MICROFLUIDIC CHEMOTAXIS ASSAY USING HYDROGEL-STABILISED GRADIENTS

by

Iftikhar Azam

B.A.Sc., The University of British Columbia, 2013

A THESIS SUBMITTED IN PARTIAL FULFILLMENT OF

THE REQUIREMENTS FOR THE DEGREE OF

MASTER OF APPLIED SCIENCE

in

THE FACULTY OF GRADUATE AND POSTDOCTORAL STUDIES

(Mechanical Engineering)

THE UNIVERSITY OF BRITISH COLUMBIA

(Vancouver)

May 2019

The following individuals certify that they have read, and recommend to the Faculty of Graduate and Postdoctoral Studies for acceptance, a thesis/dissertation entitled:

Microfluidic Chemotaxis Assay Using Hydrogel-Stabilised Gradients

submitted by Iftikhar Azam in partial fulfillment of the requirements for

the degree of Master of Applied Science

in Mechanical Engineering

Examining Committee:

Hongshen Ma, Mechanical Engineering
Supervisor

Mu Chiao, Mechanical Engineering
Supervisory Committee Member

Kenichi Takahata, Electrical Engineering
Supervisory Committee Member

Additional Examiner

Additional Supervisory Committee Members:

Supervisory Committee Member

Supervisory Committee Member

Abstract

Chemotaxis is the migration of cells in response to a chemical stimulus. This phenomenon is a part of many physiological and pathological processes, such as the neutrophilic response to bacterial invasion, as well as tumour invasion and metastasis. Since the 1960s, assays have been developed to study cell chemotaxis. Early assays mostly measured the number of cells migrating across a membrane, but do not allow tracking of individual cells. Recently, microfluidic assays have enabled single-cell tracking, but they are only able to maintain a stable chemical gradient for a limited time, or require continuous perfusion to maintain a chemical gradient.

Here, we developed a microfluidic chemotaxis assay which is capable of maintaining a stable chemical gradient for an extended period of time without the need for a fluid flow system. This capability is achieved by forming a linear chemoattractant gradient in a hydrogel prepolymer in a microchannel, then polymerising the hydrogel by exposure to UV light, thereby fixing the gradient in place. Cells are dispensed on top of the polymerised hydrogel and the cell response to the chemoattractant gradient is observed. Compared to many existing chemotaxis assays, this device requires significantly less time and user expertise to operate.

Two versions of the hydrogel-stabilized chemotaxis assay have been developed. Version 1 is manufactured using polydimethylsiloxane (PDMS), while Version 2 is manufactured using 3D printing of translucent epoxy resin. For both versions, the manufacturing methods and operation protocol have been optimised to achieve a device reliability of 80%. Version 2 dramatically reduced the number of failure modes and simplified device operation. A simulation study was

conducted to better understand the diffusion process that forms the chemical gradient, and verify the gradient profile applied to the cell sample.

Lay Summary

Chemotaxis is the migration of cells towards a chemical. Chemotaxis assays are devices that are used to study cell chemotaxis. Many types of chemotaxis assays have been developed at present. However, none are unable to maintain stable gradients for long without the aid of external equipment, which makes chemotaxis assays difficult to use. We have developed a new chemotaxis assay that is able to maintain a stable gradient for an extended period of time without the aid of external equipment. This is achieved by forming the gradient in a hydrogel prepolymer, then polymerising the hydrogel, thereby fixing the liquid in place. Cells can be placed on top of the hydrogel and their behaviour observed. We have shown that gradients can be consistently generated in this device without failure, and that the same gradient also exists in the cell solution where cells settle just above the top surface of the hydrogel.

Preface

Early iterations of Version 1 (described in Section 3.2) were developed by Dr. Hongshen Ma and Jisun Lee. This version was prone to the failure modes described in Section 5.1.

Dr. Emily Park assisted with some of the chemotaxis experiments conducted with PC3 cells. Cell cultures were maintained by Dr. Emily Park and Dr. Kerryn Matthews. Samuel Berryman assisted with the 3D printing of Version 2. Kevin Hodgson and Dr. Miki Fujita assisted with the FRAP experiment (Section 4.2.1). Scott Meixner assisted with the experiment conducted with the SpectraMax Gemini EM spectrofluorometer (Section 4.3.2.1). Cell tracking images were generated using custom software developed by Jeffrey Chiu.

All other work described in this thesis, including device development, operating protocol development, device validation experiments, and simulation, were performed by the author.

Table of Contents

Abstract ..... **iii**

Lay Summary ..... **v**

Preface ..... **vi**

Table of Contents ..... **vii**

List of Tables ..... **xii**

List of Figures ..... **xiii**

List of Abbreviations ..... **xxii**

Acknowledgements ..... **xxiv**

Dedication ..... **xxv**

Chapter 1: Introduction **1**

1.1 Contribution of Thesis Work 3

1.2 Research Goals 3

Chapter 2: Background **5**

2.1 Transwell Assay 5

2.2 Source-Sink Well Assays 6

2.2.1 Traditional Source-Sink Well Assays 6

2.2.2 Microfluidic Source-Sink Well Assays 7

2.3 Continuous Perfusion Assays 9

2.4 Scratch-Wound Assays 11

2.5 Micropipette Assays 12

2.6 Hydrogel Assays 13

2.7 Commercial Chemotaxis Assays 15
2.7.1 High Throughput Automated Chemotaxis Systems 16
2.8 Challenges for Existing Chemotaxis Assays 17
2.8.1 Performance Metrics 18
2.8.1.1 Gradient stability and control 18
2.8.1.2 Ease of assay operation 19
2.8.1.3 Assay experiment time 19
2.8.1.4 Single cell visualisation 19
2.8.1.5 External equipment/hardware 20
2.8.2 Assessment of Existing Chemotaxis Assays against Performance Metrics 20
2.9 PEGDA in Biomedical Engineering and Cell Migration 21
Chapter 3: Device Design, Fabrication, and Operation 23
3.1 Hydrogel and Cell Solution Preparation 23
3.1.1 Hydrogel Preparation 23
3.1.2 Cell Culture 24
3.2 Version 1: Design, Manufacture, and Operation 25
3.2.1 Conceptual Design Overview 25
3.2.2 Manufacturing Methods 26
3.2.3 Operation Protocol 27
3.2.3.1 Hydrogel Gradient Formation 30
3.2.3.2 Cell Sample Dispensing and Observation 31
3.3 Version 2: Design, Manufacture, and Operation 32
3.3.1 Conceptual Design Overview 32

3.3.2 Manufacturing Methods 32
3.3.3 Operation Protocol 35
3.3.3.1 Hydrogel Gradient Formation 37
3.3.3.2 Cell Dispensing 37
3.4 Advantages of Version 2 over Version 1 38
Chapter 4: Gradient Modelling 39
4.1 Methods 39
4.1.1 Overview of Transport of Diluted Species physics 39
4.2 Gradient formation in hydrogel prepolymer 40
4.2.1 FRAP experiment to determine diffusion constant in hydrogel prepolymer 40
4.2.2 Setup of hydrogel prepolymer gradient simulation 43
4.2.3 Results of hydrogel prepolymer gradient simulation 44
4.3 Simulation of chemoattractant effusion from polymerised hydrogel 44
4.3.1 Determining initial concentration distribution from experimental data 47
4.3.2 Determining diffusion constant of rhodamine B in polymerised hydrogel 49
4.3.2.1 Experiment: Concentration change in PBS due to Rhodamine B Effusion 49
4.3.2.2 Simulation: Concentration change in PBS due to Rhodamine B Effusion 50
4.3.3 Setup of rhodamine B effusion from polymerised hydrogel simulation 50
4.3.4 Results of rhodamine B effusion from polymerised hydrogel simulation 51
Chapter 5: Testing and Validation 56
5.1 Modes of Failure during Device Preparation 56
5.1.1 Leaking between Layers 57
5.1.2 Bubble Formation in Prepolymer & Cell Solution 58

5.1.3 Inconsistent Gradient Profile in Microchannels 60
5.2 Experimental Validation of Gradient Generation 61
5.2.1 Methods for Experimental Gradient Visualisation 62
5.2.2 Formation of the Gradient in Hydrogel Prepolymer 63
5.2.3 Experimental Validation of Gradient Stability 67
5.2.4 Experimental Validation of Gradient Consistency 70
5.3 Chemotaxis Experiments to Validate Device Functionality 74
5.3.1 Methods for Chemotaxis Experiments 75
5.3.2 Chemotaxis Experiment Results of dHL60 Cells in fMLP Gradient 76
5.3.3 Chemotaxis Experiment Results of PC3 Cells in FBS Gradient 76
5.3.4 Discussion of dHL60 & PC3 Chemotaxis Experiment Results 78
5.4 Modification to Hydrogel Composition to Improve Cell Adhesion to Hydrogel 79
5.4.1 Embedding of Polystyrene Beads in Hydrogel 80
5.4.2 Mixing Dopamine solution with Hydrogel 81
5.4.3 Discussion: Reason for Failure of Hydrogel Composition Modification Experiments 83
5.5 Investigation and Resolution of Internal Flows in the Microchannel 84
5.5.1 Investigation into the Cause of Internal Flow 84
5.5.1.1 Description of New Device to Investigate Cause of Flow 84
5.5.1.2 Cell Trajectory on Plasma-Activated Glass Surface 85
5.5.1.3 Cell Trajectory on PEGDA surface 87
5.5.2 Reduction of Internal Flow by Modifying Device Geometry to Reduce Hydrogel Swelling 89

5.5.2.1 Substitution of PDMS with 3D printed Epoxy Resin 89

5.5.2.2 Cell Trajectory on 3D Printed Linear Device with Thin Hydrogel Bottom.....91

5.6 Chemotaxis Experiment to Validate Functionality of 3D Printed Device.....94

Chapter 6: Conclusion 97

References.....100

List of Tables

Table 2.1 Comparison of existing chemotaxis assays.....21

Table 5.1 Molar mass of fMLP and Rhodamine B.....62

Table 5.2 Geometries of circular 3D printed device tested.....90

Table 5.3 Geometries of linear 3D printed device tested.....92

List of Figures

Figure 2.1 Transwell assay. The lower compartment is filled with buffer solution mixed with chemoattractant, and the upper compartment is filled with cell solution. Cells migrate towards the chemical gradient by squeezing through the pores of the membrane. Adapted from Toetsch *et al.* [7] by permission from Oxford University Press. 6

Figure 2.2 Zigmond chamber. (a) Wells and bridge are cut into the glass slide and covered with coverslip seeded with cells on the bottom side. (b) Cells migrate in response to chemical gradient formed at bridge area. Adapted from Keenan and Folch [6] with permission from the Royal Society of Chemistry. 7

Figure 2.3 Passive pumping chemotaxis assay. Addition of fluid droplets of pre-determined volume induce fluid flow in the source channel, generating a robust chemical gradient in the cell microchannels for a limited time. Adapted from Berthier *et al.* [8] by permission of Oxford University Press. 8

Figure 2.4 Passive pumping mechanism. Droplet of different size induces fluid flow towards larger droplet. Adapted from Berthier *et al.* [8] by permission of Oxford University Press. 8

Figure 2.5 Tree-like continuous perfusion gradient generator developed by Jeon *et al.* Chemoattractant and buffer solution flow is generated via external pumps connected to the inlets. Adapted from Jeon *et al.* [21] copyright © 2000 American Chemical Society. 10

Figure 2.6 Ladder chamber developed by Saadi *et al.* Cell suspension is flowed through the one of the large microchannels, while chemoattractant solution is flowed through the alternate large microchannel. Gradient forms in the small connecting microchannels, where cell chemotaxis is observed. Adapted from Saadi *et al.* [23] by permission of Springer Nature copyright © 2007. . 10

Figure 2.7 Scratch-wound healing assay and some similar variations. Adapted from Kramer *et al.* [5] with permission from Elsevier. 11

Figure 2.8 Soon chamber micropipette assay. The micropipette and micromanipulator system dispenses chemoattractant on the coverslip wall at strategic times, 17 μm from the top surface where cells are grown. Adapted from Soon *et al.* [24] with permission from John Wiley and Sons copyright © 2005 Wiley-Liss Inc. 12

Figure 2.9 Under-agarose chemotaxis assay. Reservoirs punched into the agarose gel are filled with chemoattractant and cell suspension respectively. Chemoattractant diffuses into the gel, and cells migrate under the gel. Adapted from Toetsch *et al.* [7] by permission of Oxford University Press. 13

Figure 2.10 PDMS microfluidic device with center hydrogel region (collagen or fibrin) (pink). Buffer solution is filled on one side channel (blue), while chemoattractant is filled on the other side (green). Chemoattractant diffuses into the hydrogel, forming a chemical gradient. Cells are seeded onto the hydrogel surface, which then exhibits chemotactic behaviour. Adapted from Moreno-Arotzena *et al*. [26] with the permission of AIP Publishing. 14

Figure 2.11 Printing-on-gel gradient generation. Chemoattractant is printed in parallel lines of decreasing print density on collagen gel. High-precision control equipment is required to achieve this. Adapted from Rosoff *et al*. [27] with permission from John Wiley and Sons copyright © 2005 Wiley-Liss Inc. 15

Figure 2.12 Schematic of Ibidi μ-Slide chemotaxis assay. Adapted from Biswenger *et al.* [14] under CC-BY-4.0. 16

Figure 2.13 iuvo^{TM} chemotaxis assay. (A) Top-view schematic. (B) 3D schematic. Reprinted from Mayvantsson *et al.* [30] with permission from Elsevier. 17

Figure 3.1 Chemotaxis assay Version 1, illustrating functional design. (a) Hydrogel prepolymer is dispensed from one end, and chemoattractant prepolymer from the other. 30 minutes is given for the gradient to form. The hydrogel is then polymerised, fixing the gradient in place. (b) The top layer from (a) is removed and a new top layer is placed, forming a microchannel on top of the polymerised hydrogel into which cells can be dispensed. Cells that settle on the surface of the polymerised hydrogel with stable gradient can detect the change in concentration and move towards the concentration gradient. 26
Figure 3.2 Layer 1, Layer 2, and Layer 3 of chemotaxis assay, Version 1. (a)-(c) CAD model of single channel (all dimensions in mm). (d)-(f) Physical devices.....28
Figure 3.3 Steps to prepare device for experiment. (a) Layer 2 is sealed on Layer 1, removing any air pockets. (b) 50 μL of hydrogel prepolymer is dispensed. (c) 25 μL of chemoattractant prepolymer is dispensed on opposite end. Wait for 30 minutes for gradient to form. (d) PEGDA is polymerised by exposure to UV light for 5 seconds. (e) Layer 2 is removed. (f) Layer 3 is sealed on Layer 1. (g) 90 μL of cell solution is dispensed.....29
Figure 3.4 Custom apparatus for gradient formation. (a) Custom pipette stand. (b) E1-ClipTip electronic pipette. (c) Jack. This apparatus completely removes the user from the gradient formation process, vastly increasing gradient consistency.....30
Figure 3.5 Chemotaxis assay Version 2, illustrating functional design. (a) Hydrogel prepolymer is dispensed through the inlet well on the left, followed by chemoattractant prepolymer dispensed through the same location. 30 minutes is given for the gradient to form. The hydrogel is then polymerised, fixing the gradient in place. (b) The top PDMS Layer is removed, leaving a reservoir that can accommodate the cell solution. Cells that settle on the surface of the

polymerised hydrogel with stable gradient can detect the change in concentration and move towards the concentration gradient. 33
Figure 3.6 Layer 1 and Layer 2 of Version 2. All dimensions in mm. (a) CAD model of single channel for Layer 1 and Layer 2. (b) Section view through midplane showing internal features.34
Figure 3.7 Physical Version 2 devices. (a) Layer 1 is 3D printed out of Clear Resin (FLGPCL04, Formlabs, Somerville, MA). (b) Layer 2 is made of PDMS. (c) Polymerised hydrogel with reservoir feature. 35
Figure 3.8 Steps to prepare Version 2 for experiment. (a) Layer 2 is positioned on Layer 1 (no sealing required). (b) 25 μL of hydrogel prepolymer is dispensed above the inlet well. (c) 20 μL of chemoattractant prepolymer is also dispensed above the inlet well. Wait for 30 minutes for gradient to form. (d) Hydrogel is polymerised by exposing to UV light for 10 seconds. (e) Layer 2 is removed. (f) 60 μL of cell solution is dispensed directly onto polymerised hydrogel reservoir. 36
Figure 4.1 Results of FRAP experiment, showing recording of bleached region and its recovery over 3 time frames. (a) Recorded images from FRAP experiment. (b) Corresponding averaged intensity plots obtained from Fiji [44]. The intensity plots form a Gaussian distribution, which were used to determine the diffusion constant. 42
Figure 4.2 Plot of full width at half maximum squared vs. time, obtained from the intensity plots in Figure 4.1. A clear linear trendline can be drawn through the data points. The diffusion constant is the trendline gradient divided by 2. 43
Figure 4.3 3D representation of gradient formation of hydrogel prepolymer simulation. (a) Concentration distribution at t = 0 min. (b) Concentration distribution at t = 60 min. For initial

conditions, it is assumed that hydrogel prepolymer and rhodamine B prepolymer are equally divided along the microchannel midplane. 45
Figure 4.4 Simulation of gradient change in hydrogel prepolymer on top surface over 1 hour. 46
Figure 4.5 Gradient data from prepolymer gradient formation experiment. (a) Image of gradient from experiment at 30 minutes. Yellow rectangle indicates area over which averaged intensity plot was generated. (b) Corresponding averaged intensity plot with units converted to generate a trendline equation that could be directly used in COMSOL. (c) Concentration distribution in COMSOL at top surface of hydrogel based on trendline equation. The COMSOL gradient profile reasonably matches that of the experiment. 48
Figure 4.6 Simulation geometry replicating effusion of rhodamine B from polymerized hydrogel into a 6-well plate containing 5 mL of PBS. 50
Figure 4.7 3D representation of rhodamine B effusion from polymerized hydrogel at: (a) t = 0 min and 52
Figure 4.8 Concentration profiles along midplane of channel. (a) At 30 minutes, in hydrogel and 1 μm, 5 μm, and 10 μm above the hydrogel top surface. There is no appreciable change in concentration profile at 1 μm, 5 μm, and 10 μm above the hydrogel top surface, but the concentration profile in the hydrogel is higher with steeper gradient. (b) 5 μm above hydrogel top surface, at 15, 30, 45, & 60 minutes. A persisting linear gradient of ~1.2 nM/mm exists between 1.5-10.0 mm along microchannel length, within the cell vicinity. 53
Figure 4.9 Concentration distribution 5 μm above hydrogel top surface, every 15 min over 60 min. A persisting linear gradient indeed exists within the cell vicinity. The gradient softens over 1 hour, but Figure 4.8b confirms that the actual concentration change is negligible. 55
Figure 5.1 Hydrogel prepolymer leak between Layer 1 and Layer 2 57

Figure 5.2 Air bubbles trapped in hydrogel prepolymer 59
Figure 5.3 Ragged Layer 1 edge (left) compared to a clean edge (right) 60
Figure 5.4 Rhodamine B gradient formation in prepolymer hydrogel in the same microchannel over 1 hour. Provided time is that after rhodamine B prepolymer dispensing. Gradient smoothens to a linear profile by 28 minutes. After 35 minutes, gradient boundary sharpens. The gradient formation is driven by a combination of weight of liquid at inlet and evaporation from inlet. 65
Figure 5.5 Intensity plots for gradient formation in the same microchannel over 1 hour. Provided time is after rhodamine B dispensing. Profile is irregular until 28 minutes, when a reasonably linear profile forms up to 8 mm. After 35 minutes, the gradient changes to become 2 flat regions separated by a sudden drop at 6 mm. 66
Figure 5.6 Change in gradient of the same channel after polymerization over 1 hour. Provided time is that after polymerisation. Once the hydrogel is polymerized, there negligible change in gradient profile. 68
Figure 5.7 Averaged intensity plots of gradient along microchannel after polymerisation over 1 hour. Provided time is that after polymerisation. Once the hydrogel is polymerized, there negligible change in gradient profile. 69
Figure 5.8 Gradient profile in all 10 channels of a single Version 2 device. Differences in gradient profiles are noticeable, and could be potentially improved. However, all channels have a gradient across the middle region of the channel. 71
Figure 5.9 Averaged intensity plots of gradient along microchannel length for all 10 microchannels on a single Version 2 device. 72
Figure 5.10 Results of linear regression of averaged intensity plots in Figure 5.9, in the 5-7 mm range. (a) Slopes of best fit lines. (b) Standard errors of best fit lines compared to raw data. Best

fit lines with standard errors more than 275 μm are considered failed (coloured orange). Results demonstrate that the device has a gradient consistency of 80%. 73
Figure 5.11 Time lapse image over 15 minutes showing typical results of a chemotaxis experiment with dHL60 cells in gradient formed using (a) 100 nM and (b) 0 nM fMLP. The numbers indicate the position of the last tracked position for each cell. The fMLP concentration is higher on the left hand side. The general trajectory of cells is towards the right. Similar cell trajectory was observed in both experiments (with and without chemoattractant). Therefore, the migration of cells is due to internal flow rather than chemotaxis. 77
Figure 5.12 Time lapse over 15 minutes showing typical results of a chemotaxis experiment with 24 hour starved PC3 cells in gradient formed using (a) 30% FBS and (b) 0% FBS. The numbers indicate the position of the last tracked position for each cell. The FBS concentration is higher on the right hand side. There is low velocity trajectory of cells downwards. Similar cell trajectory was observed in both experiments (with and without chemoattractant). Therefore, the migration of cells is due to internal flow rather than chemotaxis. 78
Figure 5.13 Time lapse over 15 minutes showing typical cell trajectory of dHL60 cells dispensed in a device with 100 nm beads embedded in hydrogel. The numbers indicate the position of the last tracked position for each cell. There is significant cell trajectory towards the right. Therefore, beads have failed to improve cell adhesion to the hydrogel, and the cells are still susceptible to internal flow. 82
Figure 5.14 Time lapse over 15 minutes showing typical cell trajectory of dHL60 cells dispensed in a device with dopamine in hydrogel. The numbers indicate the position of the last tracked position for each cell. There is significant cell trajectory towards the right. Therefore, dopamine

has failed to improve cell adhesion to the hydrogel, and the cells are still susceptible to internal flow. 83
Figure 5.15 Circular device used to investigate cause of internal flow. (a) Images of the devices. (b) Schematic design of device. This design is similar to the Version 2 device, consisting of hydrogel with a reservoir to accommodate the cell solution, except that the geometry is larger and circular, and Layer 1 is made of PDMS.....85
Figure 5.16 Time lapse over 15 minutes showing cell trajectory of dHL60 cells dispensed in a well with plasma-activated glass bottom. The numbers indicate the position of the last tracked position for each cell. There is no significant cell trajectory. This serves as a positive control, and a target which we wish to achieve on a PEGDA surface. 86
Figure 5.17 Time lapse over 15 minutes showing typical cell trajectory of dHL60 cells dispensed in the circular device with PEGDA reservoir. The numbers indicate the position of the last tracked position for each cell. No significant motion is detected for the first 5 minutes. Then suddenly significant motion begins due to hydrogel deformation. This is indicated in the cell trajectories by earlier cell location points being closer together than later cell location points. ...88
Figure 5.18 Deformed hydrogel after exposure to cell solution. (a) Isometric view. (b) View from side, showing deformed profile. 88
Figure 5.19 Schematic design of 3D printed circular device used in the attempt to reduce hydrogel swelling. 90
Figure 5.20 Schematic design of 3D printed linear device used in the attempt to reduce hydrogel swelling. 92
Figure 5.21 Time lapse over 15 minutes showing typical cell trajectory of PC3 cells dispensed in 3D printed linear device with hydrogel bottom thickness of 250 μm. The numbers indicate the

last tracked position for each cell. There is no significant cell trajectory. Therefore, making the PEGDA bottom floor very thin and using 3D printed Layer 1 successfully eliminates internal flow in then microchannel. 93
Figure 5.22 Time lapse image over 15 minutes showing results of a chemotaxis experiment in Version 2 device with dHL60 cells in gradient formed using (a) 100 nM and (b) 0 nM fMLP. The numbers indicate the position of the last tracked position for each cell. The fMLP concentration is higher on the left hand side. Cells in 0 nM gradient show limited motion, as expected. Cells in 100 nM gradient appear to show a low velocity trajectory bias towards the right; i.e. the end with lower concentration of chemoattractant. 95

List of Abbreviations

3D	Three Dimensional
CAD	Computer Aided Design
dHL-60	Differentiated Human Leukemia -60
DMEM	Dulbecco's Modified Eagle Media
DMSO	Dimethylsulphoxide
EDTA	Ethylenediaminetetraacetic acid
EGF	Epidermal Growth Factor
FACS	Fluorescence Activated Cell Sorting
FBS	Fetal Bovine Serum
FDM	Fused Deposition Modelling
fMLP	formyl-*Met-Leu-Phe*
FRAP	Fluorescence Recovery After Photo-bleaching
HL-60	Human Leukemia -60
IL8	Interleukin-8
PBS	Phosphate Buffered Saline
PC3	Prostrate Cancer 3
PDMS	Polydimethylsiloxane
PEGDA	Poly(ethylene glycol) Diacrylate
RGDS	*Arg-Gly-Asp-Ser*
RPMI	Roswell Park Memorial Institute
SLA	Stereolithography Apparatus
TLGG	Tree-Like Gradient Generator

Tris	Tris(hydroxymethyl)aminomethane
UV	Ultra Violet

Acknowledgements

Achievements of the present day are rarely accomplished alone, and this was no exception. First and foremost, thanks to Dr. Hongshen Ma, who took me under his wing and gave me the opportunity to take the next step in my career. Sampath Satti, the giant whose shoulders I stood on. Dr. Emily Park, the person who shone the light when I lost my way. Dr. Kerryn Matthews, for her reassuring practicality. Samuel Berryman, who showed me solutions outside the box. And all other members of the Multi-scale Design lab, for constantly reminding me that I was not alone.

Equally important, if not more, are my family members & family friends. Without your support & advice I would have made a lot more mistakes than I did. Special thanks to my Mum, Hasina, without whom I would not have started. Thanks most of all to my wife, Hanika, without whom I would not have finished. You have all been incredibly supportive and patient. Thank you.

Dedication

To Dr. Helal Azam, who dreamed of his son exceeding his father's achievements. You are sorely missed.

and

Dr. Syeda Hasina Azam, who planted the seed that now bears fruit.

Chapter 1: Introduction

Chemotaxis is the migration of cells in response to external chemical stimulus, typically in the form of a chemical gradient [1]. Chemotaxis has been shown to be an important part of a wide range of biological processes, including cancer metastasis [2], immune cell trafficking [1], embryonic morphogenesis [3], and nervous system development [4] [5] [6]. Extensive research and development, consisting of a combination of *in vivo* studies and *in vitro* methods (i.e. chemotaxis assays), has significantly improved our understanding of these phenomena [6].

Cell chemotaxis assays are important tools for disease diagnosis and drug development [5] [7] [8] [9]. *In vitro* assays present several advantages over *in vivo* assays, including: (i) simple to operate, (ii) capable of producing repeatable results, (iii) can be integrated with high content analysis systems, (iv) less expensive, and (v) fewer ethical concerns [5]. However, existing *in vitro* assays are limited in their ability to accurately replicate *in vivo* conditions [5].

Neutrophils are the first cells to migrate to the areas of infection and tissue damage. Neutrophils have been shown to respond to a variety of chemoattractants, including formyl-*Met-Leu-Phe* (fMLP) which is generated by bacteria [1], and interleukin-8 (IL8) [10]. The inability of neutrophils to chemotax towards fMLP can be an indication of immunodeficient diseases. In 2010, Berthier *et al*. developed a chemotaxis assay which was used to determine the ability of neutrophil chemotaxis towards fMLP. The device was tested with blood samples from a patient suffering from primary immunodeficiency and healthy donors. The neutrophils from the patient with immunodeficiency showed impaired migration in the presence of an fMLP gradient [8]. This is an example of how a chemotaxis assay can be used as a diagnosis tool.

Chemotaxis assays also play a vital role to improving our understanding biological process mechanisms such as cancer metastasis, which in turn is crucial to the development of antimetastatic drugs [5]. Cancer is the 6th most common cause of death [11], with 9.6 million deaths in 2018 [12], the majority of which can be attributed to cancer metastasis [5]. A study was conducted by Biswenger *et al.* on the chemotaxis of MDA-MB-231 breast cancer cells starved in different types of cell media. The chemoattractant used was recombinant human epidermal growth factor (EGF). The commercial Ibidi μ-Slide Chemotaxis assay [13] was used to conduct the experiment. It was discovered that a defined growth medium is required to obtain reliable chemotaxis results; solely starving cells in a custom serum-free medium can lead to unpredictable cell behaviour [14].

These examples illustrate how chemotaxis assays can help improve our understanding of cell migration mechanisms, and their potential as diagnostic tools. Many different types of chemotaxis assays are currently in existence [5] [6] [7] [15]. However, all existing assays come with limitations. Transwell assays are presently the most popular type of assays due to ease of use, but do not allow single cell visualisation [15]. All passive types of assays are unable to maintain a stable gradient for an indefinite period. Only assays where gradient generation relies on continuous perfusion can maintain a constant gradient indefinitely. However, connection to an external flow actuation and control system is required to achieve continuous perfusion, which increases the difficulty of operating the assay. Therefore, there is a need to develop a stand-alone assay that can maintain a stable gradient indefinitely without the need of external equipment.

1.1 Contribution of Thesis Work

In this thesis, I have developed a new chemical gradient generation method in a microfluidic chemotaxis assay. This method involves forming a chemical gradient in hydrogel prepolymer, then fixing the gradient in place by polymerising the hydrogel. The gradient generated by this method is linear and stable for an extended period of time without the need of external equipment. Single cell visualisation is possible in this assay, which allows results to be immediately viewed in real time. This assay meets the need for a stand-alone assay that can generate a stable gradient without the need for external equipment.

I developed 2 versions of the hydrogel-stabilized chemotaxis assay. For both versions, I identified the failure modes, optimised the design, developed manufacturing methods and operation protocol to eliminate the failure modes and improve ease of operation. I have conducted experiments to validate gradient formation and device functionality. I have also conducted a simulation study to verify that the gradient formed in the hydrogel also applies to the cell sample.

1.2 Research Goals

The goals of this thesis are:

- Identify the failure modes of the new assay
- Improve the assay design, manufacturing methods, and operation protocol in order to eliminate the failure modes
- Develop simulated models of gradient generation to improve understanding of the gradient formation mechanism, and verify that the gradient profile applies to the cell sample
- Conduct experiments to validate device robustness and functionality

Chapter 2 provides an overview of different types of existing chemotaxis assays. At the end of chapter 2, performance metrics to determine good chemotaxis assays are introduced, and existing assays are assessed against the performance metrics. Chapter 3 describes the device design, manufacturing methods, operation protocol, and experiment material preparation protocols. Chapter 4 provides details on the simulation study of gradient formation and effusion of chemoattractant from polymerised hydrogel, and discusses the results. Chapter 5 describes the experiments conducted to validate robustness and functionality of the device, presents the results and provides a discussion. Chapter 6 concludes this thesis with a summary of results and future work.

Chapter 2: Background

This chapter provides an overview of the different types of existing chemotaxis assays, with focus on how gradients are generated. In Section 2.8, performance metrics are introduced, which are used to assess the different types of chemotaxis assays presented. In Section 2.9, relevant work done with poly(ethylene glycol) diacrylate (PEGDA) is briefly discussed.

2.1 Transwell Assay

The transwell assay was developed by Boyden in the 1960s [16], and has been improved and simplified over the years [5]. The transwell assay consists of cell suspension in the upper chamber, and buffer solution mixed with chemoattractant in the lower chamber. A chemical gradient is formed across the porous membrane division (Figure 2.1) [7]. Cells are incubated for a period of time on the top side of the porous membrane, and react to the chemical gradient by squeezing through the pores to the bottom side. After the incubation period, the number of cells on the bottom side can be quantified.

Transwell assays are easy to operate and readily provide results [6] [7], and therefore are still one of the most popular chemotaxis assays at present [7]. However, transwell assays do not allow the real-time visualisation of cell trajectories, and cannot sustain a stable gradient over time [17].

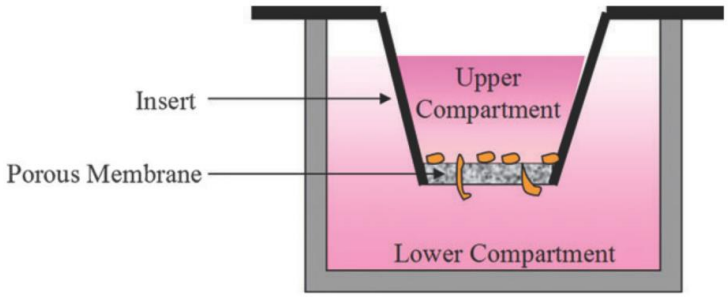

Figure 2.1 Transwell assay. The lower compartment is filled with buffer solution mixed with chemoattractant, and the upper compartment is filled with cell solution. Cells migrate towards the chemical gradient by squeezing through the pores of the membrane. Adapted from Toetsch *et al.* [7] by permission from Oxford University Press.

2.2 Source-Sink Well Assays

Source-sink well assays were developed in the 1970s to meet the need of real-time visualisation and better gradient control [6]. In general, these assays contain at least 2 reservoirs: 1 with chemoattractant solution, and the other with buffer solution, connected by a relatively small microchannel in which cells are placed and observed.

2.2.1 Traditional Source-Sink Well Assays

In the 1970s, Zigmond presented a device consisting of a plexiglass slide with 2 linear wells divided by a shallow ridge [18]. One of the wells is filled with chemoattractant solution, and the entire system is covered with a glass coverslip seeded with cells on the bottom side (Figure 2.2) [6]. Cells in the glass ridge area can be viewed in real time under a microscope.

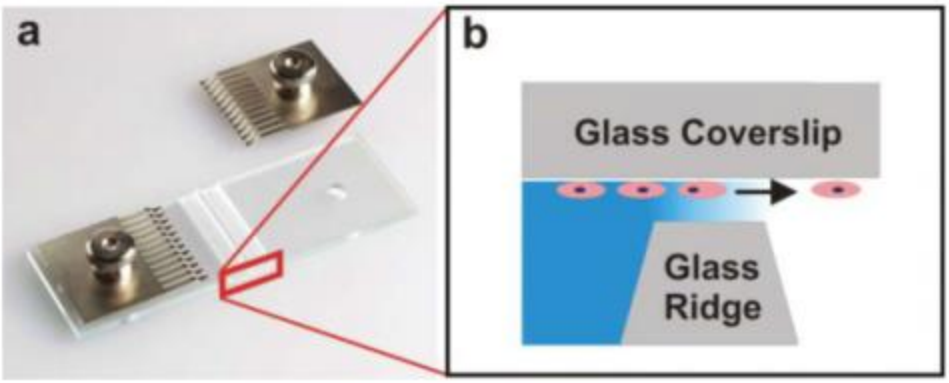

Figure 2.2 Zigmond chamber. (a) Wells and bridge are cut into the glass slide and covered with coverslip seeded with cells on the bottom side. (b) Cells migrate in response to chemical gradient formed at bridge area. Adapted from Keenan and Folch [6] with permission from the Royal Society of Chemistry.

The Dunn chamber [19] and the Insall chamber [20] improve the Zigmond chamber through geometric modifications. However, all these chambers are only able to maintain a stable gradient for 1-2 hours [6].

2.2.2 Microfluidic Source-Sink Well Assays

Recent advances in microfabrication methods have enabled the development of chemotaxis assays with more complex geometries on the micrometer-scale [6] [7]. Majority of these devices create microfeatures in polydimethylsiloxane (PDMS) using soft lithography, which is then plasma bonded to a glass slide to form microchannels.

Berthier *et al.* developed an assay in which a robust gradient is generated using passive pumping (Figure 2.3) [8]. Passive pumping works on the principle that in a microchannel with two droplets of different size at either inlets, a pressure gradient induces fluid flow towards the end with the

larger-sized droplet (Figure 2.4) [8]. Therefore, simply adding a droplet of fluid of pre-determined volume at the prescribed ports can induce fluid flow in the source port, hence generating a constant chemical gradient in the cell microchannel. The advantages of this device are: (i) very easy to use, (ii) small amounts of volume required, and (iii) short experiment time [8]. However, a stable gradient can be maintained for only a limited time.

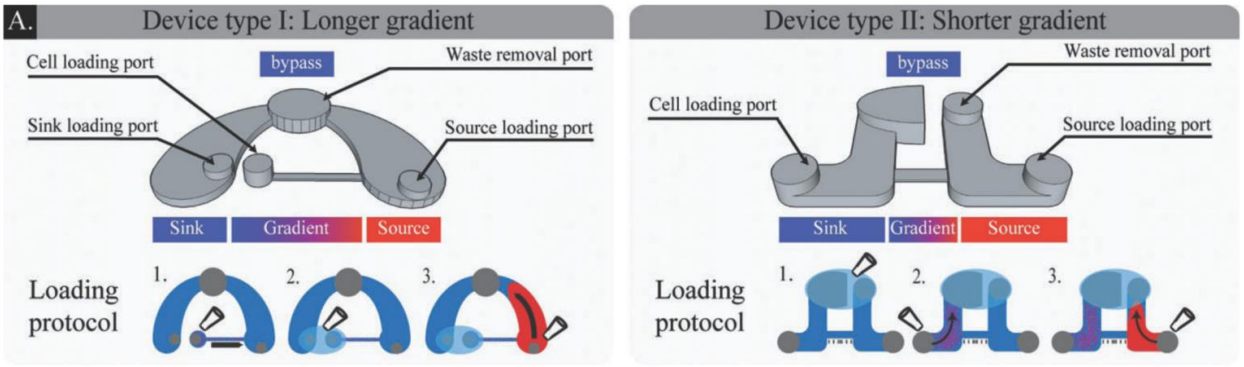

Figure 2.3 Passive pumping chemotaxis assay. Addition of fluid droplets of pre-determined volume induce fluid flow in the source channel, generating a robust chemical gradient in the cell microchannels for a limited time. Adapted from Berthier *et al.* [8] by permission of Oxford University Press.

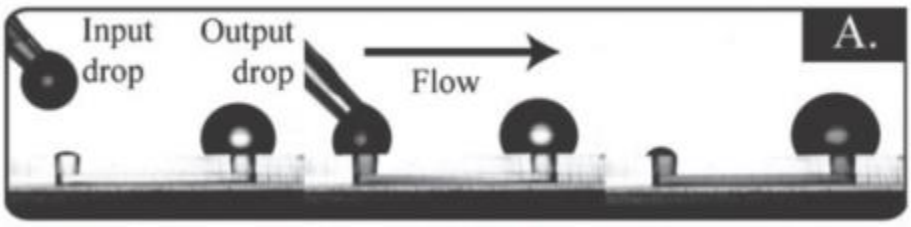

Figure 2.4 Passive pumping mechanism. Droplet of different size induces fluid flow towards larger droplet. Adapted from Berthier *et al.* [8] by permission of Oxford University Press.

2.3 Continuous Perfusion Assays

The gradient in continuous perfusion assays is created and maintained by parallel laminar flow of chemoattractant solutions of varying concentrations. An early example is the tree-like gradient generator (TLGG) design developed by Jeon *et al.* in 2000 (Figure 2.5) [21]. Continuous perfusion gradient generators exploit the phenomenon that the parallel fluid flow of two liquids in microchannels is primarily laminar, therefore there is negligible convection mixing and any mixing is predominantly by diffusion. This allows a constant chemical gradient to be maintained for a potentially limitless time (for as long as fluid flow is maintained). The same group later demonstrated the chemotaxis of neutrophils across interleukin-8 (IL8) chemoattractant gradient in a TLGG assay [10]. Lin and Butcher later developed a "Y" type gradient generator which does not require a microfluidic mixing region, and demonstrated T cell chemotaxis in competing CCL19 and CXCL12 gradients [17]. Irimia *et al.* developed a device that is able to generate a smooth gradient from two starting concentrations using position dividers [22].

The main problem with assays like the TLGG is that cells are exposed to shear forces induced by fluid flow. Saadi *et al.* addressed this problem by developing the Ladder chamber (Figure 2.6) [23] where cell suspension and chemoattractant solutions are respectively flowed through two relatively separate large microchannels connected through several smaller microchannels. Chemical gradients are thereby established in the smaller microchannels. Neutrophils positioned at the non-chemoattractant end of the middle channels were demonstrated to migrate towards IL8 chemoattractant at the opposite end. Since there is no fluid flow in the smaller channels, cells are protected from shear forces.

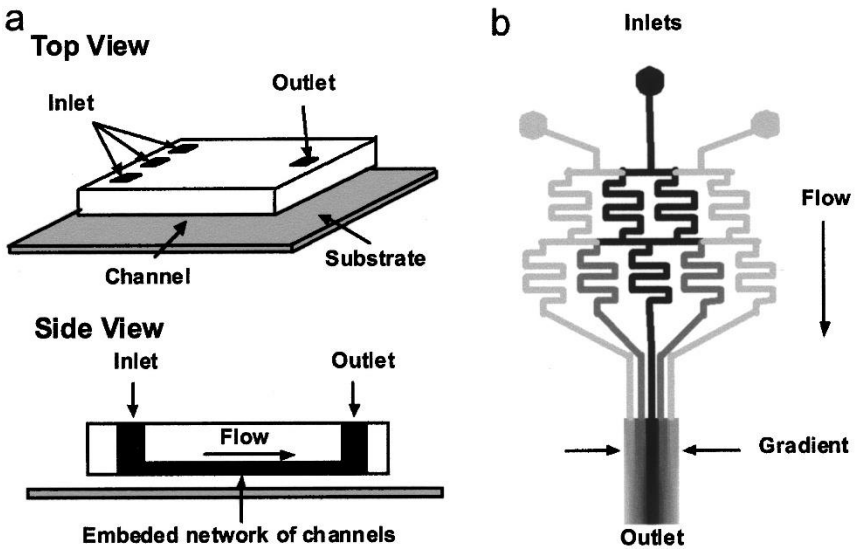

Figure 2.5 Tree-like continuous perfusion gradient generator developed by Jeon *et al.* Chemoattractant and buffer solution flow is generated via external pumps connected to the inlets. Adapted from Jeon *et al.* [21] copyright © 2000 American Chemical Society.

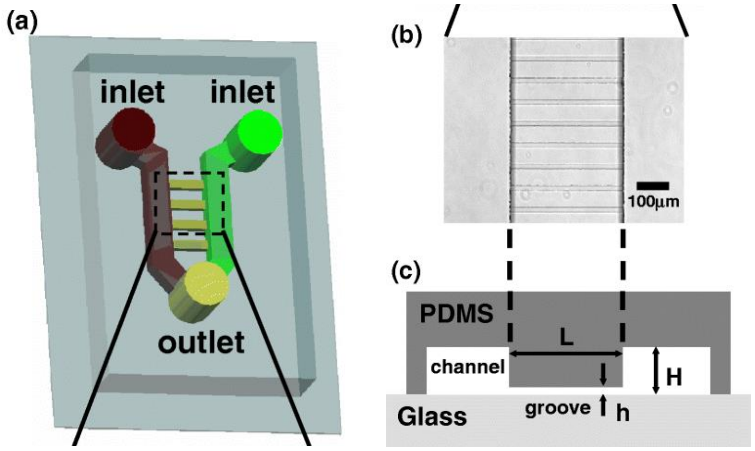

Figure 2.6 Ladder chamber developed by Saadi *et al.* Cell suspension is flowed through the one of the large microchannels, while chemoattractant solution is flowed through the alternate large microchannel. Gradient forms in the small connecting microchannels, where cell chemotaxis is observed. Adapted from Saadi *et al.* [23] by permission of Springer Nature copyright © 2007.

The main disadvantage of continuous perfusion chemotaxis assays is the need for an external active pumping system which can generate a precise velocity of fluid flow. This adds complexity, expense, and increased required user expertise to operate the system.

2.4 Scratch-Wound Assays

Scratch-wound assays consist of a single layer of cells grown in the cell chamber. A sharp tip is used to remove cells in a region, and the migration of cells in the scratch area is observed. As seen in Figure 2.7 [5], this type of assay can be modified in various ways, but follow the same principle. Scratch-wound type assays are very simple to setup and execute. However, they are not suitable for analysing neutrophil or cancer cell chemotaxis.

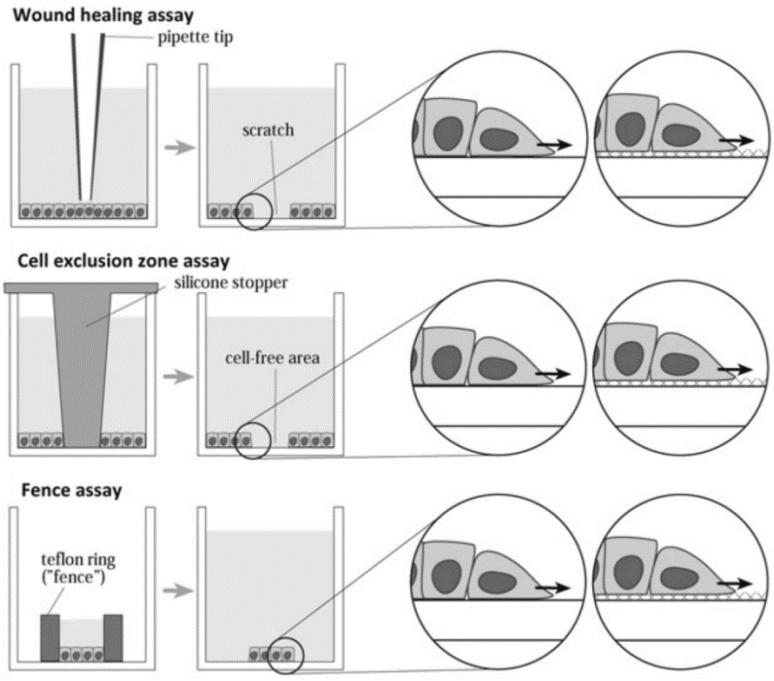

Figure 2.7 Scratch-wound healing assay and some similar variations. Adapted from Kramer *et al.* [5] with permission from Elsevier.

2.5 Micropipette Assays

Micropipette assays generate gradient by dispensing minute amounts of chemoattractant solution at strategic times and locations in the cell chamber. The Soon chamber is an example of a micropipette chemotaxis assay (Figure 2.8) [24]. Cells are grown on top of a coverslip, and a micropipette and micromanipulator used to dispense chemoattractant solution on the coverslip wall.

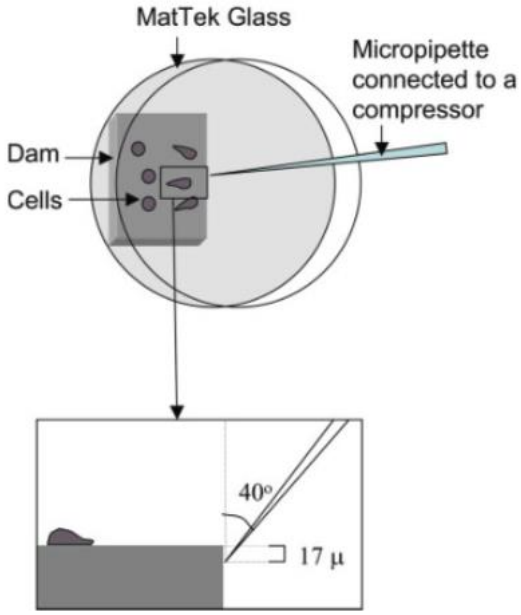

Figure 2.8 Soon chamber micropipette assay. The micropipette and micromanipulator system dispenses chemoattractant on the coverslip wall at strategic times, 17 µm from the top surface where cells are grown. Adapted from Soon *et al.* [24] with permission from John Wiley and Sons copyright © 2005 Wiley-Liss Inc.

Micropipette assays allow the precise, real-time control of gradients throughout the duration of the experiment. However, the setup typically requires expensive tools for precision chemoattractant dispensing, and even then it is difficult to reproduce the same conditions in multiple experiments

[9]. Use of external equipment means increased complexity, expense, and required user expertise to operate the system.

2.6 Hydrogel Assays

Hydrogels provide a matrix for cells similar to what cells experience *in vivo*. This property has motivated researchers to develop chemotaxis assays that can mimic *in vivo* conditions *in vitro* [6]. Heit and Kubes used an under-agarose assay with chemoattractant and cell wells (Figure 2.9) [25] [7]. The chemoattractant diffuses into the agarose gel forming a chemical gradient. Cells migrate from the cell well under the agarose gel towards the chemoattractant.

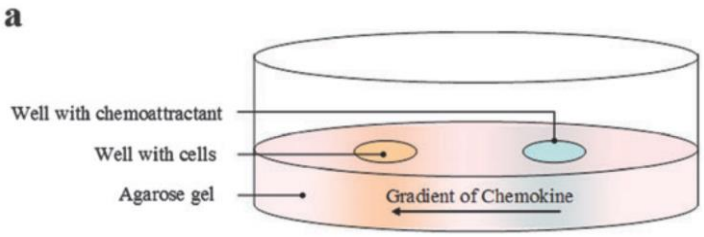

Figure 2.9 Under-agarose chemotaxis assay. Reservoirs punched into the agarose gel are filled with chemoattractant and cell suspension respectively. Chemoattractant diffuses into the gel, and cells migrate under the gel. Adapted from Toetsch *et al.* [7] by permission of Oxford University Press.

Moreno-Arotzena *et al*. developed a hydrogel assay consisting of 3 PDMS microchannels (Figure 2.10) [26]. The side channels are filled with buffer and chemoattractant solution respectively, while the center channel is filled either collagen or fibrin as the hydrogel. Chemoattractant diffuses into the hydrogel to create a gradient. It takes about 1 hour for a suitable gradient to form. Cells are seeded onto the hydrogel surface, upon which cell migration and morphology can be observed.

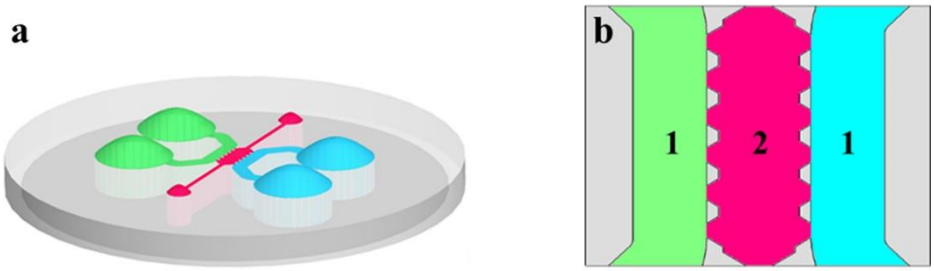

Figure 2.10 PDMS microfluidic device with center hydrogel region (collagen or fibrin) (pink). Buffer solution is filled on one side channel (blue), while chemoattractant is filled on the other side (green). Chemoattractant diffuses into the hydrogel, forming a chemical gradient. Cells are seeded onto the hydrogel surface, which then exhibits chemotactic behaviour. Adapted from Moreno-Arotzena *et al*. [26] with the permission of AIP Publishing.

Another methodology used to create gradient in hydrogels uses technology similar to inkjet printing. An example of just an assay is presented by Rosoff *et al*., where parallel lines of chemoattractant was dispensed onto a collagen gel in decreasing density (Figure 2.11) [27]. This method is able to achieve smooth gradient profiles that remain stable for 1-2 days. However, high-precision equipment is required to achieve this, increasing expense and user expertise requirements.

Though the chemical gradient can be maintained for longer than source-sink assays (e.g.: 1-2 days for Rosoff *et al*.'s assay [27]), there is still slight variation in gradient during this time.

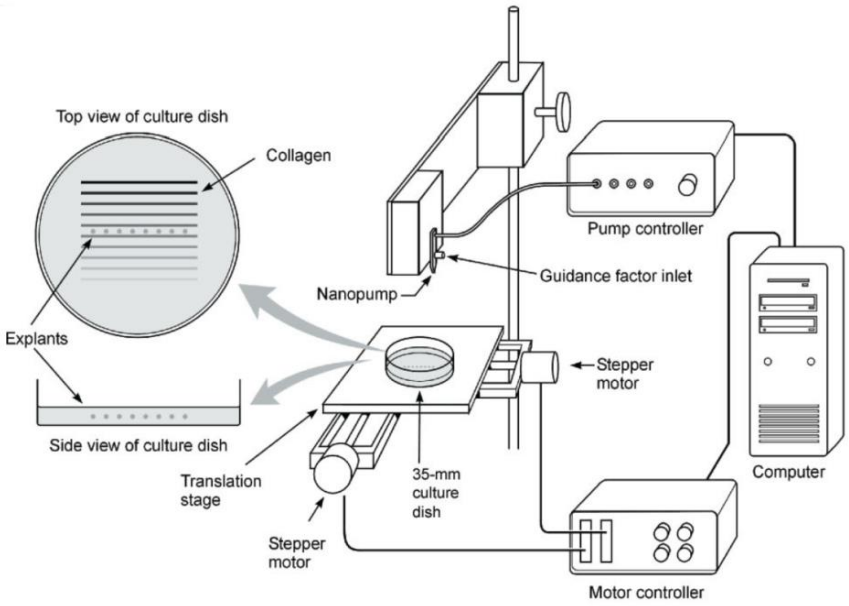

Figure 2.11 Printing-on-gel gradient generation. Chemoattractant is printed in parallel lines of decreasing print density on collagen gel. High-precision control equipment is required to achieve this. Adapted from Rosoff *et al.* [27] with permission from John Wiley and Sons copyright © 2005 Wiley-Liss Inc.

2.7 Commercial Chemotaxis Assays

Several chemotaxis assays have been developed based on those existing in academia, which are commercially available for purchase. For example, Neuro Probe manufactures a variety of disposable transwell assays and Zigmond chambers [28].

Ibidi GmbH offer the μ-Slide Chemotaxis [13], which consists of two side reservoir channels and a central cell channel (Figure 2.12) [14]. The center channel can be filled with hydrogel or cell suspension. Ibidi GmbH also offers the μ-Slide III 3in1 [29], which is a Y-shaped continuous perfusion assay [17].

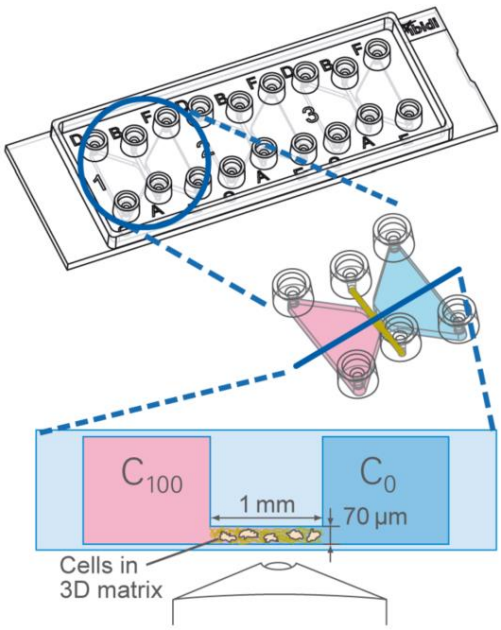

Figure 2.12 Schematic of Ibidi µ-Slide chemotaxis assay. Adapted from Biswenger *et al.* [14] under CC-BY-4.0.

The iuvo^{TM} chemotaxis assay was presented by Meyvantsson *et al*. from BellBrook Labs (Figure 2.13) [30]. This assay employs a specialised geometry that allows a stable gradient to be maintained for at least 3 hours, and can be easily integrated with automated high content analysis systems.

2.7.1 High Throughput Automated Chemotaxis Systems

Commercial chemotaxis assays are typically designed to be integrated with automated high content analysis systems. One such system is the EZ-TAXIScan, which was first presented by Kanegasaki *et al*. [31]. The chemotaxis chamber itself is a source-sink well assay, but can be integrated with a custom portable system which can automatically record images of cell motion in real time, and analyse and generate processed data. Essen BioScience offers transwell assays which can be used with their IncuCyte high content analysis system [32]. The main disadvantage with the above

systems is that they are very expensive. Several research labs have successfully demonstrated low-cost automated chemotaxis platforms [33] [34] [35].

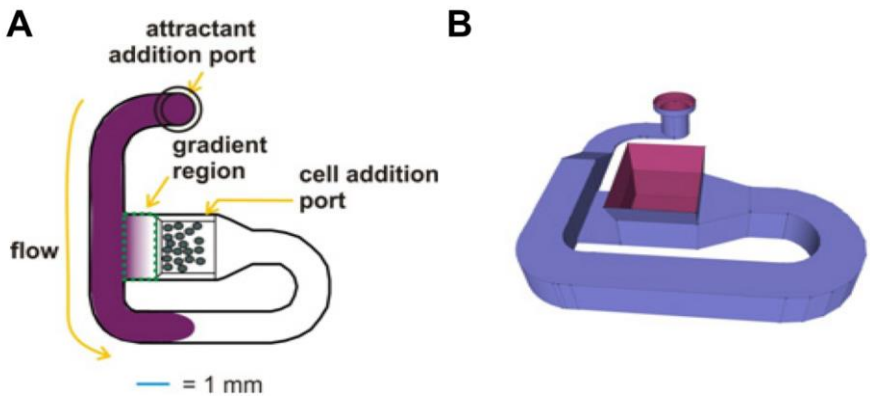

Figure 2.13 iuvo^{TM} chemotaxis assay. (A) Top-view schematic. (B) 3D schematic. Reprinted from Mayvantsson *et al.* [30] with permission from Elsevier.

2.8 Challenges for Existing Chemotaxis Assays

From the above review of existing chemotaxis assays, it can be seen that a number of challenges still remain. Almost all types of assays are unable to maintain a stable gradient for an extended period of time. Some microfluidic source-sink assays and hydrogel assays are able to slow down the gradient variation rate; but there is still some variation that occurs throughout the duration of the experiment. For example, in the Insall Chamber, which is a source-sink well assay with improved performance achieved through recent microfluidic design and manufacturing techniques, the gradient gradually decreases by 65% over a 24 hour period [20]. By comparison, Biswenger *et al.* generated a gradient in a collagen I hydrogel on the Ibidi μ-Slide assay (Figure 2.12 in Section 2.7), and demonstrated a 31% gradient decrease over a 24 hour period after the gradient formation period [14]. However in both cases, the gradient still varies over time.

Only continuous perfusion assays are able to maintain a constant gradient indefinitely. However, continuous perfusion assays require connection to external, often high-precision, equipment that can provide flow actuation and control. This increases the difficulty of assay operation. There is a need for an assay that can maintain a constant gradient for an indefinite period without the aid of external equipment.

2.8.1 Performance Metrics

Since there are several different types of chemotaxis assays with fundamentally different designs, it is difficult to compare them without a systematic approach. Carefully chosen performance metrics can provide a framework for assessing the strengths and weaknesses of chemotaxis assays, thereby identifying good chemotaxis assays. In this sub-section, a number of performance metrics will be described. Those performance metrics will be used in the following sub-section to assess the different types of chemotaxis assays presented in this chapter.

2.8.1.1 Gradient stability and control

A good quality assay should be able to maintain a constant and quantifiable gradient throughout the duration of the experiment. Much research and development has been undertaken to achieve this [6] [9] [15].

Early chemotaxis assays are simple to set up and operate, but their gradients vary over time and cannot be controlled [16] [18] [19]. More recent microfluidic assays have demonstrated precise control of gradient for an indefinite period, but require external pumps or fluid flow control equipment to operate [17] [21] [24].

2.8.1.2 Ease of assay operation

A good quality assay should require minimal user expertise to operate. This reduces the learning curve required by a new user to conduct good quality experiments. In addition, this improves experiment throughput, since assays that are easy to operate can typically be set up faster with less mistakes. Approaches that can be taken to improve ease of assay operation include: (i) reduce number of operation steps; (ii) simplify operation steps; (iii) eliminate the need for external equipment during experiment.

2.8.1.3 Assay experiment time

A good quality assay should be able to provide results in a short period of time. This is sometimes crucial for samples obtained directly from patients, which can have short shelf life [8]. Existing assays can provide results in as little as 1 hour [8] [28]. Short experiment time also means higher experiment throughput, which ultimately allows research goals to be achieved faster. This is highly desirable in cases such as drug development [36].

2.8.1.4 Single cell visualisation

A good quality assay should allow the visualisation of single cells in real time during the experiment. Single cell visualisation allows the cell migration trajectory and morphology to be observed and recorded in response to specific gradients, which provides important insight on cell chemotactic behaviour [6]. At present, all commonly used chemotaxis assays, except transwell assays, allow for single cell visualisation.

2.8.1.5 External equipment/hardware

A good quality assay should not require any external equipment connected to it during the experiment to maintain a stable gradient. In general, the only type of chemotaxis assays that can maintain constant, precisely controlled gradients are continuous perfusion assays, which require connection to an external fluid flow control system [17] [21] [22]. This greatly increases the complexity of the assay operation (particularly integration with microscopic imaging systems), experiment time, and operation cost.

2.8.2 Assessment of Existing Chemotaxis Assays against Performance Metrics

In Table 2.1, the different types of chemotaxis assays described in this chapter are assessed against the performance metrics presented in the previous sub-section.

It can be seen from Table 2.1 that most chemotaxis assays are able to maintain a gradient for only a limited time period. Continuous perfusion can maintain a constant gradient indefinitely, but require connection to external equipment to actively maintain the gradient. This makes continuous perfusion assays more difficult to operate than other types of assays, since there is a higher learning curve, and the operation protocol consists of many additional steps. An assay that can generate a constant gradient for an indefinite amount of time, without the need of external equipment, will fulfil all the performance metrics listed above. In this work, we present a device that achieves this.

Table 2.1 Comparison of existing chemotaxis assays

Assay Type	Gradient Stability	Gradient Control	Ease of Operation	External Equipment Requirement	Single Cell Visualisation
Transwell	Variable	Not controllable	Easy	No	No
Traditional Source-Sink	Variable	Not controllable	Easy	No	Yes
Microfluidic & Commercial Source-Sink	Constant (for duration of experiment)	Not controllable	Easy	No	Yes
Continuous Perfusion	Constant	Controllable	Difficult	Yes	Yes
Scratch-Wound[1]	Not applicable	Not applicable	Easy	No	Yes
Micropipette	Active control required	Controllable	Difficult	Yes	Yes
Hydrogel	Variable	Not controllable	Easy[2]	No	Yes

[1]Only useful for studying cell growth
[2]Printing-on-gel gradient generation assay can be considered difficult

2.9 PEGDA in Biomedical Engineering and Cell Migration

Poly(ethylene glycol) diacrylate (PEGDA) is a hydrogel whose prepolymer form is liquid, but when exposed to ultra violet light polymerises into a solid with mechanical, chemical, and biological properties closely similar to living tissue [37]. The mechanical properties of PEGDA can be tuned by varying the chemical composition and fabrication method [38]. Therefore, PEGDA has been widely researched in a variety of biomedical applications, particularly tissue engineering [4] [38].

The use of PEGDA in cell migration has mainly focused on altering the properties of PEGDA itself to control cell growth. Tuturro and Papavasiliou was able to influence the direction of fibroblast aggregate growth by forming a mechanical properties gradient within PEGDA [39]. DeLong *et al*. formed a gradient of the adhesive peptide *Arg-Gly-Asp-Ser* (RGDS) in PEGDA and demonstrated the realignment of human dermal fibroblast along the gradient [40].

Chapter 3: Device Design, Fabrication, and Operation

This chapter describes the design, fabrication, and operation of two versions of the microfluidic chemotaxis assay using hydrogel stabilized gradients. Section 3.1 provides methods for hydrogel preparation and cell cultures used in both versions of the devices. Sections 3.2 and 3.3 describe the conceptual design, manufacturing method, and operational protocol for Versions 1 and 2. Finally, Section 3.4 compares the two devices and summarises the benefits of Version 2 over Version 1.

3.1 Hydrogel and Cell Solution Preparation

3.1.1 Hydrogel Preparation

The hydrogel prepolymer is prepared by mixing Poly(ethylene glycol) diacrylate (PEGDA) (50% v/v) (Mn 575, Sigma-Aldrich, St. Louis, MO) , Tris/EDTA (40% v/v) (10mM/1mM, Thermo Fisher Scientific, Waltham, MA), 70% ethanol (10% v/v), and Irgacure 819 photo-initiator (1% w/v) (ChemFine International, Wuxi, China). This mixture is thoroughly mixed, incubated overnight at 37°C, then sterile-filtered using a 0.22 μm syringe filter.

The formyl-*Met-Leu-Phe* (fMLP) chemoattractant prepolymer is prepared by dissolving fMLP (Sigma-Aldrich, St. Louis, MO) in hydrogel prepolymer at 0.1% w/v, then diluted to desired concentration. For experiments described in Chapter 5, fMLP prepolymer was diluted to 100 nM.

The fetal bovine serum (FBS) chemoattractant prepolymer is prepared by mixing heat-inactivated fetal bovine serum (30% v/v) (Gibco, Carlsbad, CA), Poly(ethylene glycol) diacrylate (50% v/v) (Mn 575, Sigma-Aldrich, St. Louis, MO) , Tris/EDTA (10% v/v) (10 mM / 1 mM, Thermo Fisher

Scientific, Waltham, MA), 70% ethanol (10% v/v), and Irgacure 819 photo-initiator (1% w/v) (ChemFine International, Wuxi, China). This mixture is thoroughly mixed, incubated overnight at 37 °C, then sterile-filtered using a 0.22 μm syringe filter.

In experiments where visualisation of gradient was necessary, rhodamine B powder (Sigma-Aldrich, St. Louis, MO) was dissolved in hydrogel prepolymer at 0.1% w/v, then diluted to desired concentration.

After preparation, all above prepolymers are stored in thoroughly covered 2 mL tubes (Eppendorf, Hamburg, Germany) at -20 °C to prevent premature polymerisation from ambient light.

3.1.2 Cell Culture

HL-60/S4 (ATCC CRL-3306) is cultured in RPMI 1640 medium with L-glutamine (Gibco, Carlsbad, CA), supplemented with 10% heat-inactivated fetal bovine serum (FBS) (Gibco, Carlsbad, CA), 50 μM Betamercaptoethanol (Sigma-Aldrich, St. Louis, MO), 1 mM sodium pyruvate, and 1% Penicillin/Streptomycin (Sigma-Aldrich, St. Louis, MO). HL-60 is incubated in 75 cm^2 culture flasks (T-75, Corning, Corning, NY) at 37 °C and 5% CO_2. dHL-60 cells are prepared from HL-60 cells by adding 1.3% DMSO (Sigma-Aldrich, St. Louis, MO), and culturing for an additional 5-6 days. Before the experiments, the dHL-60 cells are washed in RPMI 1640 and L-glutamine medium, centrifuged at 2000 rpm for 5 minutes, and resuspended in medium.

PC3 (ATCC CRL-1435) is cultured in DMEM(1X) with 4.5 g/L D-glucose and L-Glutamine supplemented with 10% heat-inactivated fetal bovine serum (FBS) (Gibco, Carlsbad, CA) and 1%

Penicillin/Streptomycin (Sigma-Aldrich, St. Louis, MO). PC3 is incubated in 75 cm^2 culture flasks (T-75, Corning, Corning, NY) at 37 °C and 5% CO_2. To prepared starved PC3, the cell culture is detached from culture flask wall by adding Trypsin-EDTA, then resuspended in DMEM with no (FBS) in a round-bottomed glass FACS tube (Corning, Corning, NY), and incubated at 37 °C and 5% CO_2 for 4-24 hours.

3.2 Version 1: Design, Manufacture, and Operation

3.2.1 Conceptual Design Overview

Figure 3.1 provides an illustration of the device design. In Figure 3.1a, the device consists of a polydimethylsiloxane (PDMS) microchannel (middle) on top of a glass slide, with another PDMS layer (top) with inlet holes to both ends of the microchannel. Hydrogel prepolymer is dispensed from one end, and chemoattractant prepolymer is dispensed from the other. After waiting for 30 minutes for a gradient to form, the hydrogel is polymerised by exposure to ultra-violet (UV) light, which fixes the chemical gradient in place. The top layer is removed, and a second top layer is positioned on top of the middle layer, forming another microchannel on top of the polymerised hydrogel into which cell solution can be dispensed (Figure 3.1b). Cells that settle onto the top of the polymerised hydrogel detect the chemical gradient and respond by moving towards the concentration gradient.

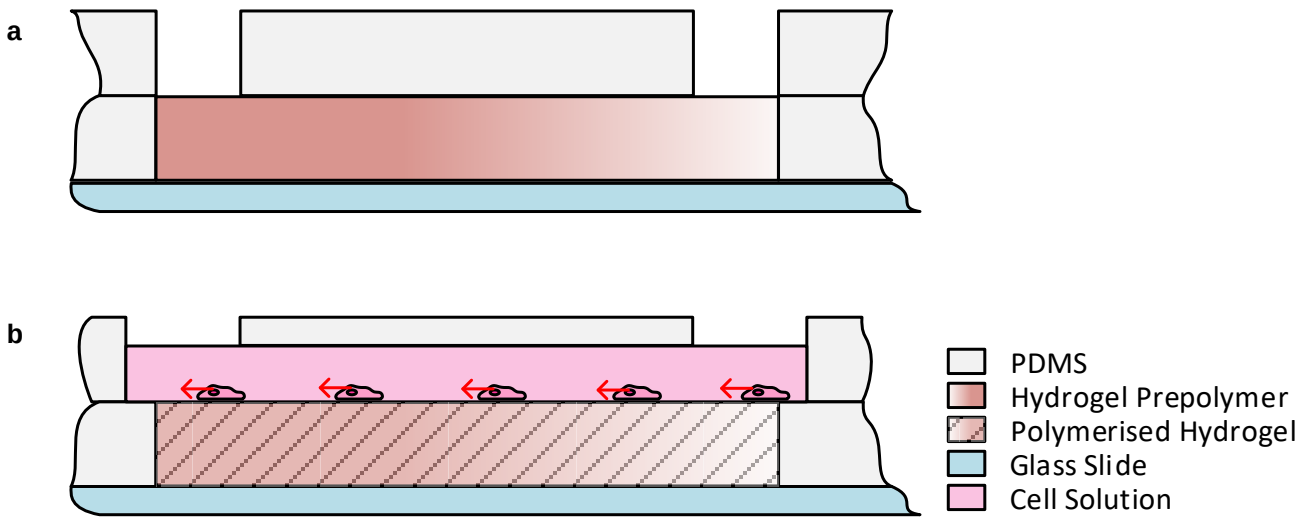

Figure 3.1 Chemotaxis assay Version 1, illustrating functional design. (a) Hydrogel prepolymer is dispensed from one end, and chemoattractant prepolymer from the other. 30 minutes is given for the gradient to form. The hydrogel is then polymerised, fixing the gradient in place. (b) The top layer from (a) is removed and a new top layer is placed, forming a microchannel on top of the polymerised hydrogel into which cells can be dispensed. Cells that settle on the surface of the polymerised hydrogel with stable gradient can detect the change in concentration and move towards the concentration gradient.

3.2.2 Manufacturing Methods

The device can be categorised into 3 distinct components: Layer 1, Layer 2, and Layer 3 (Figure 3.2). All three layers are made of a mixture of polydimethylsiloxane (PDMS) base with its hardener (Sylgard-184, Ellsworth Adhesives, Germantown, WI) in the ratio 15:1.

To manufacture Layer 1, 25 g of pre-cured PDMS is poured into a 150 mm diameter petri dish. This mixture is then degassed for 30 minutes, cured overnight at room temperature, then cured for an additional 1 hour at 65 °C, all on a flat surface. A .dxf file of the Layer 1 layout was created in SOLIDWORKS 2019 (Dassault Systèmes, Vélizy-Villacoublay, France), which is then imported

into a laser cutter (PLS4.75, Universal Laser Systems, Scottsdale, AZ). The cured PDMS sheet is laser-cut based on this layout. Laser-cutting results in charred PDMS debris fused to the cut edges, which is removed by soaking in 2-propanol (Sigma-Aldrich, St. Louis, MO), shaving off debris using a blade, then sonicating in a 2-propanol bath. The cleaned Layer 1 is finally bonded onto a 50 x 75 mm glass slide (Fisher Scientific, Hampton, NH) using oxygen plasma (Harrick Plasma, Ithaca, NY) for 60 seconds.

Molds for Layer 2 and Layer 3 are 3D printed from Protolabs (Maple Plain, MN) out of unfinished WaterShed XC 11122 material. Prior to use, the molds are surface-treated by detergent washing, sonicating in detergent water for 3 minutes, sonicating in 2-propanol for 3 minutes, and leaving at 65 °C for 48 hours. 4.5 g of the pre-cured mixture of PDMS is poured into both Layer 2 and Layer 3 molds. This mixture is then degassed for 30 minutes, cured overnight at room temperature, then cured for an additional 1 hour at 65 °C. The cured layers can then simply be removed from the mold and used.

3.2.3 Operation Protocol

Figure 3.3 illustrates the steps to prepare the device for the experiment, including gradient formation and cell dispensing. The gradient formation steps require the custom apparatus shown in Figure 3.4.

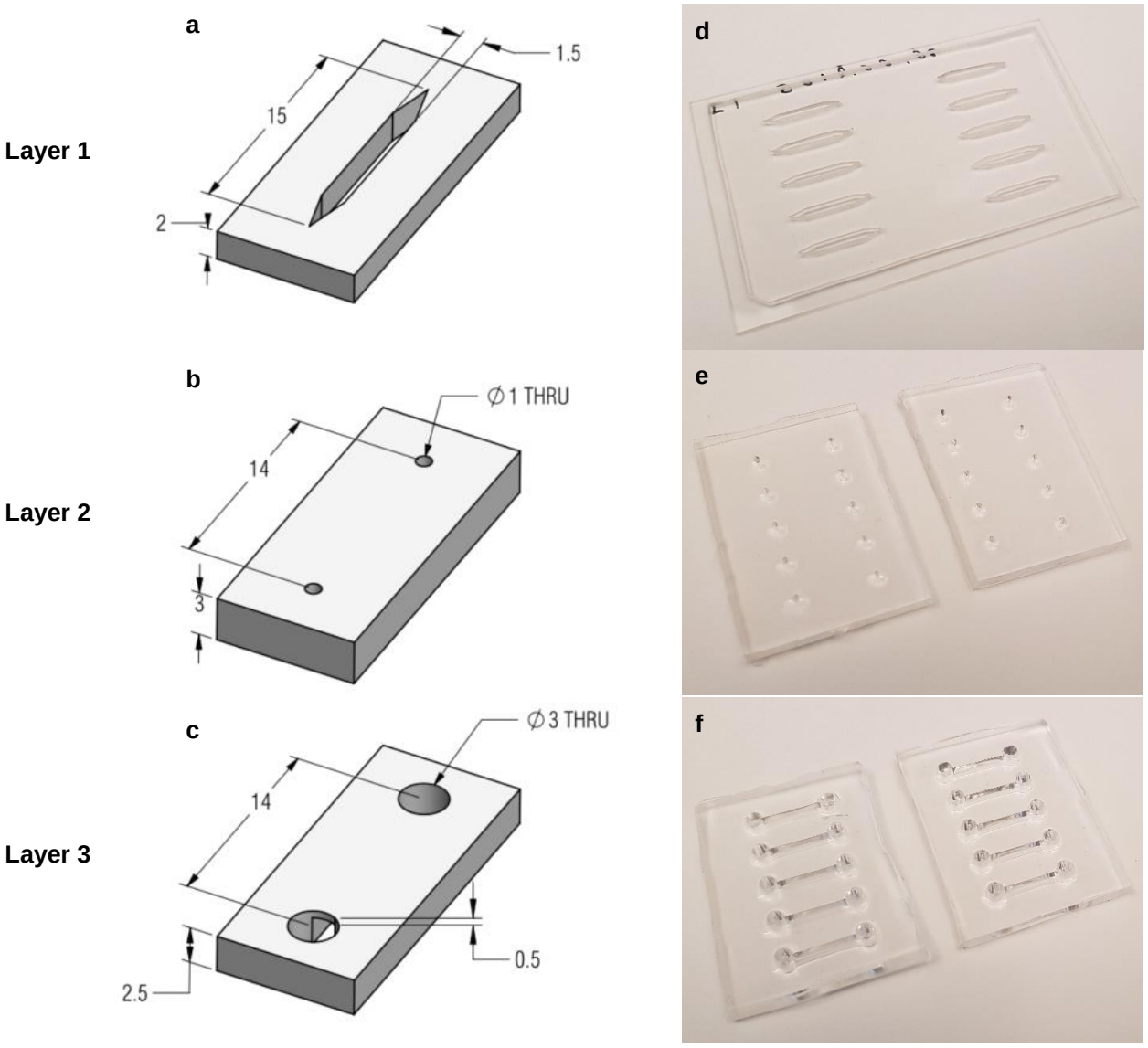

Figure 3.2 Layer 1, Layer 2, and Layer 3 of chemotaxis assay, Version 1. (a)-(c) CAD model of single channel (all dimensions in mm). (d)-(f) Physical devices

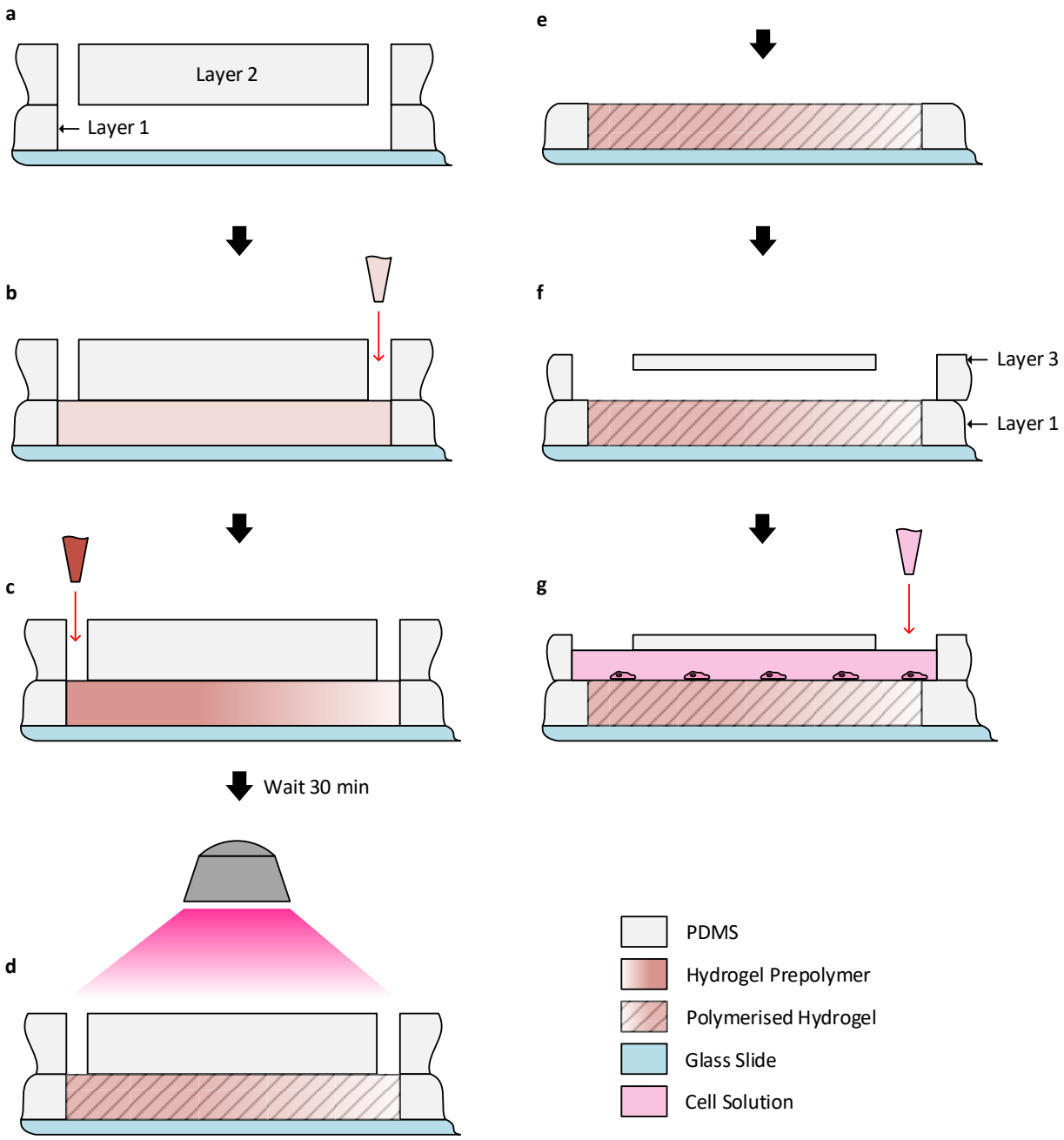

Figure 3.3 Steps to prepare device for experiment. (a) Layer 2 is sealed on Layer 1, removing any air pockets. (b) 50 μL of hydrogel prepolymer is dispensed. (c) 25 μL of chemoattractant prepolymer is dispensed on opposite end. Wait for 30 minutes for gradient to form. (d) PEGDA is polymerised by exposure to UV light for 5 seconds. (e) Layer 2 is removed. (f) Layer 3 is sealed on Layer 1. (g) 90 μL of cell solution is dispensed.

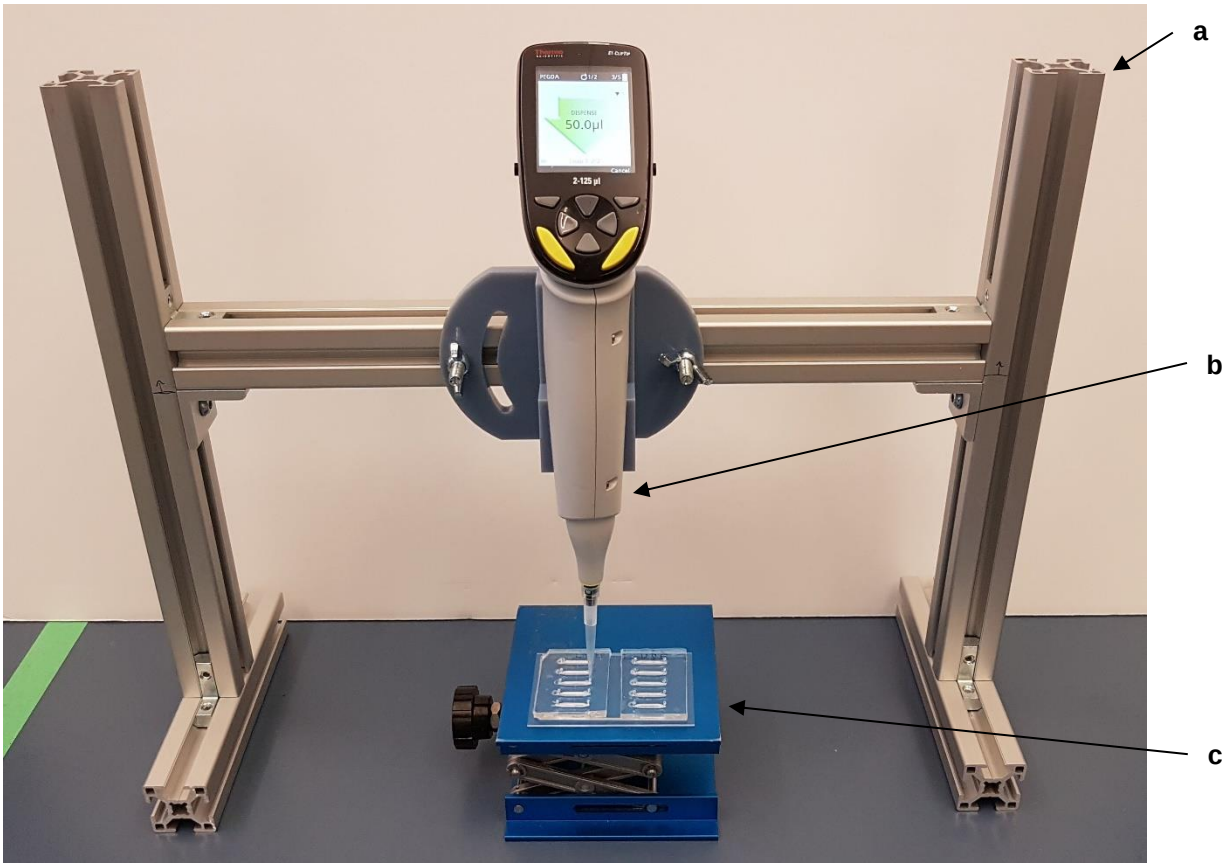

Figure 3.4 Custom apparatus for gradient formation. (a) Custom pipette stand. (b) E1-ClipTip electronic pipette. (c) Jack. This apparatus completely removes the user from the gradient formation process, vastly increasing gradient consistency.

3.2.3.1 Hydrogel Gradient Formation

This sub-section describes the operation protocol that must be executed in order to form a consistent gradient in the hydrogel. Layer 2 is sealed upon Layer 1 by manually compressing the layers together and removing any air pockets formed. The device is then placed on the jack. For each channel, 50 µL of hydrogel prepolymer is drawn into the electronic pipette (E1-ClipTip 4670020 BT, Thermo Fisher Scientific, Waltham, MA), and then placed on the custom pipette

stand. The jack is positioned so that the tip of pipette is inserted into one of the Layer 2 inlets, then 50 μL of hydrogel prepolymer is dispensed into the channel. Similarly, to dispense chemoattractant prepolymer, 25 μL of is drawn into the electronic pipette and placed on the custom stand. The jack is positioned so that the tip of pipette is inserted into the opposite Layer 2 inlet. 25 μL of chemoattractant prepolymer is then dispensed into the channel. For control channels, 25 μL of hydrogel prepolymer is dispensed instead of chemoattractant prepolymer.

Once all 10 channels of the device are filled, the setup covered for 30 minutes for the gradient to form. Then the device is exposed to ultra-violet light (λ = 395nm) for 10 seconds to polymerise the hydrogel in the channel.

3.2.3.2 Cell Sample Dispensing and Observation

Layer 2 is removed and Layer 3 is sealed upon Layer 1 by manually compressing the layers together and removing any air pockets formed. A manual pipette is used to thoroughly aspirate the cell solution. Then the manual pipette is used to dispense 90 μL of cell solution through any of the two Layer 3 inlets into the channel. The device is immediately transferred to a stage-top adapter, which is placed on the stage of a Nikon Eclipse Ti2 inverted microscope (Nikon, Tokyo, Japan). The cells are allowed to settle for 15 minutes before commencing with experiment. All experiments are conducted using the NIS-Elements Ar imaging software (Nikon, Tokyo, Japan), which is used to control the microscope and obtain data. Further details of experiments performed are provided in Chapter 5.

3.3 Version 2: Design, Manufacture, and Operation

3.3.1 Conceptual Design Overview

Figure 3.5 provides an illustration of the device design. In Figure 3.5a, the device consists of a 3D printed translucent epoxy resin microchannel bonded on top of a glass slide, and a PDMS Layer with extruded tab loosely position on top. Hydrogel prepolymer is dispensed through the inlet well on the left, followed by the chemoattractant prepolymer dispensed through the same location. After waiting for 30 minutes for the gradient to form, the hydrogel is polymerised by exposure to ultraviolet light, which fixes the gradient in place. The PDMS top layer is then removed, leaving a reservoir in the polymerised hydrogel which can accommodate cell solution (Figure 3.5b). As with Version 1, cells that settle onto the top of the polymerised hydrogel detect the chemical gradient and respond by moving towards the concentration gradient.

3.3.2 Manufacturing Methods

Version 2 consists of 2 components: 3D printed Layer 1 and PDMS Layer 2 (Figures 3.6 & 3.7). To manufacture Layer 1, a 3D CAD model of Layer 1 was developed in SOLIDWORKS 2019 (Dassault Systèmes, Vélizy-Villacoublay, France). The CAD model is exported in .stl format, which is then loaded onto a Form 2 SLA 3D printer (Formlabs, Somerville, MA). Clear Resin is used as the print material (FLGPCL04, Formlabs, Somerville, MA). Once the 3D print is complete, the part is removed, washed in 2-propanol (Sigma-Aldrich, St. Louis, MO), and left to dry at room temperature for 15 minutes. A clean 75 x 50 mm glass slide (Fisher Scientific, Hampton, NH) is taken and precured Clear Resin coated on the top. The 3D printed part is then positioned on top of the Clear Resin coated glass slide. Any trapped air bubbles must be removed by carefully pressing

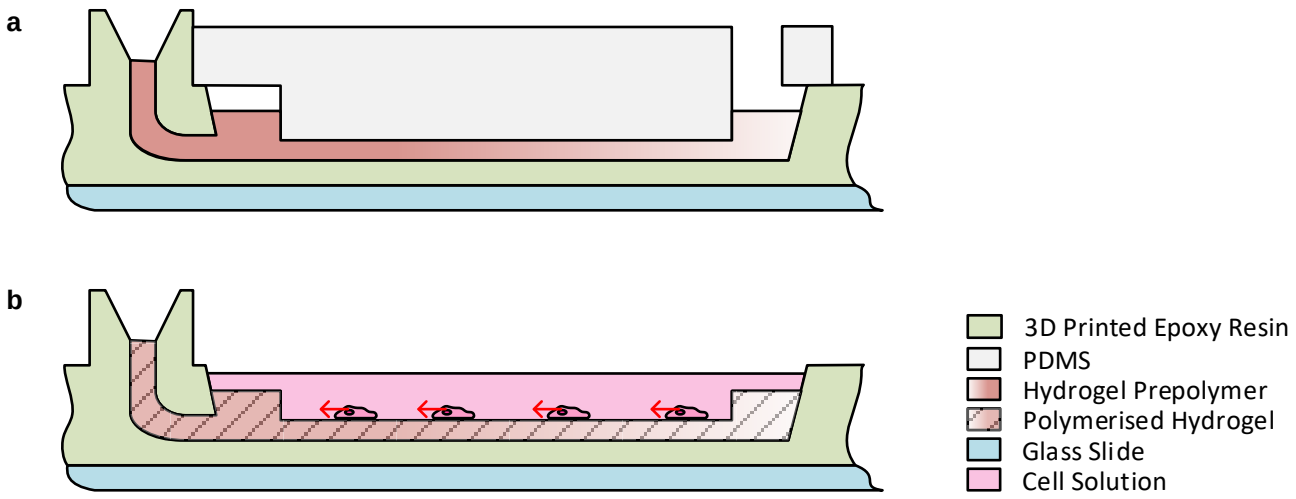

Figure 3.5 Chemotaxis assay Version 2, illustrating functional design. (a) Hydrogel prepolymer is dispensed through the inlet well on the left, followed by chemoattractant prepolymer dispensed through the same location. 30 minutes is given for the gradient to form. The hydrogel is then polymerised, fixing the gradient in place. (b) The top PDMS Layer is removed, leaving a reservoir that can accommodate the cell solution. Cells that settle on the surface of the polymerised hydrogel with stable gradient can detect the change in concentration and move towards the concentration gradient.

the 3D printed part against the glass slide. Next, a manual pipette is used to coat the bottom floor of the microchannels with a thin layer of Clear Resin. The viscous precured Clear Resin fills the surface imperfections that form on the 3D print surface, forming a transparent continuous optical medium between the bottom of the glass slide and the bottom of the Layer 1 channel. This allows cells at bottom of channel to be clearly visible through a microscope. Lastly, Layer 1 is put into the Form Cure (Formlabs, Somerville, MA) ultra-violet curing chamber for 20 minutes and no heat.

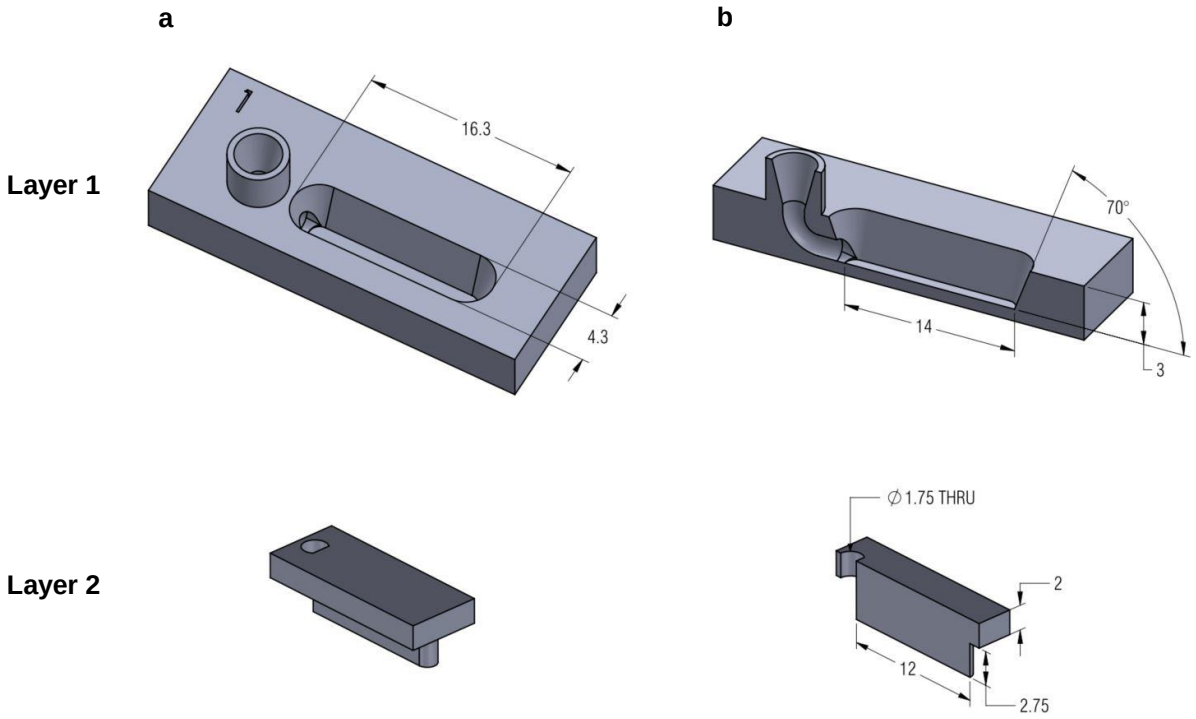

Figure 3.6 Layer 1 and Layer 2 of Version 2. All dimensions in mm. (a) CAD model of single channel for Layer 1 and Layer 2. (b) Section view through midplane showing internal features.

The mold for Layer 2 was fabricated using an Objet 30 Pro FDM 3D printer (Stratasys, Eden Prairie, MN), using VeroWhite material (Stratasys, Eden Prairie, MN). Prior to use, the mold is surface treated by detergent washing, sonicating in detergent water for 3 minutes, sonicating in 2-propanol for 3 minutes, then leaving at 65 °C for 48 hours. Precured PDMS mixture is prepared by mixing polydimethylsiloxane (PDMS) base with its hardener (Sylgard-184, Ellsworth Adhesives, Germantown, WI) in the ratio 15:1. 4.0 g of the pre-cured mixture is poured into the Layer 2 mold. This mixture is then degassed for 30 minutes, cured overnight at room temperature, then cured for an additional 1 hour at 65 °C. The cured Layer 2s can then simply be removed from the mold and used.

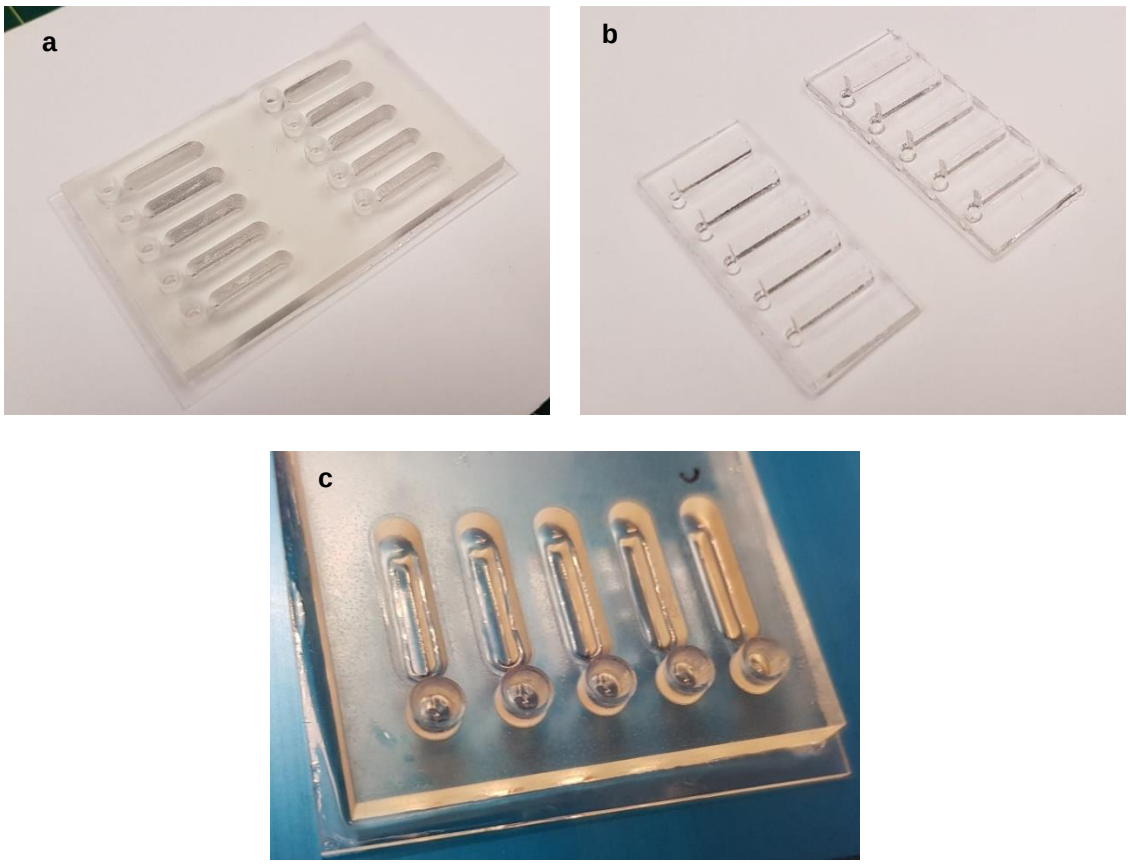

Figure 3.7 Physical Version 2 devices. (a) Layer 1 is 3D printed out of Clear Resin (FLGPCL04, Formlabs, Somerville, MA). (b) Layer 2 is made of PDMS. (c) Polymerised hydrogel with reservoir feature.

3.3.3 Operation Protocol

Figure 3.8 illustrates the steps to prepare the device for the experiment, including gradient formation and cell dispensing. The same custom apparatus shown in Figure 3.4 must also be used for Version 2.

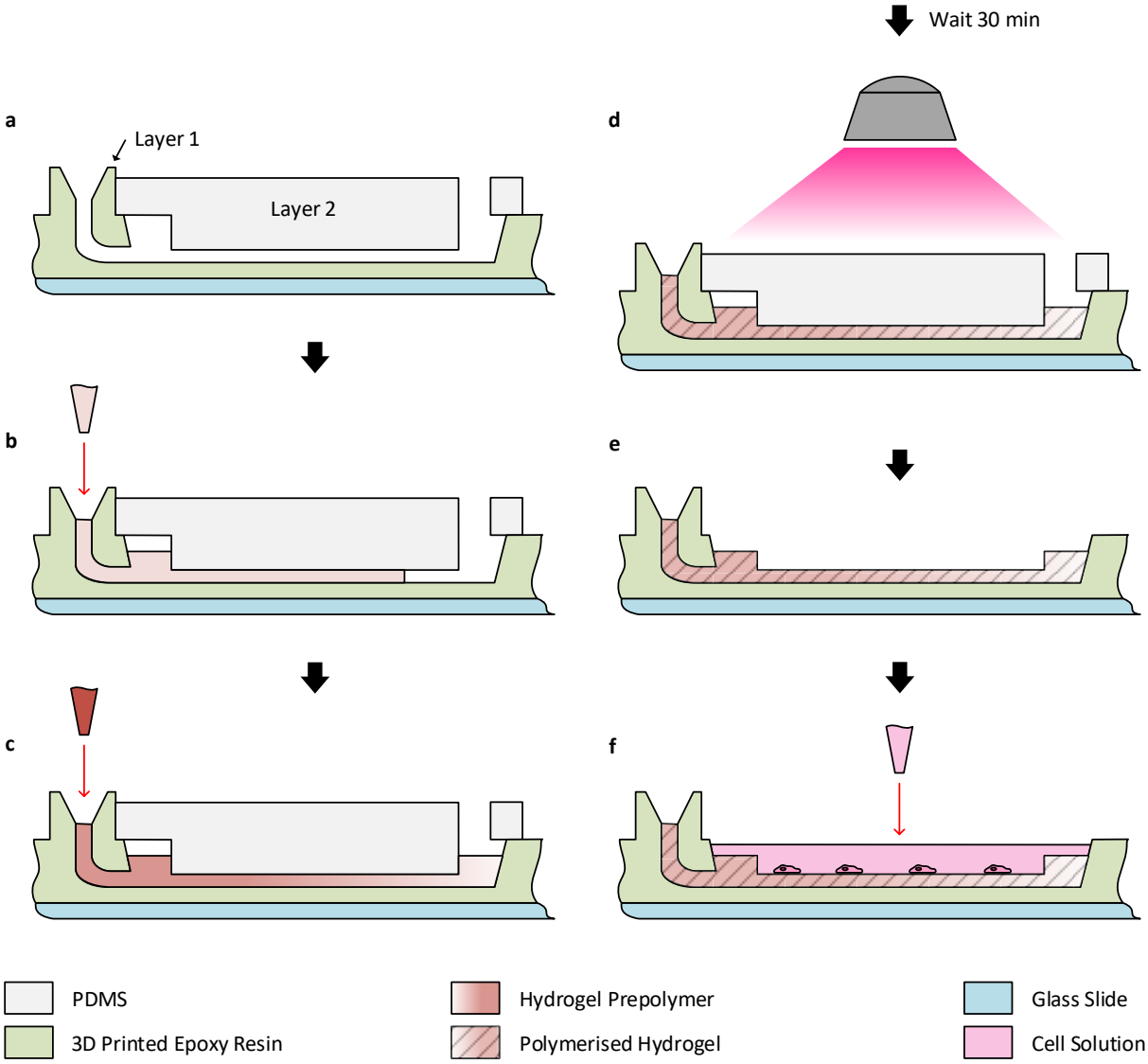

Figure 3.8 Steps to prepare Version 2 for experiment. (a) Layer 2 is positioned on Layer 1 (no sealing required). (b) 25 µL of hydrogel prepolymer is dispensed above the inlet well. (c) 20 µL of chemoattractant prepolymer is also dispensed above the inlet well. Wait for 30 minutes for gradient to form. (d) Hydrogel is polymerised by exposing to UV light for 10 seconds. (e) Layer 2 is removed. (f) 60 µL of cell solution is dispensed directly onto polymerised hydrogel reservoir.

3.3.3.1 Hydrogel Gradient Formation

This sub-section describes the operation protocol that must be executed in order to form a consistent gradient in the hydrogel. Layer 2 is positioned upon Layer 1, taking care that the Layer 2 tab is centered with respect to Layer 1. The device is then placed on the jack. For each channel, 25 μL of hydrogel prepolymer is drawn into the electronic pipette, and then placed on the custom pipette stand. Using the jack, the device is positioned so that the tip of the pipette is 1-2 mm above the inlet well. After positioning for the first channel, the jack height does not need to be adjusted for the remaining channels. Once in position, 25 μL of hydrogel prepolymer is dispensed into the channel through the inlet well. Similarly, to dispense chemoattractant prepolymer, 20 μL is drawn into the electronic pipette and then placed on the custom stand. Using the jack, the device is positioned so that the pipette tip is at the same position, 1-2 mm above the inlet well. 20 μL of chemoattractant prepolymer is then dispensed into the device. For control channels, 20 μL of hydrogel prepolymer is dispensed instead of chemoattractant prepolymer.

Once all 10 channels of the device are filled, the setup covered for 30 minutes for the gradient to form. Then the device is exposed to ultra-violet light (λ = 395nm) for 10 seconds to polymerise the hydrogel in the channel.

3.3.3.2 Cell Dispensing

Layer 2 is removed. A manual pipette is used to thoroughly aspirate the cell solution. Then the manual pipette is used to dispense 60 μL of cell solution directly into the hydrogel reservoir. The device is immediately transferred to a stage-top adapter, which is placed on the stage of a Nikon

Eclipse Ti2 inverted microscope (Nikon, Tokyo, Japan). The cells are allowed to settle for 15 minutes before commencing with experiment. All experiments are conducted using the NIS-Elements Ar imaging software (Nikon, Tokyo, Japan), which is used to control the microscope and obtain data. Further details of experiments performed are provided in Chapter 5.

3.4 Advantages of Version 2 over Version 1

The advantages of Version 2 over Version 1 are as follows:

1. Hydrogel dispensing is contactless. Prior the dispensing in the first microchannel, the pipette tip is positioned 1-2 mm above the inlet. Droplets from the pipette fill the microchannel through a combination of gravity and capillary action. Once the jack height is set for the first microchannel, it does not need to be changed for the remaining microchannels.
2. No seal between Layer 1 and Layer 2 required. 25 μL of hydrogel prepolymer and 20 μL of chemoattractant prepolymer is used with this system. This volume fills the bottom half of the channel without overflowing. Therefore, there is no risk of leaking.
3. No Layer 3 required. 60 μL of cell solution is directly dispensed into the polymerised hydrogel reservoir.

Overall, Version 2 requires fewer steps and less pipette positioning accuracy compared to Version 1. Thus, Version 2 faster to prepare and easier to operate.

Chapter 4: Gradient Modelling

This chapter provides details on the work done to simulate gradient formation in hydrogel prepolymer and chemoattractant effusion from the polymerised hydrogel. Since rhodamine B was used to experimentally validate the gradient (discussed in Section 5.2 in Chapter 5), the diffusion of rhodamine B in PEGDA hydrogel is simulated.

Section 4.1 provides some background on the modelling method. Section 4.2 describes the work done to simulate the gradient formation in the hydrogel prepolymer and discusses the results. Section 4.3 describes the work done to simulate the effusion of rhodamine B from polymerised hydrogel and discusses the results.

4.1 Methods

COMSOL Multiphysics® 5.4 (COMSOL AB, Stockholm, Sweden) was used to perform all simulations. SOLIDWORKS 2019 (Dassault Systèmes, Vélizy-Villacoublay, France) was used to model all geometries, and COMSOL's built-in LiveLink™ for SOLIDWORKS (COMSOL AB, Stockholm, Sweden) was used to import the geometry into COMSOL. The Transport of Diluted Species is a built-in physics mechanism in COMSOL that was used to model the concentration distribution of rhodamine B as it diffused over time.

4.1.1 Overview of Transport of Diluted Species physics

The Transport of Diluted Species uses Fick's Laws of Diffusion to simulate the diffusion of a species in a fluid. Fick's First and Second Laws of Diffusion are provided in mathematical form in Equations 4.1 and 4.2 respectively [41]:

$$N_i = -D_i \nabla c_i \tag{4.1}$$

$$\frac{\partial c_i}{\partial t} = D_i \nabla^2 c_i \tag{4.2}$$

where for species ***i***, N_i is the molar flux (mol/m^{2}s), D_i is the diffusion constant (m^2/s), c_i in the concentration (mol/m^3), and ***t*** is time (s) [42].

COMSOL's Transport of Diluted Species numerically solves the above equations to determine how the concentration within the provided geometry varies over time due to diffusion. Two input parameters need to be provided: (i) initial concentration c_0 (mol/m^3), and (ii) diffusion constant of the species in the fluid ***D*** (m^2/s).

4.2 Gradient formation in hydrogel prepolymer

For the simulation of hydrogel prepolymer gradient formation, the initial concentration is simply the concentration of chemoattractant dispensed into the device (100 nM, Section 3.1.1 in Chapter 3). The diffusion constant of rhodamine B in 50% PEGDA prepolymer is not documented, and so needed to be determined experimentally.

4.2.1 FRAP experiment to determine diffusion constant in hydrogel prepolymer

Fluorescence recovery after photo-bleaching (FRAP) is an experimental technique that can be used to determine the diffusion constant of a species. In a FRAP experiment, the certain region of a fluorescently labelled sample is irreversibly bleached by exposure to a short intense light pulse.

The bleached region slowly recovers as fluorescent species from the surrounding region diffuse into the bleached area [43].

An Olympus FV1000 Laser Scanning Confocal Microscope (Olympus Corporation, Tokyo, Japan) was used to conduct the FRAP experiment. Figure 4.1 shows the results of the FRAP experiment of 10 μM rhodamine B in PEGDA hydrogel prepolymer. Fiji image processing software [44] was used to generate averaged intensity plots along the horizontal axis of the bleached region. As can be seen, the intensity plot forms a Gaussian distribution that gradually flattens over time.

The method outlined by Seiffert & Oppermann was used to evaluate the diffusion constant from FRAP data [43]. Based on the equation for Fick's second law (Equation 4.2 above), Seiffert & Oppermann derived the following equation:

$$w^2 = 2Dt \tag{4.3}$$

where $\boldsymbol{w}$ is the full width at half the maximum of the intensity plot Gaussian function, $\boldsymbol{D}$ is the diffusion constant (m^2/s), and $\boldsymbol{t}$ is time (s) [43].

From the FRAP data in Figure 4.1, three values of $\boldsymbol{w}$ and $\boldsymbol{t}$ were obtained, which were plotted in Microsoft Excel (Figure 4.2). As can be seen, a clear linear trendline can be drawn through the data points. By dividing the trendline gradient by 2, the diffusion constant was determined to be 4.7979×10^{-11} m^2/s. As expected, this diffusion constant is lower than that in water (4.2×10^{-10} m^2/s [45]), since hydrogel prepolymer is more viscous than water.

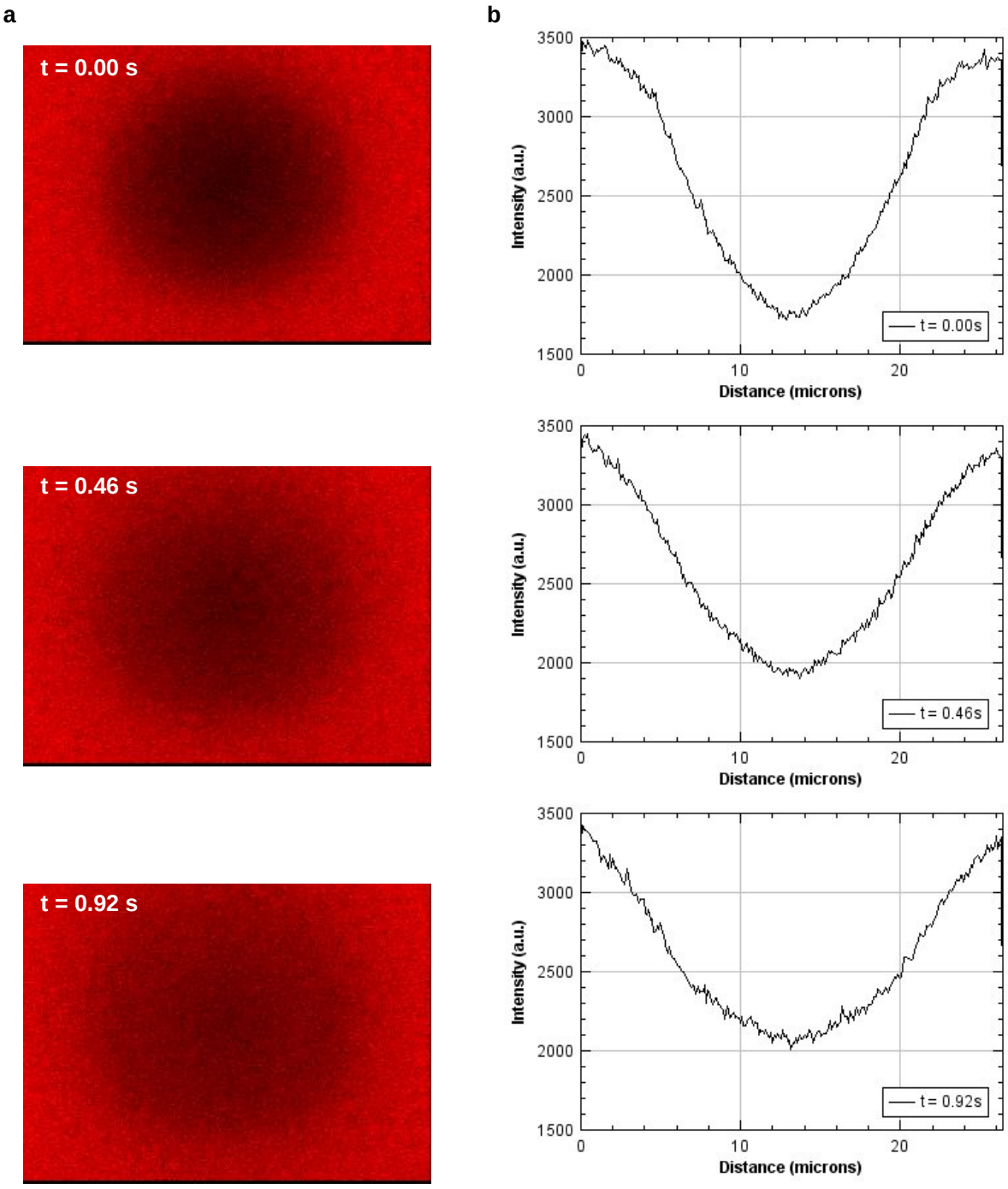

Figure 4.1 Results of FRAP experiment, showing recording of bleached region and its recovery over 3 time frames. (a) Recorded images from FRAP experiment. (b) Corresponding averaged intensity plots obtained from Fiji [44]. The intensity plots form a Gaussian distribution, which were used to determine the diffusion constant.

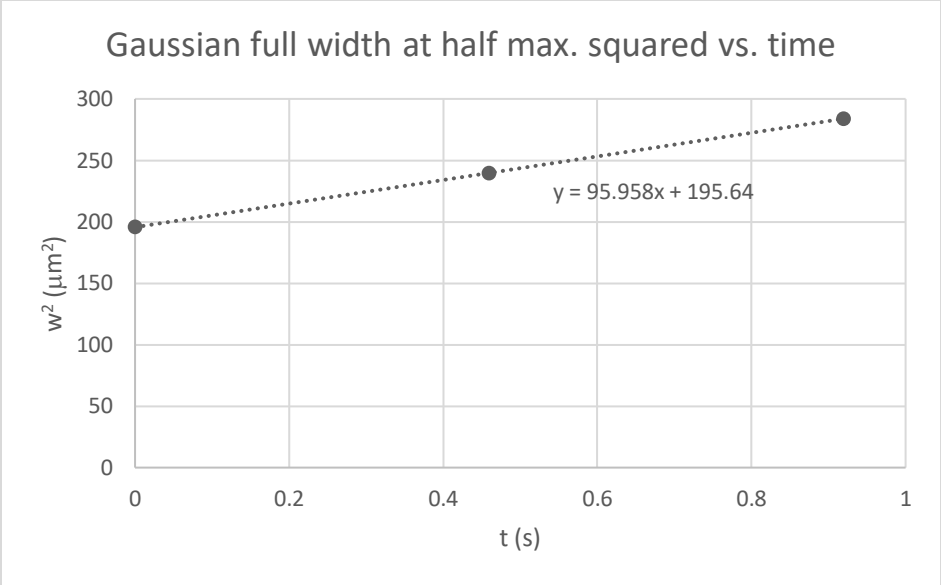

Figure 4.2 Plot of full width at half maximum squared vs. time, obtained from the intensity plots in Figure 4.1. A clear linear trendline can be drawn through the data points. The diffusion constant is the trendline gradient divided by 2.

4.2.2 Setup of hydrogel prepolymer gradient simulation

For the hydrogel prepolymer gradient simulation, the following simplified assumption is made: at the initial state, half of the channel is filled with prepolymer with rhodamine B, and the other half is filled with prepolymer with no rhodamine B.

The geometry of this simulation was setup based on Version 2 dimensions. Based on the above assumption, the geometry was divided along the mid-plane into 2 domains. 1 domain was assigned an initial concentration of 100 nM; the other 0 nM (Figure 4.3). The simulation run time was set at 3600 seconds (1 hour).

4.2.3 Results of hydrogel prepolymer gradient simulation

Figure 4.3 shows the 3D views of the concentration distribution at 0 minutes and 60 minutes. Figure 4.4 shows the concentration distribution of the top surface every 15 minutes over 1 hour. At 0 minutes, there is sharp boundary between the rhodamine B prepolymer and hydrogel prepolymer. Over time, the gradient becomes less steep. This is the expected result if only diffusion is occurring between the prepolymers.

Figure 5.4 (Section 5.2.2, Chapter 5) shows the experimental result of formation of gradient in hydrogel prepolymer. On comparing Figure 5.4 with Figure 4.4, it can be seen that the gradient formation process is completely different. Figure 5.4 shows that in reality, the gradient is formed by internal flow generated by a combination of sources, which dominate over any diffusion effects.

4.3 Simulation of chemoattractant effusion from polymerised hydrogel

The goal of this simulation is to validate that the gradient profile generated in the hydrogel applies to the cell sample. dHL60 cells are typically around 10 μm in diameter, so we wish to know whether there is a gradient in the cell solution 5-10 μm above the hydrogel top surface.

To accurately replicate the device operation conditions, the input parameters, initial concentration and diffusion constant of rhodamine B in polymerised hydrogel, need to be accurately defined. Sub-Sections 4.3.1 and 4.3.2 provides details on how these input parameters were determined. Section 4.3.3 describes the simulation setup and discusses the results.

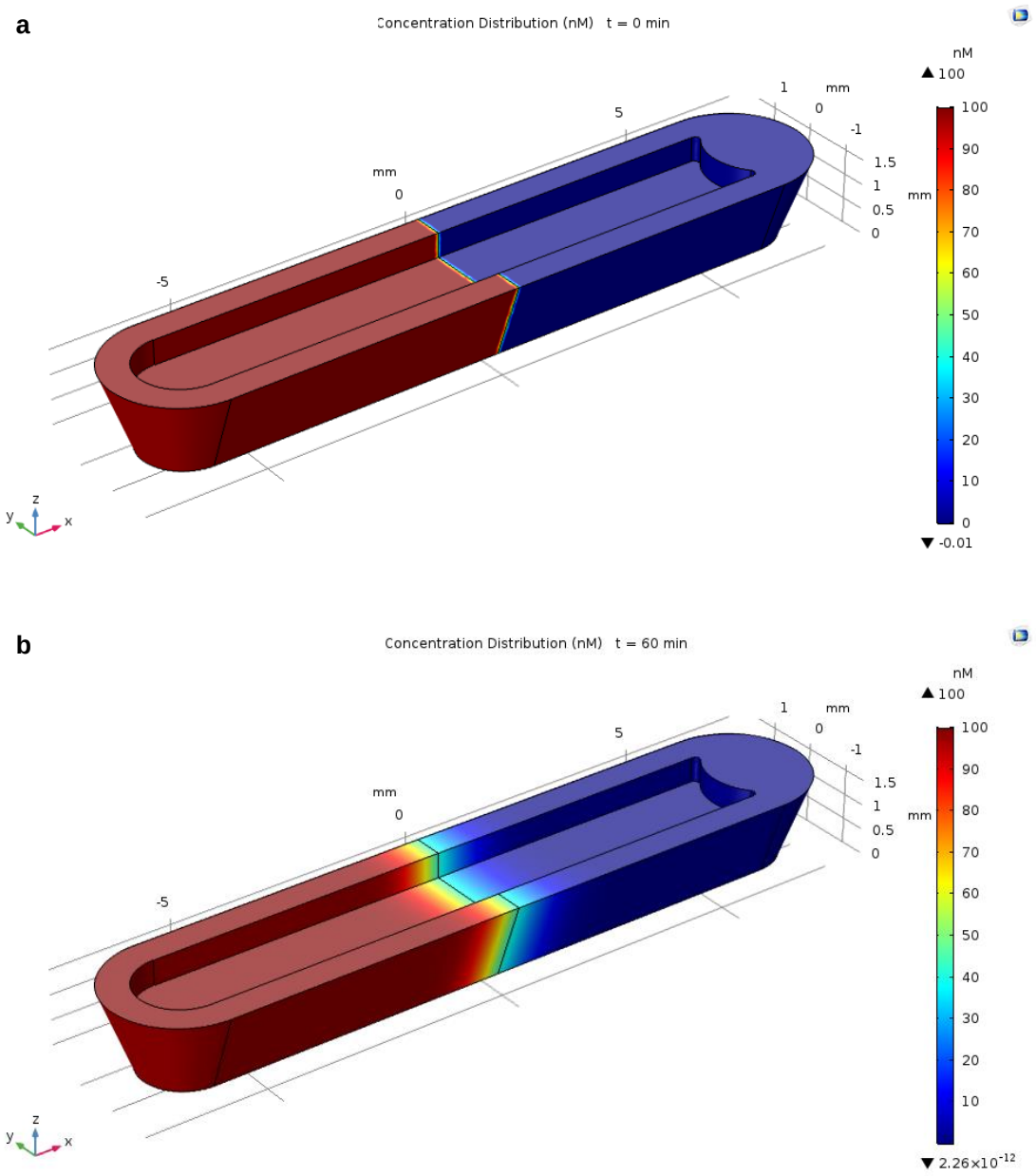

Figure 4.3 3D representation of gradient formation of hydrogel prepolymer simulation. (a) Concentration distribution at t = 0 min. (b) Concentration distribution at t = 60 min. For initial conditions, it is assumed that hydrogel prepolymer and rhodamine B prepolymer are equally divided along the microchannel midplane.

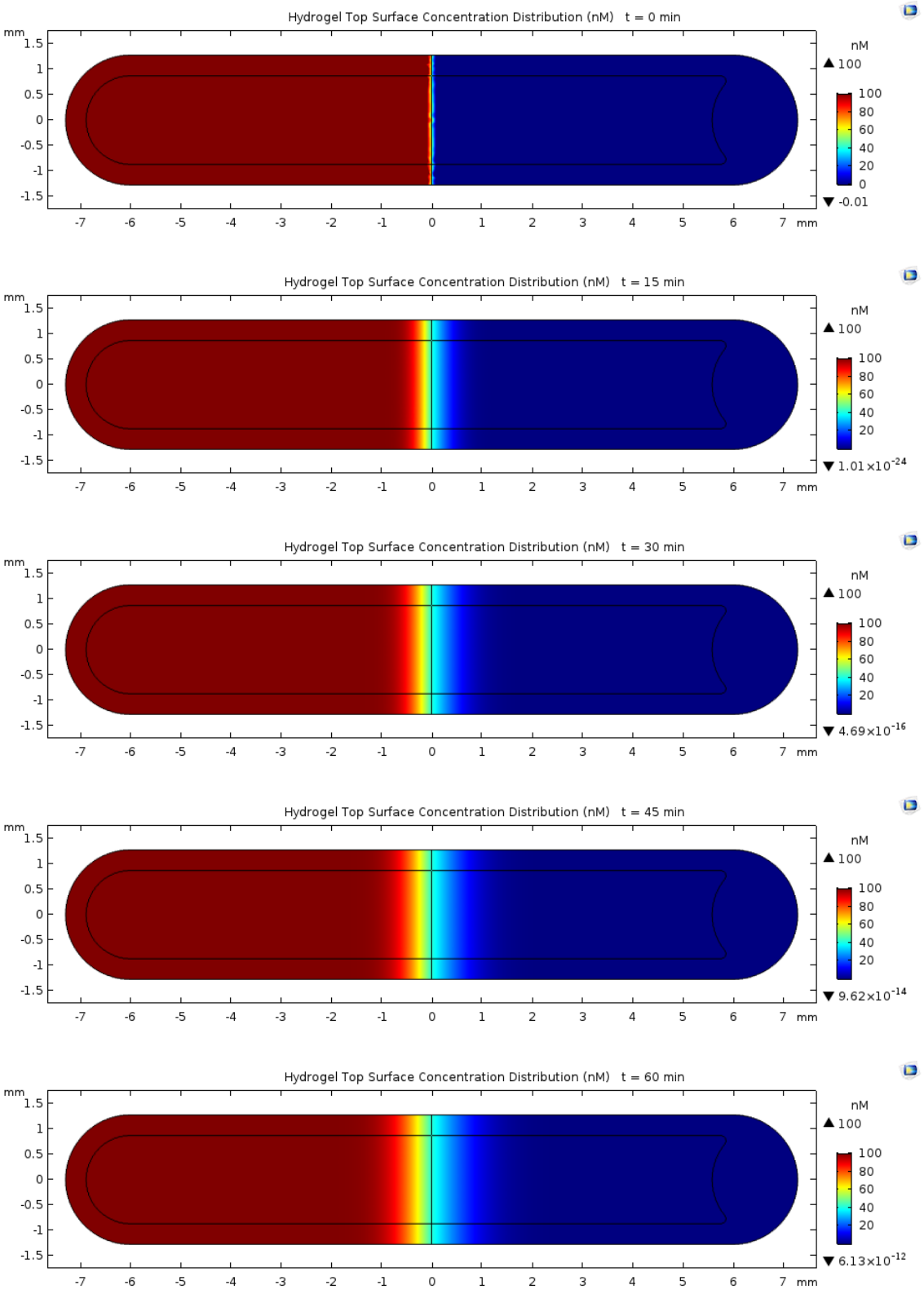

Figure 4.4 Simulation of gradient change in hydrogel prepolymer on top surface over 1 hour.

4.3.1 Determining initial concentration distribution from experimental data

Since there is no correlation between the simulation results of Section 4.2.2 and the experimental results of Section 5.2.2, it was decided to determine the initial concentration values based on the experimental data. In Section 5.2.2, it was determined that 30 minutes is a suitable wait time for the gradient to form. Therefore, an averaged intensity plot was generated from the gradient image at 30 minutes using Fiji image processing software [44].

The highest intensity region in the left part of Figure 4.5a is the inlet region of the device. It is assumed that the concentration of rhodamine B in that region is 100 nM. In this way, a calibration factor between intensity and concentration was derived, from which the intensity data was converted to concentration.

The intensity plot data was exported to Microsoft Excel, and converted into units of concentration (nM), and then the concentration profile was plotted (Figure 4.5b). From 0-10 mm, it can be seen that the concentration profile gradient linear; after 10 mm the concentration profile flattens out at a near-zero value. Therefore a linear trendline was generated for the 0-10 mm region only.

The trendline equation in Figure 4.5b was used in COMSOL to define the initial concentration distribution in the polymerised hydrogel up to 10 mm. Beyond 10 mm, the initial concentration was set to 0 nM. Figure 4.5c shows the concentration distribution at 0 minutes. It can be seen that the COMSOL gradient profile (Figure 4.5c) is reasonably close to the experimental data (Figure 4.5a).

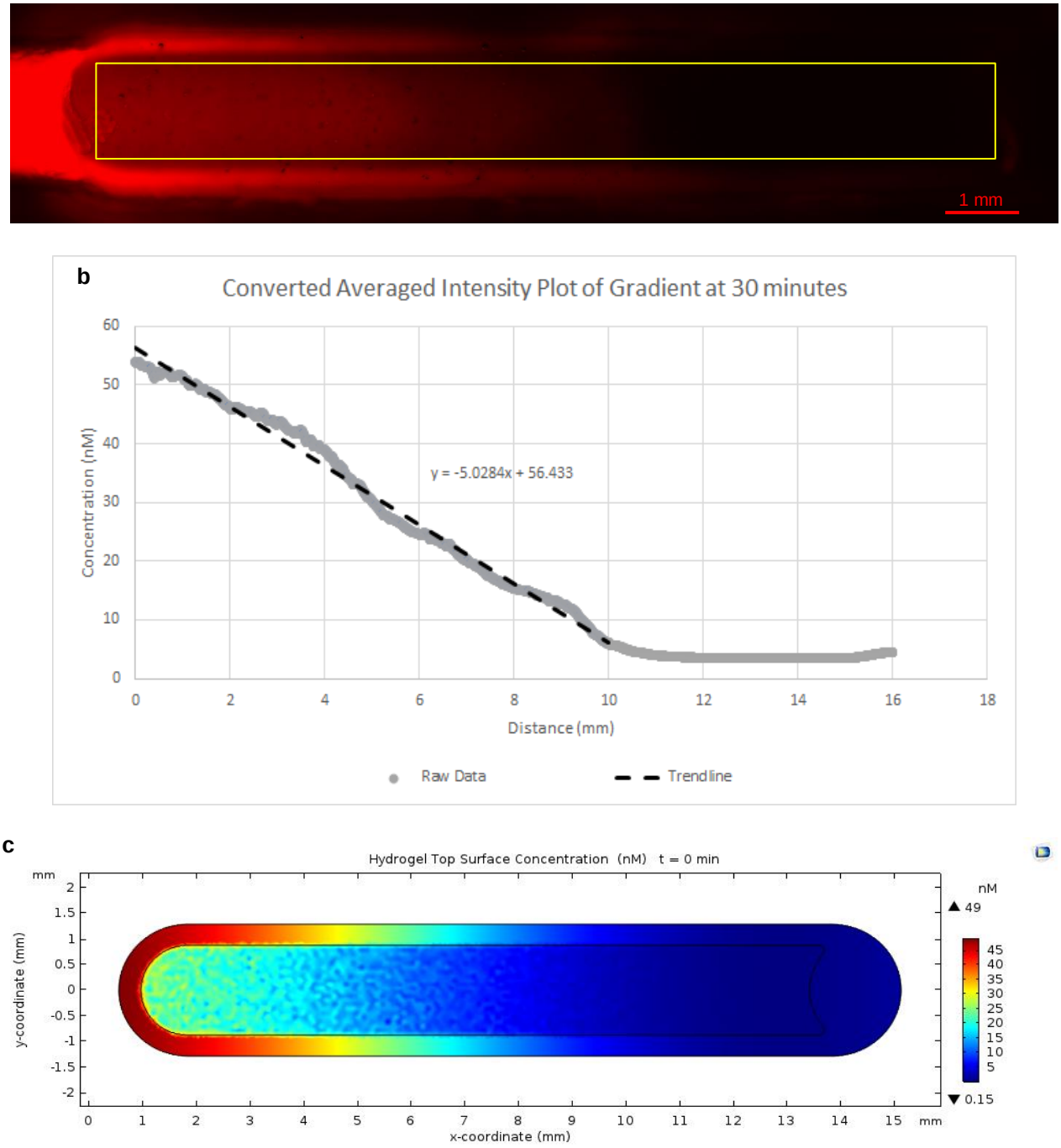

Figure 4.5 Gradient data from prepolymer gradient formation experiment. (a) Image of gradient from experiment at 30 minutes. Yellow rectangle indicates area over which averaged intensity plot was generated. (b) Corresponding averaged intensity plot with units converted to generate a trendline equation that could be directly used in COMSOL. (c) Concentration distribution in COMSOL at top surface of hydrogel based on trendline equation. The COMSOL gradient profile reasonably matches that of the experiment.

4.3.2 Determining diffusion constant of rhodamine B in polymerised hydrogel

The diffusion constant of rhodamine B in polymerised hydrogel was determined through a combination of an experiment and a COMSOL simulation of that experiment. The goal of the experiment was to immerse a sample of polymerised hydrogel containing rhodamine B in a liquid and measure the change in concentration of rhodamine B in the liquid over time as rhodamine B effused into the liquid. The simulation would be setup to replicate the experiment, and be repeated with different diffusion constants, until a diffusion constant was determined for which the simulation results most closely matched the experiment results. Hence the diffusion constant of rhodamine B in polymerised hydrogel would be determined.

4.3.2.1 Experiment: Concentration change in PBS due to Rhodamine B Effusion

75 μL of 10 μM rhodamine B prepolymer was dispensed into a Version 1 (PDMS) device and UV polymerised. The polymerised hydrogel was removed from the device and immersed into a 6-well plate well containing 5 mL of phosphate buffered saline (PBS). 100 μL of the fluid was sampled from the 6-well plate well every 5 minutes for 25 minutes, and dispensed into a 96-well plate well. In addition, 100 μL samples of known concentrations of rhodamine B in PBS, ranging from 0.1 M to 1 nM, were arrayed into the same 96 well plate.

The fluorescent intensity of rhodamine B in each of the 96 well plates were recorded using a SpectraMax Gemini EM spectrofluorometer (Molecular Devices LLC, San Jose, CA). The intensity data from the wells with known concentrations of rhodamine B was used to generate a calibration curve from which the concentration of rhodamine B in the PBS samples was determined.

4.3.2.2 Simulation: Concentration change in PBS due to Rhodamine B Effusion

A simulation was set up replicating the experiment described in Sub-Section 4.3.2.1 (Figure 4.6). This simulation was run with an initial guessed diffusion constant. Once the simulation completed, the volume averaged concentration of rhodamine B in the PBS domain was evaluated at 0, 5, 10, 15, 20, and 25 minutes. This result was compared with experimental results. This process was repeated multiple times with different diffusion constants until one was determined that produced results that was linear and reasonably matched the experimental results.

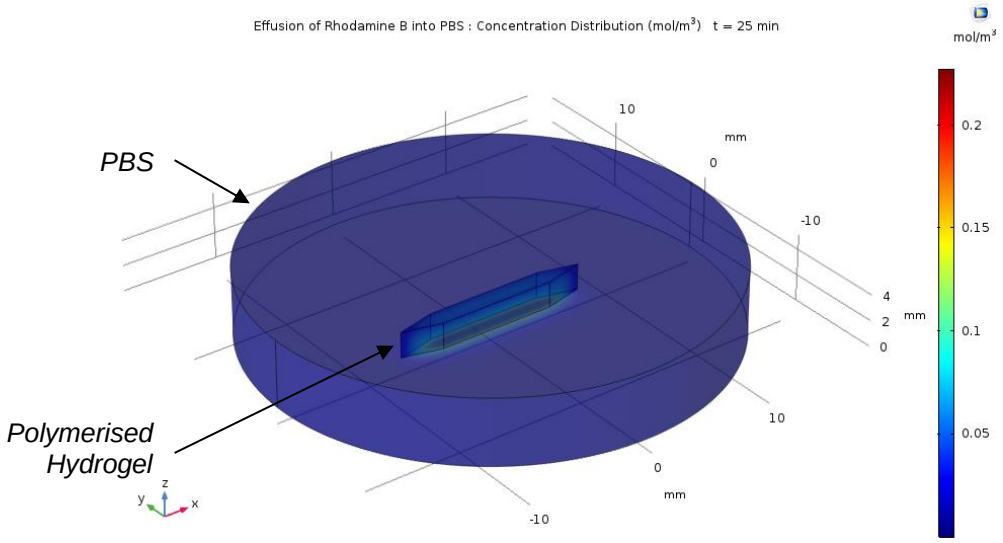

Figure 4.6 Simulation geometry replicating effusion of rhodamine B from polymerized hydrogel into a 6-well plate containing 5 mL of PBS.

4.3.3 Setup of rhodamine B effusion from polymerised hydrogel simulation

This simulation contains 3 domains (Figure 4.8). 2 are of the polymerised hydrogel, split at the x = 10 mm plane. The initial concentration in the domain of polymerised hydrogel where x < 10 mm

was defined by the trendline equation generated in Figure 4.5b. The initial concentration in the domain of polymerised hydrogel where x > 10 mm was set to 0 nM. The 3rd domain is the cell solution, in which the initial concentration was also set to 10 nM. The diffusion constant of cell solution is assumed to be the same as water, which is 4.2×10^{-10} m^2/s [45]. The simulation run time was set at 3600 s (1 hour).

4.3.4 Results of rhodamine B effusion from polymerised hydrogel simulation

The objective of this simulation was to confirm that the chemical gradient generated in the hydrogel also existed in the vicinity of the cells that were on top of the hydrogel. Since dHL60 cells are about 10 μm diameter, our interest is primarily in the concentration profile 5 μm above the top surface of the hydrogel.

Figure 4.7 shows 3D representation of the results at 0 and 60 minutes. Figure 4.8a shows the concentration profiles at 30 minutes, 1 μm, 5 μm, and 10 μm above the surface of the hydrogel. It can be seen that there is negligible difference in concentration profile at the 3 locations. This was typical a 0, 15, 45, and 60 seconds (not shown), and therefore all subsequent results were obtained at 5 μm only.

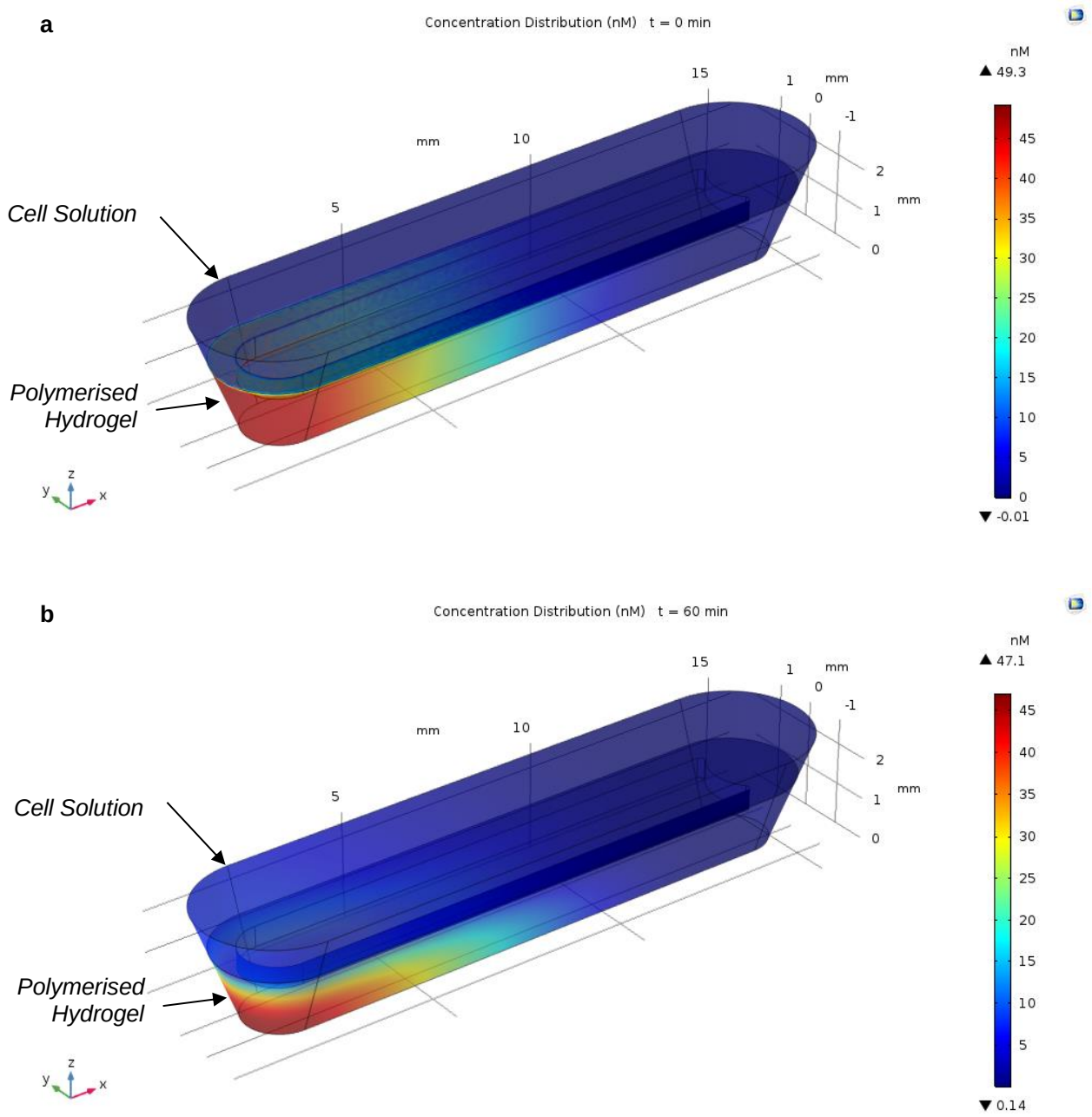

Figure 4.7 3D representation of rhodamine B effusion from polymerized hydrogel at: (a) t = 0 min and (b) t = 60 min.

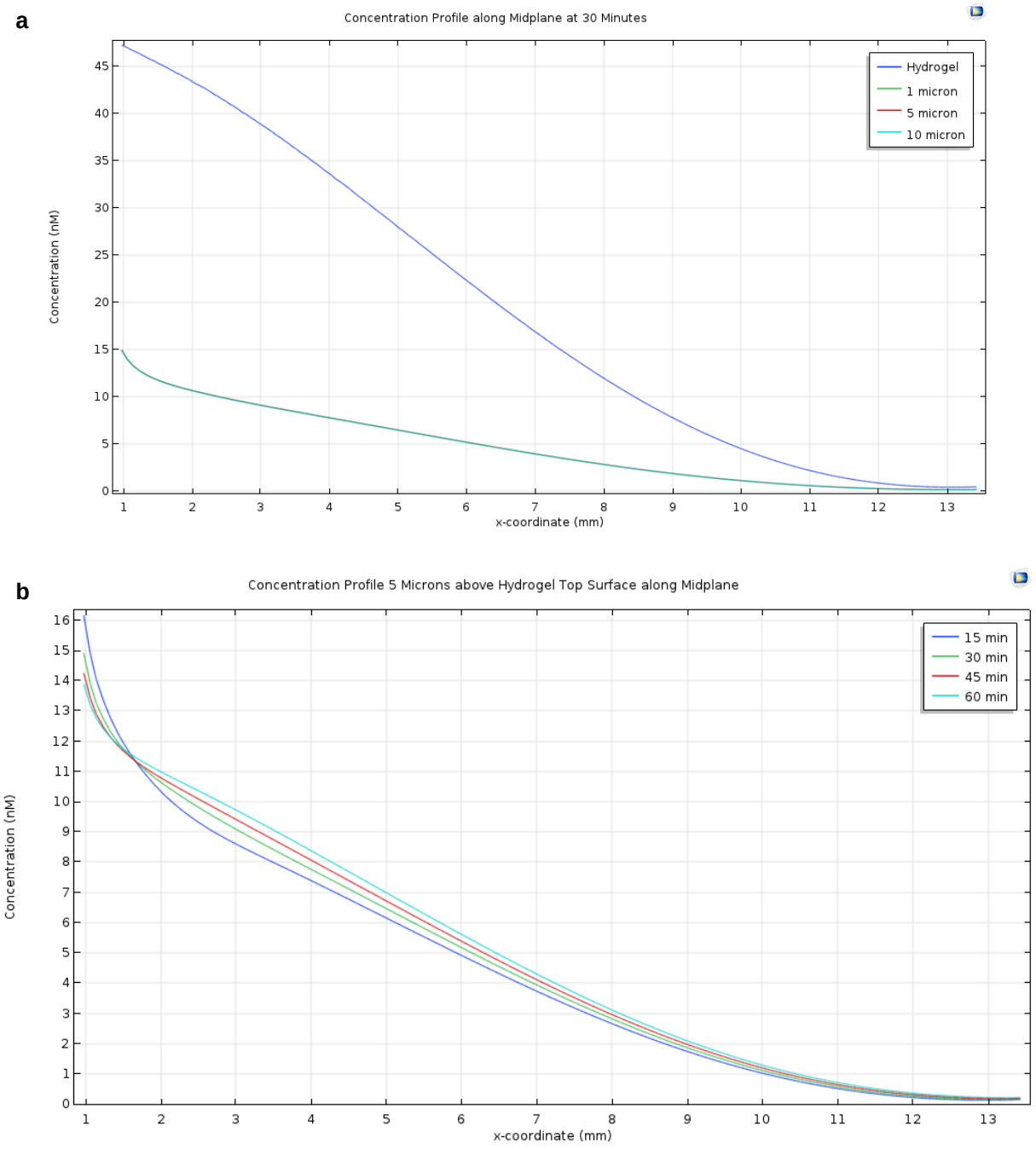

Figure 4.8 Concentration profiles along midplane of channel. (a) At 30 minutes, in hydrogel and 1 μm, 5 μm, and 10 μm above the hydrogel top surface. There is no appreciable change in concentration profile at 1 μm, 5 μm, and 10 μm above the hydrogel top surface, but the concentration profile in the hydrogel is higher with steeper gradient. (b) 5 μm above hydrogel top surface, at 15, 30, 45, & 60 minutes. A persisting linear gradient of ~1.2 nM/mm exists between 1.5-10.0 mm along microchannel length, within the cell vicinity.

Figure 4.8b shows the concentration profiles in the cell solution along the midplane of the microchannel at 15 minute intervals, 5 μm above the top surface of the hydrogel. It can be seen that from 1.5 – 10 mm, there is indeed a consistent linear gradient that stabilises within 15 minutes, and does not change significantly even after 1 hour. The concentration ranges from 1 nM to 11 nM, giving a gradient value of roughly 1.2 nM/mm . At $x < 10$ mm, the gradient decreases to a minimum value of 0.14 nM (Figure 4.10).

Figure 4.9 shows the 2D concentration distribution in the cell solution 5 μm above the top surface of the hydrogel. The concentration gradient maintains a similar profile to that set initially in the polymerised hydrogel. In this figure, the gradual softening of the gradient over 1 hour is noticeable, though Figure 4.8b confirms that the actual concentration values vary negligibly.

All these results provide ample validation that the cells at the central region of the microchannel should be able to detect a concentration gradient of about 1.2 nM/mm once dispensed in this chemotaxis assay.

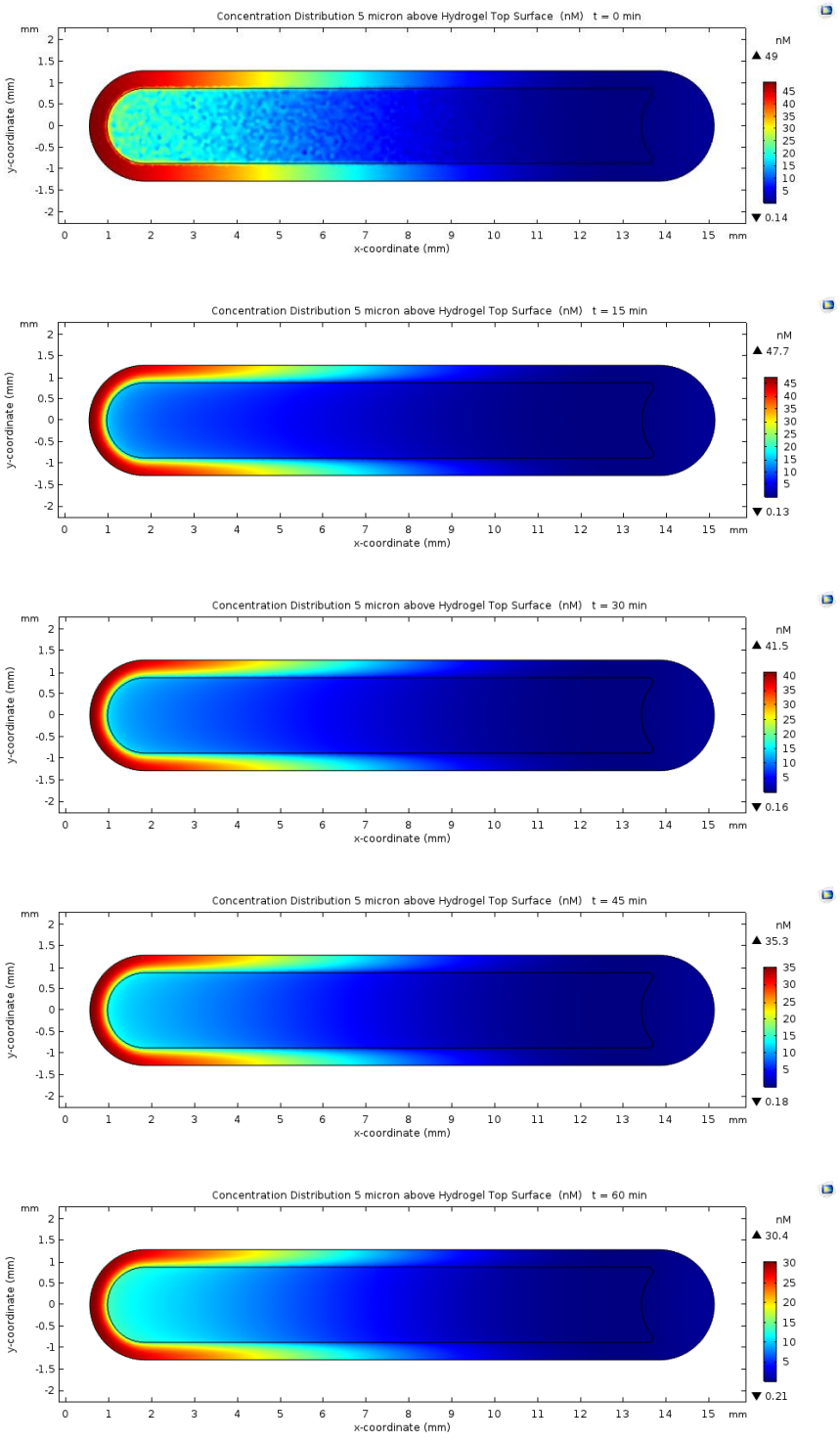

Figure 4.9 Concentration distribution 5 μm above hydrogel top surface, every 15 min over 60 min. A persisting linear gradient indeed exists within the cell vicinity. The gradient softens over 1 hour, but Figure 4.8b confirms that the actual concentration change is negligible.

Chapter 5: Testing and Validation

This chapter provides details of experiments conducted to test, validate, and troubleshoot the chemotaxis device. In Section 5.1, 3 failure modes of early iterations of Version 1 are identified, and the solutions implemented to eliminate them are described. In Section 5.2, experiments are conducted to observe the mechanisms by which gradient forms, determine a suitable wait time for gradient formation, verify that the gradient is stable, and verify that a consistent gradient forms in multiple channels. In Section 5.3, chemotaxis experiments are conducted to validate the functionality of the device. By these experiments a 4th failure mode was discovered: internal flows induced by an unknown source, which obscured any chemotactic behaviour. Therefore, in Section 5.4, attempts were made to improve cell adhesion to the hydrogel in order to the effect of flow on cells. However, these attempts had no effect. So, in Section 5.5, the source of flow was investigated, identified, and eliminated. Finally, in Section 5.6, a chemotaxis experiment is conducted again with Version 2, in which there is no internal flow.

All microscope imaging was performed with a Nikon Eclipse Ti2 inverted microscope (Nikon, Tokyo, Japan), which is controlled through the NIS-Elements Ar imaging software (Nikon, Tokyo, Japan) to obtain data.

5.1 Modes of Failure during Device Preparation

One of the goals of this thesis was to identify modes of failure of the device. This was done by attempting experiments and observing any unusual behaviour. In early iterations of Version 1, 3 failure modes were identified in the device preparation stages: (i) leaking between layers, (ii)

bubble formation in the liquid, and (iii) inconsistent gradient generation. This section will describe the failure modes, and explain the steps taken to eliminate them.

5.1.1 Leaking between Layers

In this failure mode, hydrogel prepolymer leaked out of microchannel between Layers 1 & 2 soon after dispensing (Figure 5.1). This failure mode also refers to cell solution leaking between Layers 1 and 3. The cause for both is the same: improper sealing between the PDMS layers.

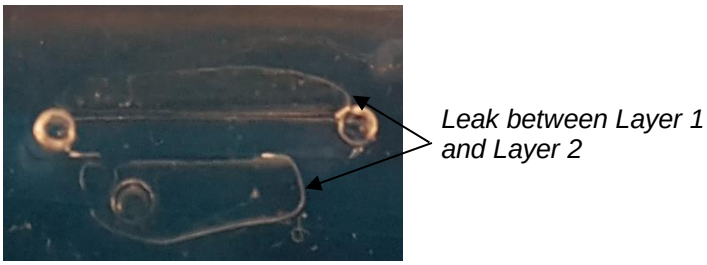

Figure 5.1 Hydrogel prepolymer leak between Layer 1 and Layer 2

Leaking of hydrogel prepolymer between Layers 1 & 2 is undesired because that would result in a gradient of unpredictable profile. Also, once exposed to UV light, the leaked areas would polymerise, and need to be carefully removed, otherwise no sealing would occur between Layers 1 & 3. Leaking between Layers 1 & 3 is undesired, because that would generate flow in the microchannel, which would induce cell motion that dominates over any chemotactic behaviour. Leaking between Layers 1 & 3 also causes loss of cells and uneven cell distribution within the channel.

In Version 1, this problem was rectified by changing the curing protocol for PDMS to make it softer and stickier. The original protocol (as recommended by manufacturer) was to mix PDMS base with its hardener in the ratio 10:1, then cure at 65 °C for 2 hours. The protocol was changed to increase the base to hardener ratio to 15:1, cure overnight at room temperature, then cure at 65 °C for 1 hour. Increasing the base to hardener ratio and curing time resulted in PDMS that was softer and stickier, but not too sticky and soft that it tore easily. Layers 1, 2 & 3 manufactured by this new protocol demonstrated a 100% success rate, i.e. it was possible to consistently prepare devices with no chance of leaking.

Another solution was pursued in parallel to rectify this problem: the design of Version 2. One of the motivations for Version 2 was to eliminate the leaking between layers failure mode by removing the need for a seal between the layers. This was achieved by designing a tab in Layer 2 (Figure 3.6b in Section 3.3.2). In this way, it was not necessary to fill the entire Layer 1 channel; simply filling it partially would submerge the bottom part of the Layer 2 tab, hence forming the reservoir once the hydrogel was polymerised. Since hydrogel prepolymer does not reach the top of the Layer 1 channel during dispensing, there is no leak between Layers 1 & 2. Since the need for Layer 3 is removed by the reservoir feature, leaking between Layers 1 & 3 is eliminated.

5.1.2 Bubble Formation in Prepolymer & Cell Solution

In this failure mode, air bubbles get trapped in the microchannel during the dispensing of the hydrogel prepolymer (Figure 5.2). This failure also refers to air bubbles getting trapped in the microchannel when dispensing the cell solution. Bubble formation in the hydrogel is unacceptable,

since it interferes with the gradient. Bubbles in the cell solution is undesired since it can influence the cell migration trajectory in unpredictable ways.

Figure 5.2 Air bubbles trapped in hydrogel prepolymer

This failure mode has been linked to 2 causes. One is inconsistent dispensing. The original protocol for dispensing involved the use of a manual pipette supported by the user's arm. A high level of user skill was required in order to hold the pipette at a constant angle and dispense liquid at a slow and steady speed. The slightest jerk could result in bubbles. With the original dispensing protocol, it was difficult to avoid bubbles consistently.

The other identified cause of bubble formation are ragged microchannel edges (Figure 5.3). Ragged edges in the Layer 1 microchannel occur when the sacrificial portion of the Layer 1 PDMS does not get removed properly, and needs to be removed manually. Due to the highly laminar nature of fluid flow in microchannels, air tends to get trapped more easily in the pockets of ragged edges.

The inconsistent dispensing problem was rectified by modifying the dispensing protocol. A custom setup was devised consisting of an electronic pipette supported by a custom stand, and positioned using the jack (Figure 3.4 in Section 3.2.3). The custom stand keeps the pipette at a constant

position. The electronic pipette is able to dispense a precise volume of fluid at a constant speed (the lowest speed setting of the pipette). The jack allows repositioning of the device without having to move the pipette. This system makes the dispensing process much more repeatable and easier.

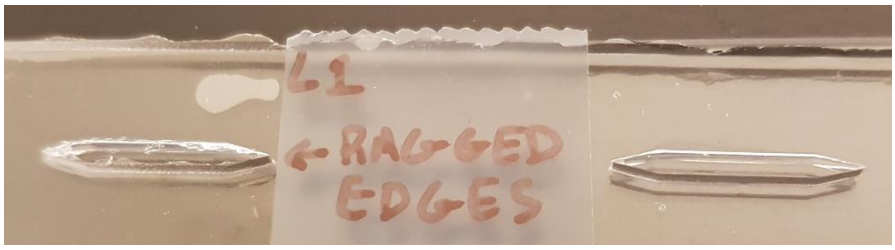

Figure 5.3 Ragged Layer 1 edge (left) compared to a clean edge (right)

Ragged edges in the current iteration of Layer 1 was rectified by testing various settings of the laser cutter. For the PLS4.75, Universal Laser Systems laser cutter, the correct setting is Power: 50%, Speed: 10, and it is recommended to run 15 passes. This cuts the PDMS sufficiently so that the unwanted pieces can be gently pushed out without the need to manually cut them out.

With the above solutions, the failure mode of trapped air bubbles was 100% eliminated. With the correct dispensing protocol and a smooth-edged Layer 1, no trapped air bubbles will form.

5.1.3 Inconsistent Gradient Profile in Microchannels

The microchannel viewing length is about 12 mm long. However, most experiments are typically conducted using a 10x objective, which on the Nikon Eclipse Ti2 inverted microscope provides a viewing range of around 1.8 x 1.8 mm. Therefore, there is a design requirement of this device is

that the gradient profile must be consistent enough so that a gradient forms within the middle 1.8 mm of the microchannel.

The original dispensing protocol using the manual pipette described in section 5.1.2 also made generating consistent gradients very difficult. A high level of user skill was required in order to hold the pipette at the same constant angle and dispense liquid at the same slow and steady speed in all microchannels.

The new dispensing protocol solution described in Section 5.1.2, consisting of the electronic pipette, custom stand, and jack (Figure 3.4 in Section 3.2.3), also eliminated this failure mode. The custom stand keeps the pipette at the exact same vertical position for each microchannel. The electronic pipette is able to dispense the exact same volume at the exact same speed for all microchannels. The jack allows precise repositioning of the device without having to move the pipette. This setup essentially removes the user from the dispensing step, thereby removing many of the human errors inherent with manual processes. The result is much higher repeatability.

5.2 Experimental Validation of Gradient Generation

The objective of the set of experiments described in the section is to determine an appropriate wait time for the gradient to form, and verify that the gradient formation meets design requirements related to the gradient for this device. There are two requirements related to the gradient: (i) gradient profile must be stable (nearly constant) over an extended period of time, and (ii) the gradient profile must be consistent in multiple channels, with the boundary forming within 1.8 mm of the channel midplane.

This section is organised as follows: Sub-Section 5.2.1 discusses methods that are common to all experiments in this section. Sub-Section 5.2.2 describes the experiment conducted to observe the formation of gradient in hydrogel prepolymer, ending with remarks and the determination of a suitable waiting period. Sub-Section 5.2.3 describes the experiment conducted to verify the stability of the gradient, and discusses the results. Sub-Section 5.2.4 describes the experiment conducted to verify the consistency of the gradient, and discusses the results.

5.2.1 Methods for Experimental Gradient Visualisation

Since fMLP is not optically visible once dissolved, a suitable fluorescent substitute must be used to visualise the gradient experimentally. Rhodamine B has a molar mass similar to fMLP (Table 5.1), and therefore is a suitable substitute. Rhodamine B prepolymer can be prepared in the exact same way as fMLP (Section 3.1.1, Chapter 3). Rhodamine B can be activated by shining fluorescent light through an mCherry HQ filter cube (Nikon, Tokyo, Japan).

Table 5.1 Molar mass of fMLP and Rhodamine B

Chemical	Molar Mass (g/mol)
fMLP	437.56
Rhodamine B	479.02

All gradient experiments were conducted on Version 2. The NIS-Elements Ar imaging software has a Large Scan feature, which can automatically take an array of images and stitch them into a single image. The Large Scan feature was used to generate images of the entire microchannel. NIS Elements also has a Time Lapse feature, by which the microscope can be set to take images at

specified intervals for a specified duration. Once all experimental images were obtained, Fiji image processing software [44] was used to analyse the images and produce averaged intensity plots over the length of the channel.

5.2.2 Formation of the Gradient in Hydrogel Prepolymer

The objective of this experiment was to analyse the mechanism of gradient formation. A suitable wait time could be determined from the results by choosing a time in which the gradient is the smoothest.

The methods for this experiment are as follows. The device was place on top of the stage-top adapter on the microscope stage. The Nikon Eclipse Ti2 inverted microscope was setup to take fluorescent images using the mCherry filter. The NIS-Elements Ar imaging software was setup to take a Large Scan image of a single microchannel, every 1 minute for 1 hour. Hydrogel prepolymer and rhodamine B prepolymer was dispensed as according to the protocol described in Sub-Section 3.3.3.1 in Chapter 3. Briefly, 25 μL of hydrogel prepolymer was dispensed into the microchannel, followed by 20 μL of rhodamine B prepolymer. Image recording was started as soon as rhodamine B prepolymer was dispensed.

Figure 5.4 shows the images taken of gradient formation every 7 minutes for 1 hour. The behaviour exhibited is similar to that studied by Du *et al.* in a similar device [46]. At 0 minutes, a parabolic profile can be seen. This is the expected profile of pressure-induced flow. At 7 minutes, 2 behaviours can be observed: (i) rhodamine B prepolymer at the gradient boundary near the microchannel centre seems to be moving upwards and downwards towards the walls, and (ii) a

second wave of rhodamine B prepolymer is flowing from the inlet. This second wave is likely caused by the weight of rhodamine B prepolymer accumulated at the inlet well. Both these behaviours proceed until a smooth gradient forms at around 28 minutes. From 35 minutes onwards, it can be seen that the gradient slowly sharpens, until a very sharp boundary forms by 60 minutes. This behaviour can be explained by the evaporation of rhodamine B prepolymer from the inlet opening, which generates a backward pressure inducing flow of prepolymer towards the channel entrance.

Figure 5.5 shows averaged intensity plots corresponding to the images in Figure 5.4. For the first 21 minutes, the intensity profile is irregular and changes unpredictably. By 28 minutes, the intensity profile smoothens to a reasonably linear gradient up until around 8 mm, beyond which there is no rhodamine B. From 35 minutes onwards, a sharp boundary starts to form. By 60 minutes, the intensity profile consists of 2 flat regions separated by a sudden drop at the 6 mm location.

The intensity profiles in Figure 5.5 were carefully considered to decide on a suitable wait time. No time before 28 minutes would be acceptable, since those intensity profiles are very irregular. The intensity profiles after 42 minutes consist of two flat regions and a narrow region with a steep gradient near the center of the channel. This steep gradient region is less than 2 mm wide, and it is difficult to ensure that the region will fall within the 1.8 mm microchannel center region that is required. Therefore, the best option is the gradient that forms near 30 minutes. The intensity profile that forms near 30 minutes is a reasonably smooth linear gradient that extends over a very wide

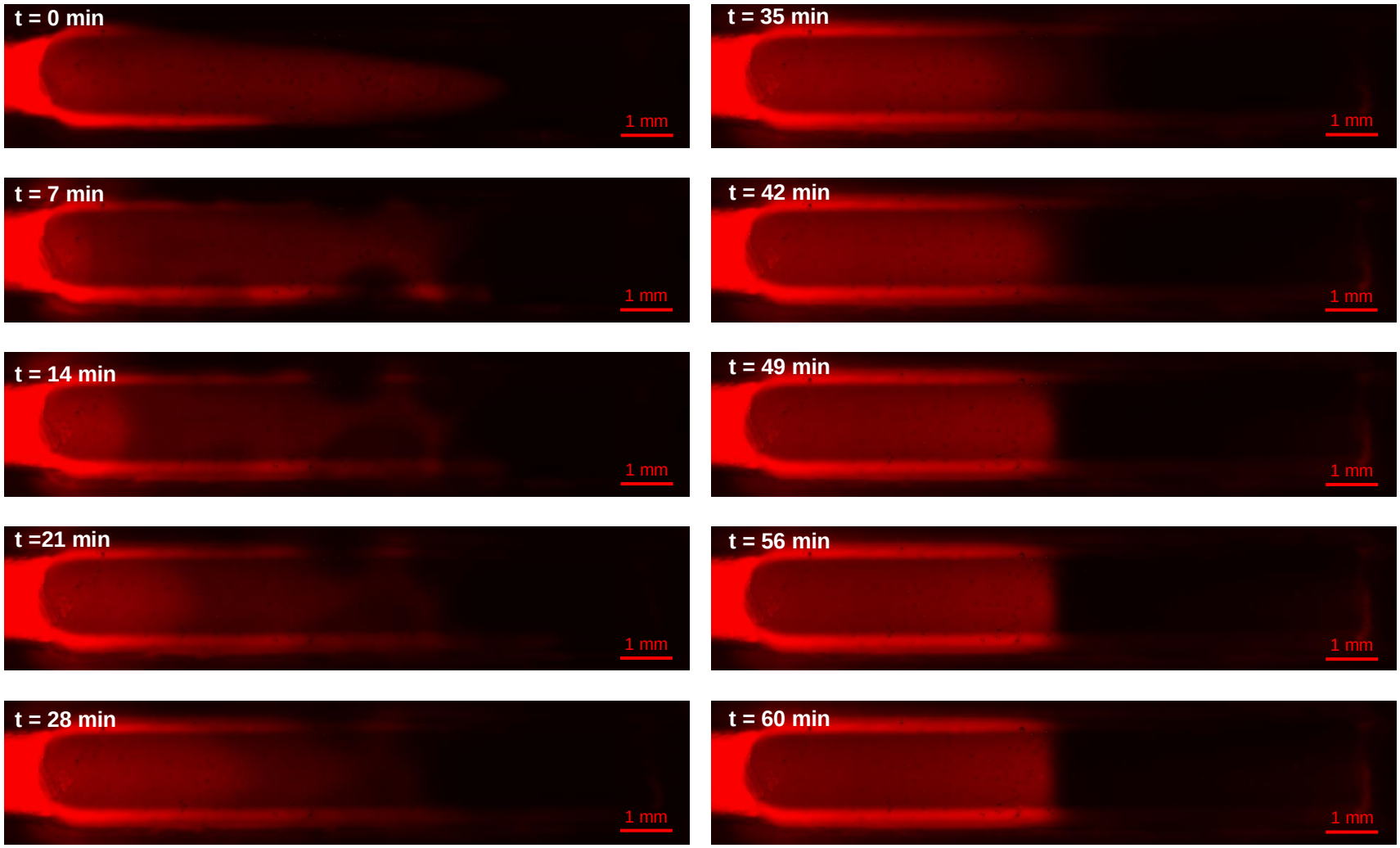

Figure 5.4 Rhodamine B gradient formation in prepolymer hydrogel in the same microchannel over 1 hour. Provided time is that after rhodamine B prepolymer dispensing. Gradient smoothens to a linear profile by 28 minutes. After 35 minutes, gradient boundary sharpens. The gradient formation is driven by a combination of weight of liquid at inlet and evaporation from inlet.

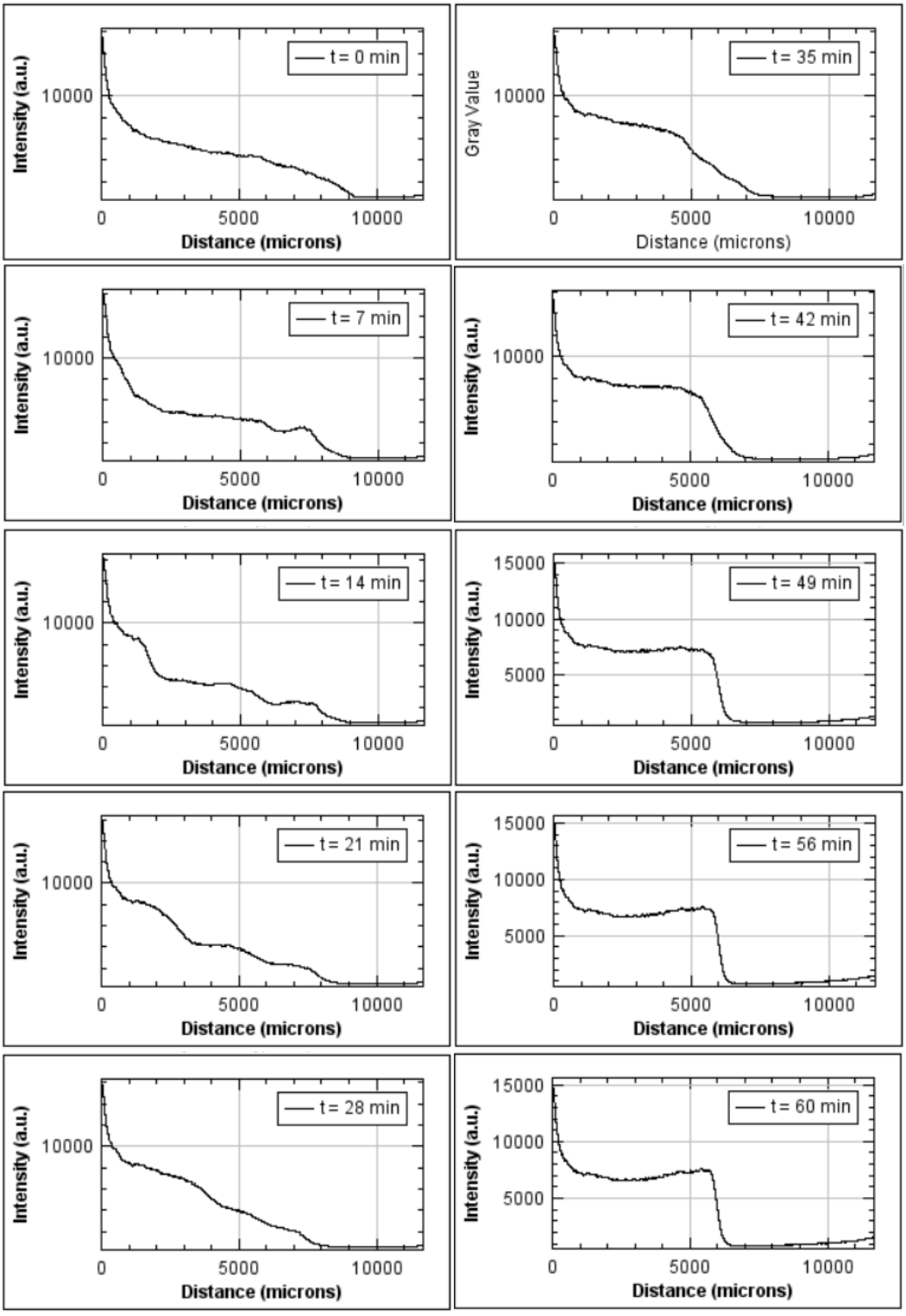

Figure 5.5 Intensity plots for gradient formation in the same microchannel over 1 hour. Provided time is after rhodamine B dispensing. Profile is irregular until 28 minutes, when a reasonably linear profile forms up to 8 mm. After 35 minutes, the gradient changes to become 2 flat regions separated by a sudden drop at 6 mm.

range. By going with this wait time, it can be ensured that there will be a gradient in the 1.8 mm region near the center of the microchannel.

5.2.3 Experimental Validation of Gradient Stability

Throughout this thesis, it has been claimed that this device is able to generate a stable gradient without the need of external equipment. The purpose of this experiment is to validate this claim.

For this experiment, a gradient was formed in a single microchannel, the hydrogel was polymerised, and cell solution was dispensed (as described in the protocol in Section 3.3.3, Chapter 3). The device was then transferred to the microscope, and Large Scan fluorescent images were taken from 15 minutes after cell solution was dispensed, every 15 minutes for 1 hour.

Figure 5.6 shows the gradient images, and Figure 5.7 shows the corresponding averaged intensity plots. From both figures, it can be seen that there is negligible change in gradient over a 1 hour period. This validates the claim that this gradient generation method can produce stable, near-constant gradients.

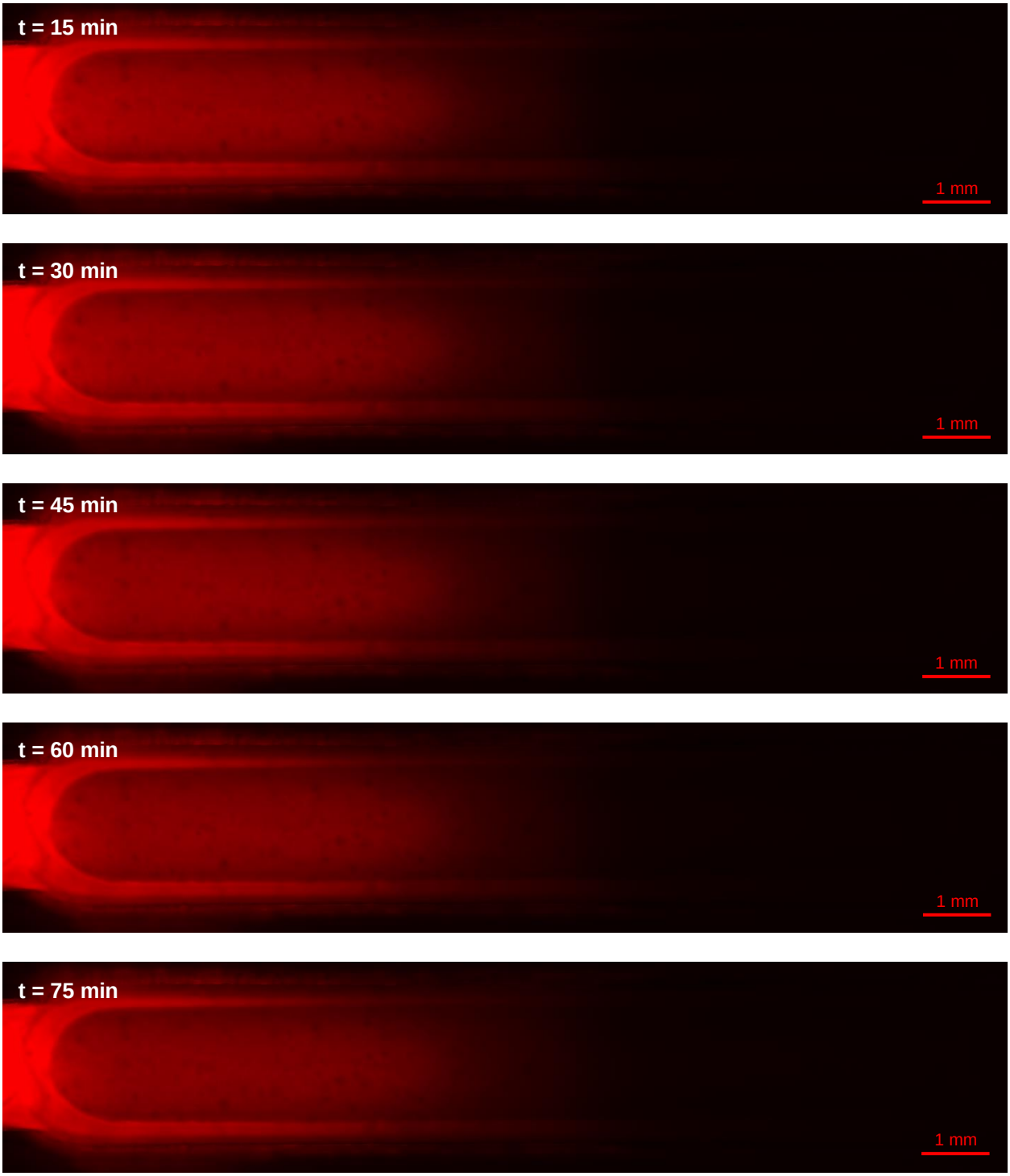

Figure 5.6 Change in gradient of the same channel after polymerization over 1 hour. Provided time is that after polymerisation. Once the hydrogel is polymerized, there negligible change in gradient profile.

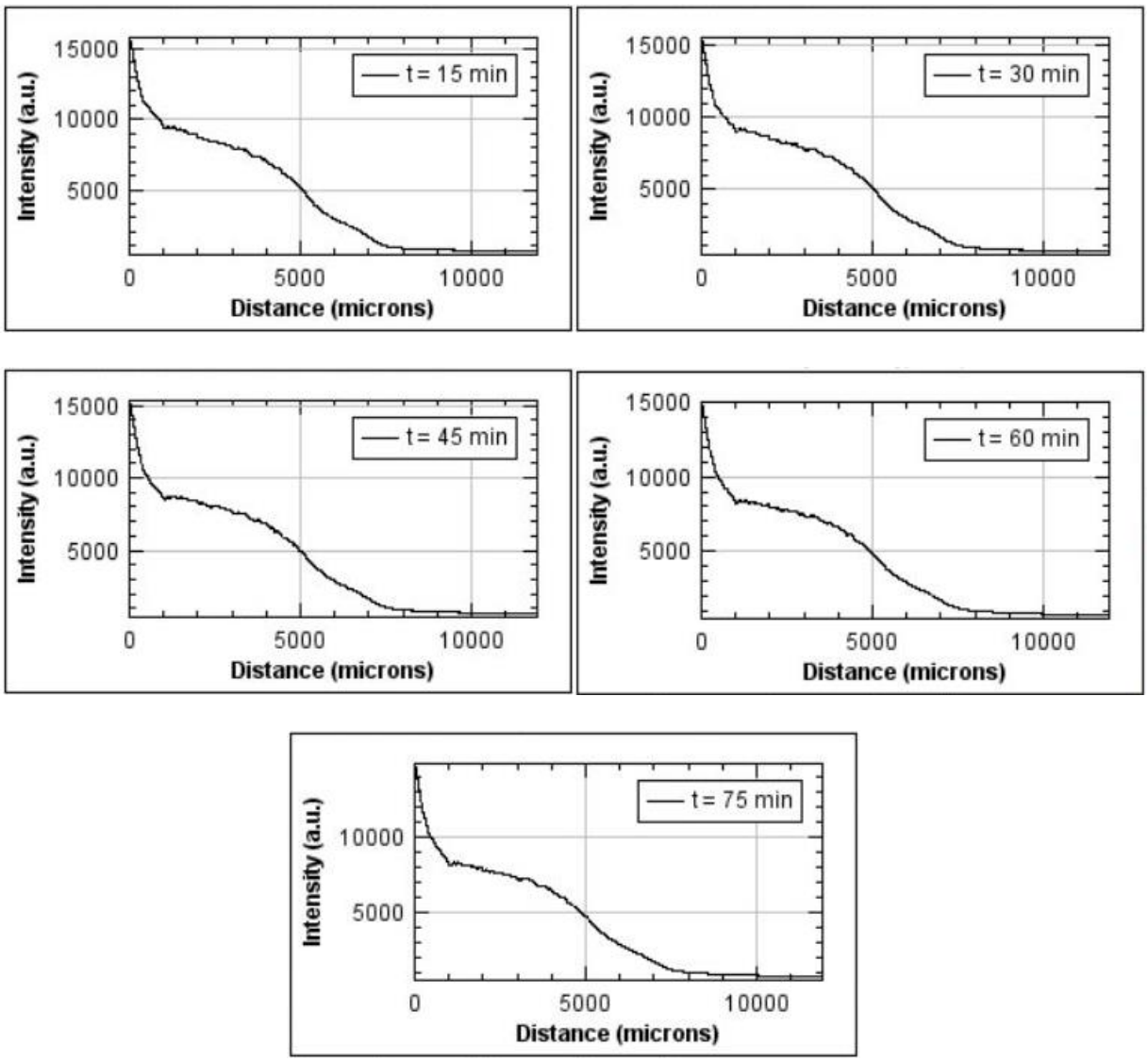

Figure 5.7 Averaged intensity plots of gradient along microchannel after polymerisation over 1 hour. Provided time is that after polymerisation. Once the hydrogel is polymerized, there negligible change in gradient profile.

5.2.4 Experimental Validation of Gradient Consistency

The purpose of this experiment is to verify that the same gradient profile forms in different microchannels. For this experiment, a single device containing 10 microchannels in a 2 x 5 array was used. In all 10 channels, gradients were formed, the hydrogel was polymerised, and cell solution was dispensed (as described in the protocol in Section 3.3.3, Chapter 3). The device was then transferred to the microscope, and Large Scan fluorescent images were taken of all 10 microchannels.

Figure 5.8 shows the images obtained from the microscope, and Figure 5.9 show the corresponding averaged intensity plots generated using Fiji. Though the profiles are roughly similar, the inconsistencies are significant enough that the results need to be analysed carefully.

As explained in Section 5.1.3, the minimum magnification required to appropriately observe cells on the Nikon Eclipse Ti2 inverted microscope is 10x, which allows 1.8 mm of the microchannel to be viewed at a time. Therefore, the requirement is that a linear gradient must consistently form along the middle 2 mm of the microchannel. The microchannel is about 12 mm long, so the middle of the microchannel is at 6 mm, and we are interested in the 5-7 mm range.

The data points from the averaged intensity plots on Figure 5.9 in the 5-7 mm range were extracted into Microsoft Excel, and linear regression was performed. The resulting slopes and standard errors are provided in Figure 5.10. Channels with significantly non-linear profiles at the middle yield standard errors greater than 275 μm (for example R2). From Figure 5.10b, it can be seen that

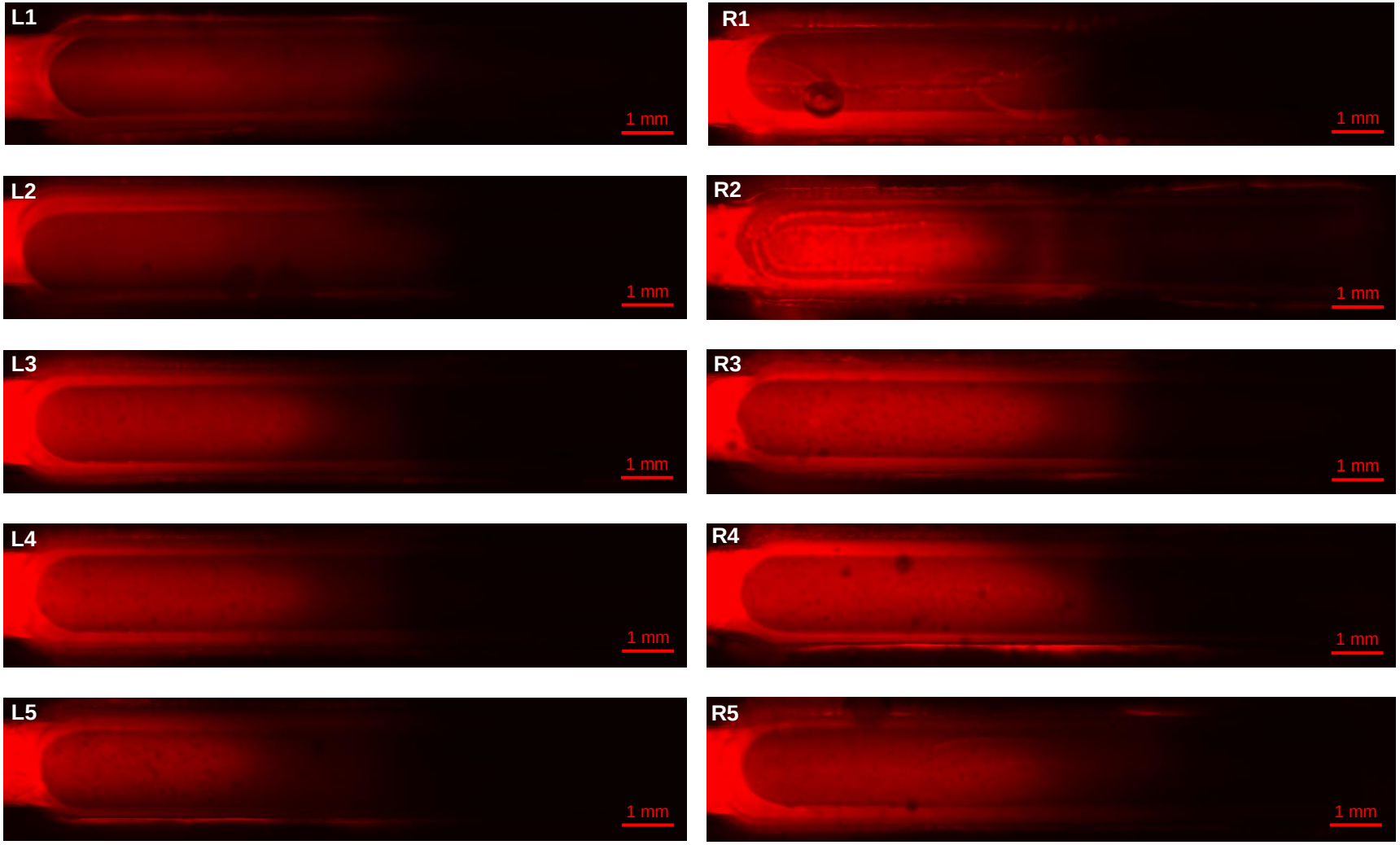

Figure 5.8 Gradient profile in all 10 channels of a single Version 2 device. Differences in gradient profiles are noticeable, and could be potentially improved. However, all channels have a gradient across the middle region of the channel.

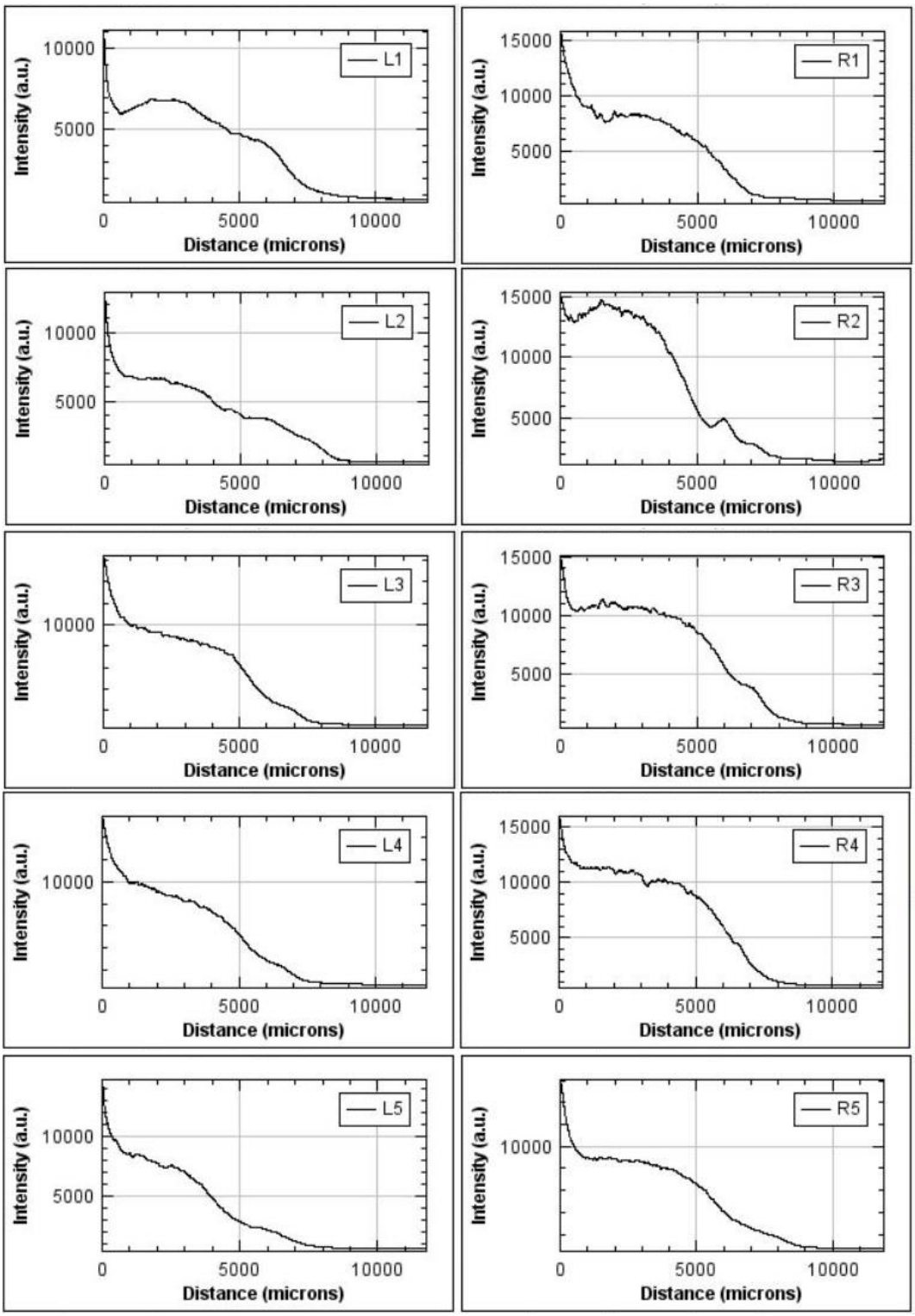

Figure 5.9 Averaged intensity plots of gradient along microchannel length for all 10 microchannels on a single Version 2 device.

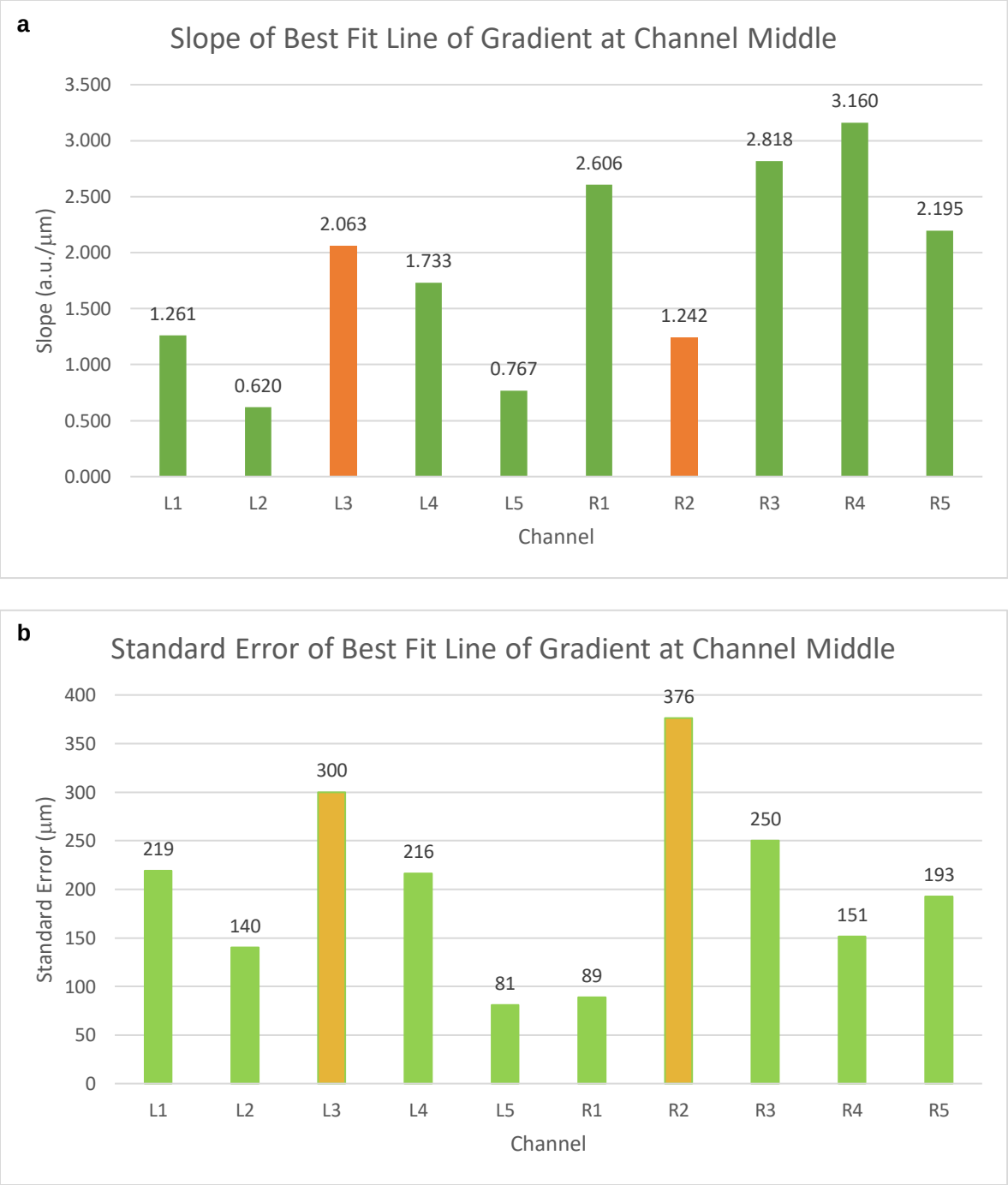

Figure 5.10 Results of linear regression of averaged intensity plots in Figure 5.9, in the 5-7 mm range. (a) Slopes of best fit lines. (b) Standard errors of best fit lines compared to raw data. Best fit lines with standard errors more than 275 µm are considered failed (coloured orange). Results demonstrate that the device has a gradient consistency of 80%.

only L3 & R2 have standard errors greater than 275 μm (coloured in orange). Therefore it can be concluded that a gradient consistency of 80% is achieved in this device.

The cause of irregularities in the gradient can be attributed to the fact that many steps in the device preparation process are still manual (Section 3.3.3, Chapter 3). The placement of Layer 2 on Layer 1 is manual, and it is not possible to exactly center the Layer 2 tabs with respect to Layer 1. The positioning of the device with respect to the pipette tip before dispensing is also manual, and will vary from channel to channel. Also, the 3D printing process is not 100% perfect, and major surface defects sometimes occur, as can be seen in R2. This interferes with the gradient profile.

Though there is definitely room for improving the gradient consistency, 80% device gradient consistency has been achieved. This is sufficient to proceed with validating the functionality of the device by performing chemotaxis experiments.

5.3 Chemotaxis Experiments to Validate Device Functionality

The purpose of the experiments described in this section was to validate the functionality of this device by performing chemotaxis experiments. A chemotaxis experiment involved dispensing cells on the polymerised hydrogel with a chemical gradient, and observing the cell trajectory through Time Lapse imaging on a microscope. The behaviour of cells on polymerised hydrogel with no chemoattractant was also recorded as a control, and the 2 sets of results compared. In a successful experiment, it was expected that there would be a clear trajectory of cells up the chemical gradient compared to control.

Experiments were performed with 2 types of cells: (i) dHL60 cells with 100 nM fMLP chemoattractant, and (ii) starved PC3 cells with 30% FBS chemoattractant. The preparation methods for the cells and chemoattractants are described in Section 3.1 in Chapter 3.

The experiments were performed with Version 1 of the device, manufactured and prepared using the methods outlined in Section 3.2, Chapter 3. The results of this section's experiments was another motivation for switching to Version 2 (discussed further in Sections 5.4 & 5.5).

In this chapter, methods common to all experiments are detailed in Sub-Section 5.3.1. Sub-Section 5.3.2 provides the results for dHL60 cells in fMLP gradient. Sub-Section 5.3.3 provides the results for PC3 cells in FBS gradient. The results for the 2 types of cells were the same, so a single discussion of results is provided in Sub-Section 5.3.4.

5.3.1 Methods for Chemotaxis Experiments

Each experiment was conducted on a single Version 1 device containing 10 microchannels in a 2 x 5 array. In a typical experiment, chemical gradients were generated in 8 of the 10 microchannels (referred to from here on as 100 nM gradients); the remaining 2 were filled with hydrogel prepolymer only (no chemoattractant, referred to from here on as 0 nM gradients). The gradients were generated and cell solution dispensed using the protocols outlined in Section 3.2.3 in Chapter 3. For the 0 nM gradient, 25 μL of hydrogel prepolymer was used instead of chemoattractant prepolymer.

After the cells were dispensed, the device was transferred to the stage-top adapter on top of the microscope stage, and left for 15 minutes for the cells to settle. The microscope was set up so that the center of each channel could be observed simultaneously. 10x objective was used for all experiments. Time Lapse of the microchannels was conducted at 30 second intervals for 15 minutes. Time lapse images were later be processed through custom image processing software (developed by Jeffrey Chiu of our group) to display cell trajectory in image format.

5.3.2 Chemotaxis Experiment Results of dHL60 Cells in fMLP Gradient

Figure 5.10 shows the typical cell trajectories of dHL60 cells at the center of the microchannel in an fMLP gradient. Figure 5.10a shows the cell trajectory in a 100 nM fMLP gradient. The fMLP concentration is higher on the left side, so it is expected that cells will move towards the left. Figure 5.11b shows the cell trajectory in 0nM gradient (no fMLP). It is expected that cells in 0 nM gradient will show no biased directional movement.

It can be seen that there is significant cell motion in both 100 nM and 0 nM gradients. Furthermore, in Figure 5.11a, the cells are moving towards the right; towards the direction of lower fMLP concentration. Further discussion of these results is continued in Sub-Section 5.3.4.

5.3.3 Chemotaxis Experiment Results of PC3 Cells in FBS Gradient

The PC3 cells used in these experiments were starved for 24 hours according to the protocol outlined in Section 3.1, Chapter 3. Figure 5.12 shows the typical cell trajectories of starved PC3 cells at the center of the microchannel in an FBS gradient. Figure 5.12a shows the cell trajectory in a 30% FBS gradient. The FBS concentration is higher on the right side, so it is expected that

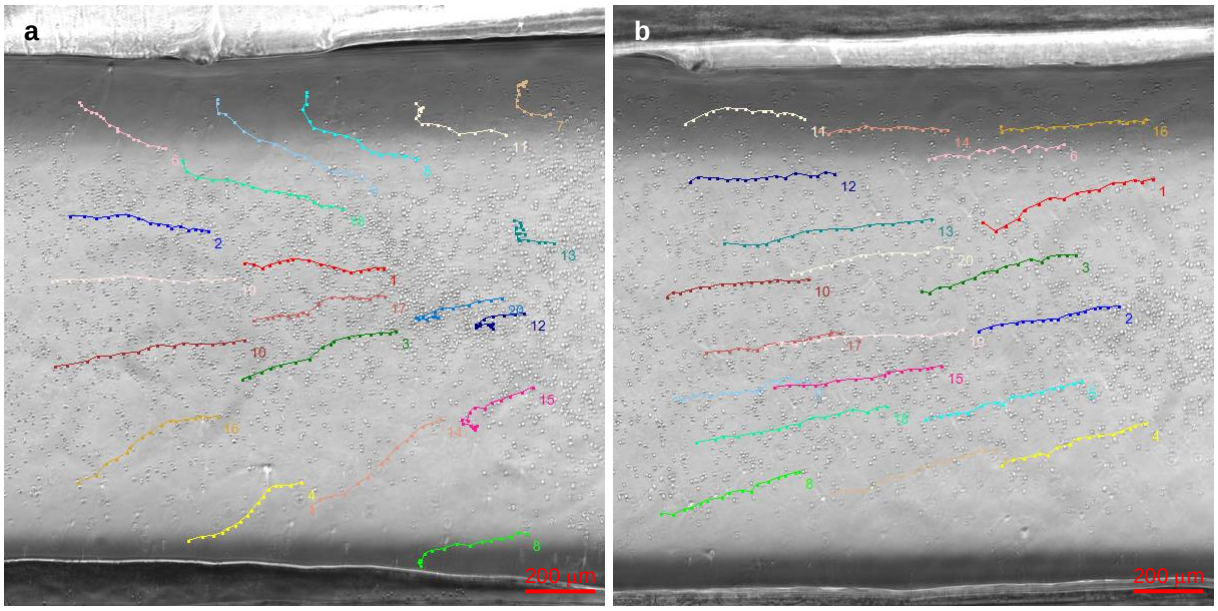

Figure 5.11 Time lapse image over 15 minutes showing typical results of a chemotaxis experiment with dHL60 cells in gradient formed using (a) 100 nM and (b) 0 nM fMLP. The numbers indicate the position of the last tracked position for each cell. The fMLP concentration is higher on the left hand side. The general trajectory of cells is towards the right. Similar cell trajectory was observed in both experiments (with and without chemoattractant). Therefore, the migration of cells is due to internal flow rather than chemotaxis.

cells will move towards the right. Figure 5.12b shows the cell trajectory in 0% gradient (no FBS). It is expected that cells in 0% gradient will show no biased directional movement.

It can be seen that there is significant cell motion in both 30% and 0% gradients. The overall trajectory of cells appears to be downwards, though at lower velocity compared to dHL60 cells. Further discussion of these results is continued in Sub-Section 5.3.4.

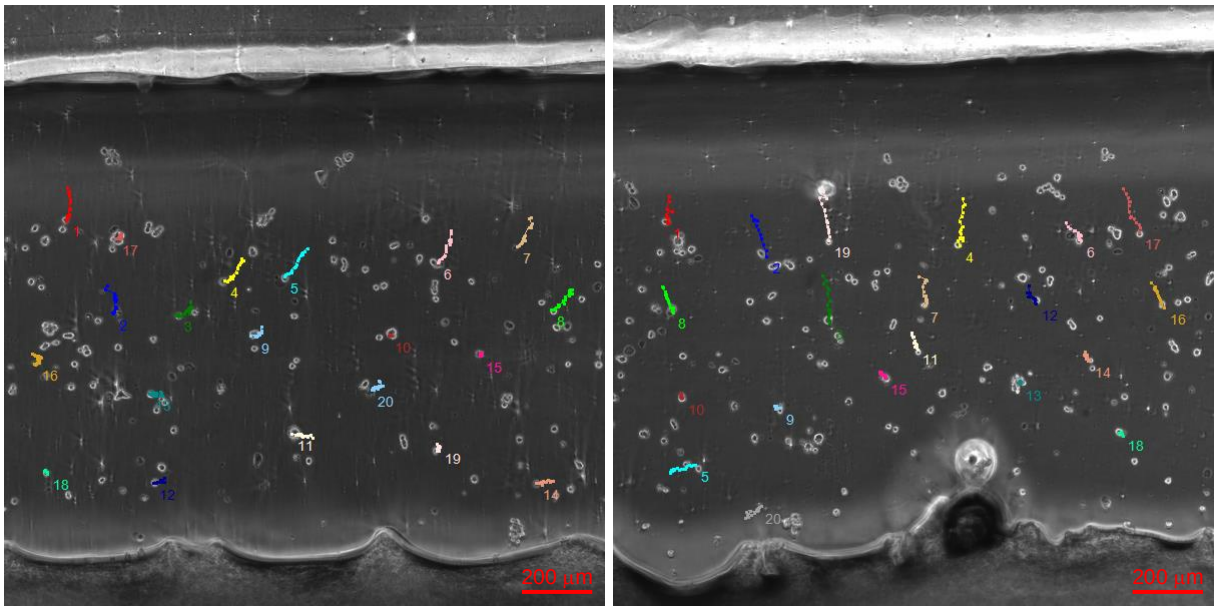

Figure 5.12 Time lapse over 15 minutes showing typical results of a chemotaxis experiment with 24 hour starved PC3 cells in gradient formed using (a) 30% FBS and (b) 0% FBS. The numbers indicate the position of the last tracked position for each cell. The FBS concentration is higher on the right hand side. There is low velocity trajectory of cells downwards. Similar cell trajectory was observed in both experiments (with and without chemoattractant). Therefore, the migration of cells is due to internal flow rather than chemotaxis.

5.3.4 Discussion of dHL60 & PC3 Chemotaxis Experiment Results

Chemotaxis experiments using dHL60 cells and PC3 cells show that the migration of cells in the presence of a chemical gradient is the same as control. Specifically, there is no difference in cell trajectories in channels with chemical gradient compared to channels with no gradient. The fact that there is a biased cell motion in channels with no gradient confirms that there is a strong source of internal flow within the cell solution in the microchannel. The direction of flow varies in the channel: it was rightwards in the device in which dHL60 experiment was conducted (Figure 5.10), and it was downwards in the device where PC3 cell experiment was conducted (Figure 5.11). However, all channels exhibited significant cell motion in a particular direction, regardless of

chemical gradient. This is undesired, since the cell motion caused by internal flow obscures any chemotactic behaviour that may be occurring.

Another conclusion can be made from these results: cells do not adhere to the hydrogel top surface. If they did adhere, they would not be influenced so strongly by flow in the cell solution. Instead, the cells float loosely on top of the hydrogel surface, are easily influenced by any internal flow currents in the cell solution, and are unable to respond to the chemical gradient.

In summary, a 4th mode of failure has been identified in Version 1 of the device: unwanted motion of cells caused by a force other than chemotaxis. This unwanted cell motion dominates over and obscures any chemotactic effects that may be occurring. Unwanted motion of cells can be attributed to 2 causes: (i) internal flow of cell solution caused by an unknown source, and (ii) failure of cells to adhere to the hydrogel surface, making it susceptible to internal flows. In Section 5.4, solutions are attempted to improve cell adhesion to the hydrogel surface. In Section 5.5, an investigation is undertaken to find the source of internal flows, and solutions are attempted to remove that source.

5.4 Modification to Hydrogel Composition to Improve Cell Adhesion to Hydrogel

The objective of this section is to apply certain techniques demonstrated in literature to improve cell adhesion to PEGDA hydrogel. The aim is to reduce the influence of internal flows on cell trajectory, so that chemotactic behaviour can be seen. The idea is that cells that adhere more to PEGDA will be much less susceptible to internal flows in the cell solution.

There are reports in literature that, despite PEGDA being a biocompatible material, cells do not naturally adhere to PEGDA unless its composition modified. The modifications serve to make available certain cell signalling molecules or nanoscopic features on the PEGDA surface to which cells can attach [47] [48].

In this section, 2 techniques are adapted from demonstrated studies in literature to improve cell adhesion: (i) embedding 100 nm polystyrene beads in PEGDA [47], and (ii) mixing dopamine solution into PEGDA prepolymer [49]. The techniques are explained further in Sub-Sections 5.4.1 and 5.4.2, along with the experiment results and conclusions. Sub-Section 5.4.3 provides additional discussion of the results.

All experiments were performed on Version 1, with the same protocol as outlined in Section 3.2.3 in Chapter 3, except that instead of 50 μL of hydrogel prepolymer and 25 μL of chemoattractant polymer, 75 μL of hydrogel polymer is dispensed in a single step into the microchannel. For all experiments, after dispensing the cell solution, the cell trajectory at the center of the channel was observed on the microscope using Time Lapse imaging every 30 seconds for 15 minutes. If the technique works, it is expected that the cell trajectory will be limited and in random directions, as opposed to a high velocity trajectory in a singly biased direction.

5.4.1 Embedding of Polystyrene Beads in Hydrogel

Yang *et al.* mixed 100 nm polystyrene beads into PEGDA prepolymer, UV polymerised it, then investigated the adhesion of L929 mouse fibroblast to PEGDA with beads compared to PEGDA with no beads. Improved cell adhesion was demonstrated to PEGDA with beads [47]. The

explanation is the beads extrude from the PEGDA top surface, forming nanoscopic attachment points for cells, thereby encouraging cells to adhere.

It was decided to trial this method to see if this worked on dHL60 cells. 100 nm polystyrene bead suspension (Sigma-Aldrich, St. Louis, MO) was mixed with hydrogel prepolymer in various proportions from 5% to 50%. UV polymerisation failed with PEGDA mixed with 25% or more bead suspension, so experiments were done with 5%, 10%, 15%, and 20%.

Figure 5.13 shows typical dHL60 trajectory on top of polymerised PEGDA with beads and no chemical gradient. A clear biased cell trajectory towards the right can still be seen. Hence we can conclude that embedding 100 nm polystyrene beads into the hydrogel has no effect. This is further discussed in Sub-Section 5.4.3.

5.4.2 Mixing Dopamine solution with Hydrogel

In a study by Ku *et al.*, a variety of materials, including PDMS, glass, poly(ethylene), and silicone rubber, was immersed in a 2 mg/mL dopamine solution for 16 hours. Ku *et al.* demonstrated improved adhesion of MC3T3-E1 and PC12 cells to all materials that underwent dopamine surface treatment. The idea is that dopamine is a cell signalling compound that is universally recognised by most living cells, and so encourages cell adhesion [49]. However, Ku *et al.*'s tests did not include PEGDA.

In our adaptation of this technique, we decided to mix dopamine with the PEGDA prepolymer instead of soaking the polymerised PEGDA for 16 hours. Dopamine solution was prepared by

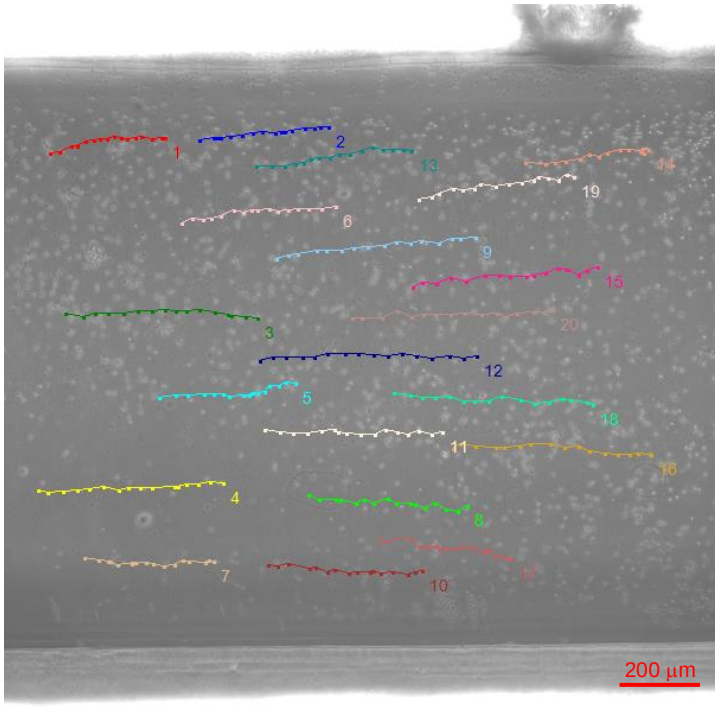

Figure 5.13 Time lapse over 15 minutes showing typical cell trajectory of dHL60 cells dispensed in a device with 100 nm beads embedded in hydrogel. The numbers indicate the position of the last tracked position for each cell. There is significant cell trajectory towards the right. Therefore, beads have failed to improve cell adhesion to the hydrogel, and the cells are still susceptible to internal flow.

taking the powdered form (Sigma-Aldrich, St. Louis, MO) and dissolving in PEGDA prepolymer. 0.2 mg/mL, 1 mg/mL, 2 mg/mL, 10 mg/mL, and 20 mg/mL, of dopamine in PEGDA were trialed.

Figure 5.14 shows typical dHL60 trajectory on top of polymerised PEGDA with dopamine solution mixed in and no chemical gradient. Once again, a clear biased cell trajectory towards the right can still be seen. Hence, we can conclude that mixing dopamine solution into the hydrogel has no effect. This is further discussed in Sub-Section 5.4.3.

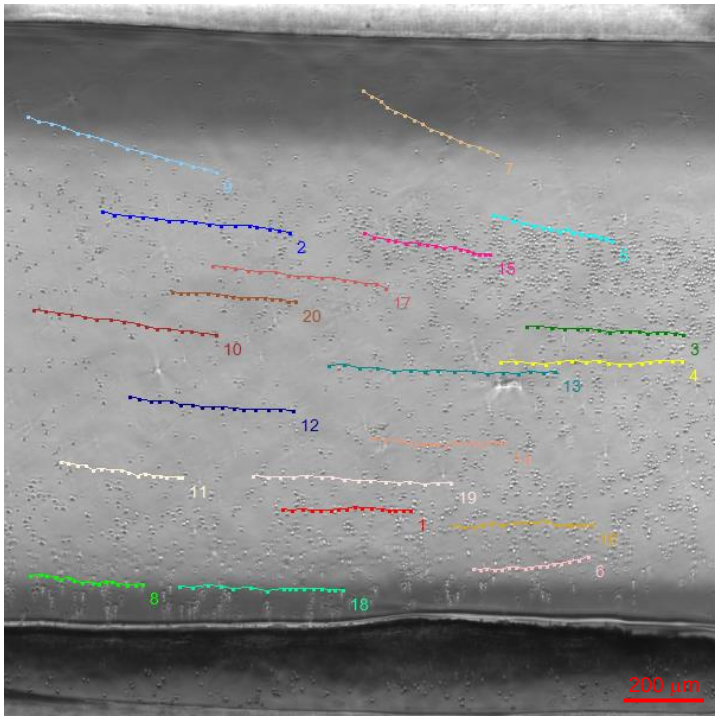

Figure 5.14 Time lapse over 15 minutes showing typical cell trajectory of dHL60 cells dispensed in a device with dopamine in hydrogel. The numbers indicate the position of the last tracked position for each cell. There is significant cell trajectory towards the right. Therefore, dopamine has failed to improve cell adhesion to the hydrogel, and the cells are still susceptible to internal flow.

5.4.3 Discussion: Reason for Failure of Hydrogel Composition Modification Experiments

On careful contemplation of this section's results, the following hypothesis is proposed as to why cells are unable to adhere to PEGDA, despite implementing modifications that are proven to work in literature. Immediately after cells are dispensed into the microchannel, they are still floating, and need some time to settle and adhere to the PEGDA. However, due to internal flows, the cells are being swept into high velocity motion before they are given the chance to adhere. Therefore, it can be concluded that in order to resolve the failure mode of unwanted cell motion, the source of internal flow must be identified and removed. This is addressed in Section 5.5.

5.5 Investigation and Resolution of Internal Flows in the Microchannel

This section is divided into 2 major sub-sections. In Sub-Section 5.5.1, an investigation is launched to find the cause of flow, and is subsequently found. The cause of flow is the sudden swelling of hydrogel due to it absorbing water from the cell solution. On confirming this, Sub-Section 5.5.2 describes steps undertaken to modify the geometry to reduce hydrogel deformation. I was ultimately able to reduce flow by switching to Version 2, and reducing the PEGDA floor thickness to ~250 μm.

5.5.1 Investigation into the Cause of Internal Flow

In this sub-section, the purpose is to discover the source of internal flow in a microfluidic device with a PEGDA bottom surface. The general approach for this was to change the geometry from the linear device to a larger circular geometry. The idea was that by moving the walls further away, the behaviour of cells near the centre may reveal some insight to the cause of internal flow.

5.5.1.1 Description of New Device to Investigate Cause of Flow

Figure 5.15 shows the new circular device used to investigate internal flow. In the new design, the hydrogel geometry was changed to a large circle with a smaller circular reservoir which could accommodate cell solution (similar to Version 2). Layer 1 was changed to a PDMS circular well 8 mm in diameter. Layer 2 followed the design of Version 2, except a 4 mm diameter circular tab was used instead of a linear tab.

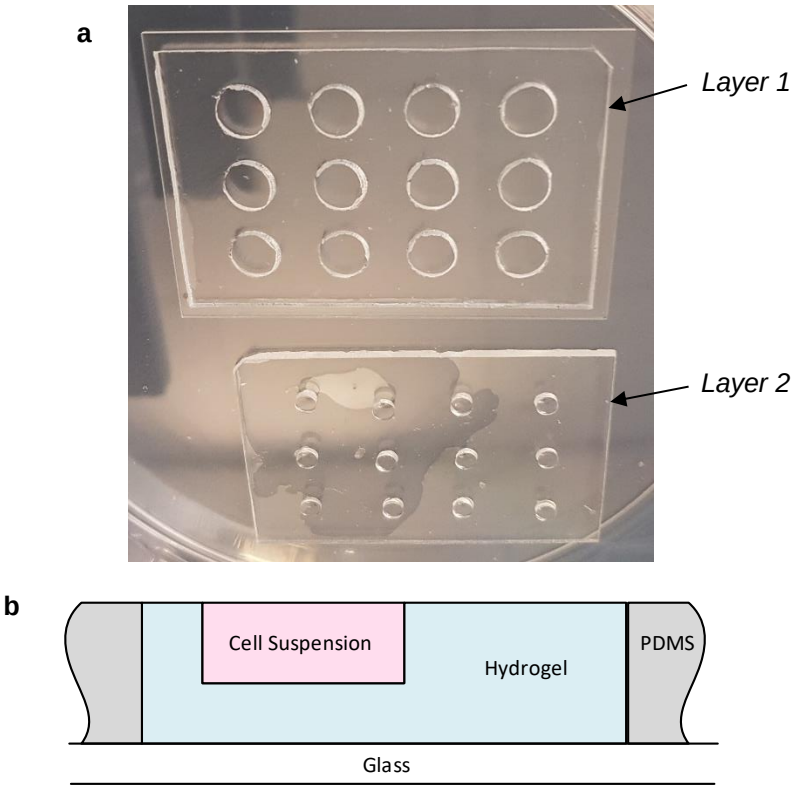

Figure 5.15 Circular device used to investigate cause of internal flow. (a) Images of the devices. (b) Schematic design of device. This design is similar to the Version 2 device, consisting of hydrogel with a reservoir to accommodate the cell solution, except that the geometry is larger and circular, and Layer 1 is made of PDMS.

5.5.1.2 Cell Trajectory on Plasma-Activated Glass Surface

An experiment was conducted to observe the cell trajectory on a plasma-activated glass surface. The purpose of this was to obtain a positive control by which the cell trajectory on hydrogel bottom could be compared.

To setup this experiment, cell solution was dispensed directly into the 8 mm diameter well of Layer 1. Since the PDMS was plasma-bonded to the glass slide (Section 3.2.2, Chapter 3), the glass surface was already plasma-activated. Immediately after dispensing cell solution into the 8 mm

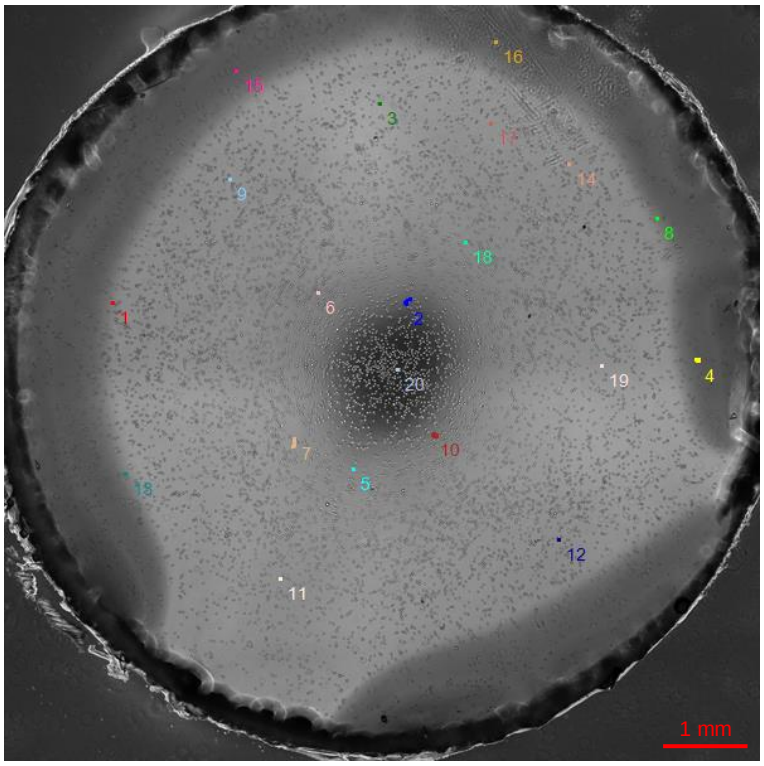

Figure 5.16 Time lapse over 15 minutes showing cell trajectory of dHL60 cells dispensed in a well with plasma-activated glass bottom. The numbers indicate the position of the last tracked position for each cell. There is no significant cell trajectory. This serves as a positive control, and a target which we wish to achieve on a PEGDA surface.

diameter well, the device was loaded onto the microscope and cell trajectory recorded using Time Lapse imaging at 30 second intervals for 15 minutes.

Figure 5.16 shows the cell trajectory on a plasma-activated glass slide. It can be seen that there is no significant cell motion. This serves as a positive control test. The objective of future tests with hydrogel would be to achieve this result.

5.5.1.3 Cell Trajectory on PEGDA surface

To setup this experiment, the 8 mm diameter Layer 1 was filled to the brim with hydrogel prepolymer. Then Layer 2 was placed on top of Layer 1, taking care not to trap any air bubbles, and positioning the 4 mm diameter Layer 2 tab so that is was roughly centered with respect to the Layer 1 well. This technique resulted in hydrogel prepolymer overflowing between the layers. However, in this case this was not a problem, since we were not trying to form a chemical gradient, and there was no Layer 3 in this setup.

Once Layer 2 was properly positioned, the hydrogel was UV-polymerised, cell solution dispensed into the reservoir, then the device immediately transferred to the microscope. Cell trajectory recorded using Time Lapse imaging at 30 second intervals for 15 minutes.

During this experiment, the following phenomena was consistently observed. During the first 5-10 minutes of the Time Lapse recording, no significant cell motion was seen. Then at one sudden moment, flow would start. At this moment, the optical properties of the device readily changed, requiring the microscope exposure to be re-adjusted.

Figure 5.17 shows the cell trajectory recorded for this experiment. Note how the earlier recorded locations of the cells are much closer together than the later recorded locations. This indicates that the cells were initially not moving, but then at a specific time point suddenly started to move.

After the experiment, the cell suspension was discarded, and the polymerised hydrogel was removed from the device and observed. The hydrogel easily detached from the device, indicating

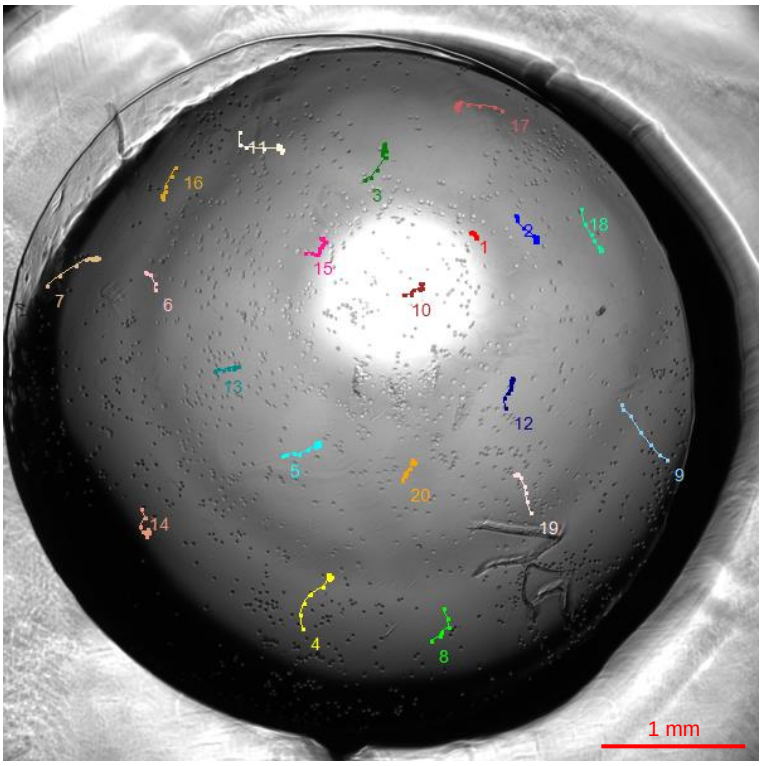

Figure 5.17 Time lapse over 15 minutes showing typical cell trajectory of dHL60 cells dispensed in the circular device with PEGDA reservoir. The numbers indicate the position of the last tracked position for each cell. No significant motion is detected for the first 5 minutes. Then suddenly significant motion begins due to hydrogel deformation. This is indicated in the cell trajectories by earlier cell location points being closer together than later cell location points.

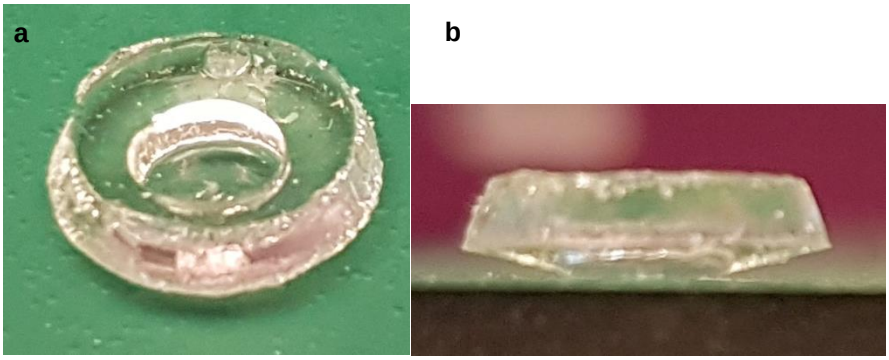

Figure 5.18 Deformed hydrogel after exposure to cell solution. (a) Isometric view. (b) View from side, showing deformed profile.

that there was no adherence of the hydrogel to PDMS or glass. The hydrogel had deformed significantly, had shown in Figure 5.18.

The characteristic of polymerised PEGDA swelling due by absorbing water is reported in literature [4] [38] [48]. From this experiment's results, it can be concluded that the polymerised hydrogel was swelling by absorbing water in the cell solution. The hydrogel deformation was the cause of internal flow.

5.5.2 Reduction of Internal Flow by Modifying Device Geometry to Reduce Hydrogel Swelling

Having identified the cause of internal flow, the purpose in this sub-section is to engineer a solution to eliminate it. The goal was to find a way to reduce hydrogel swelling. This was achieved by a combination of 3D printed epoxy resin material, and making the hydrogel bottom floor very thin.

5.5.2.1 Substitution of PDMS with 3D printed Epoxy Resin

As was seen from the results of Sub-Section 5.5.1.3, polymerised PEGDA does not adhere to PDMS or glass. However, polymerised PEGDA does irreversibly fuse with 3D printed epoxy resin. Therefore, it was decided to change the material of Layer 1 (with 8 mm diameter well) to 3D printed epoxy resin, including a 3D printed bottom. The idea was that since PEGDA fuses with the 3D printed material once polymerised, it would restrict the deformation of the hydrogel.

Figure 5.19 shows the schematic design of the 3D printed circular device, and Table 5.2 shows the different geometries that were tested. The Layer 1 has been modified to the 3D printed version,

but the previous PDMS Layer 2 has been retained. Efforts were made to make the PEGDA geometry as small and thin as possible; thinner PEGDA would not be able to absorb as much water, and hence would not be able to swell as much. However, smaller geometries are more difficult to manually operate, compromising experiment quality. This limited the size to which the device could be decreased.

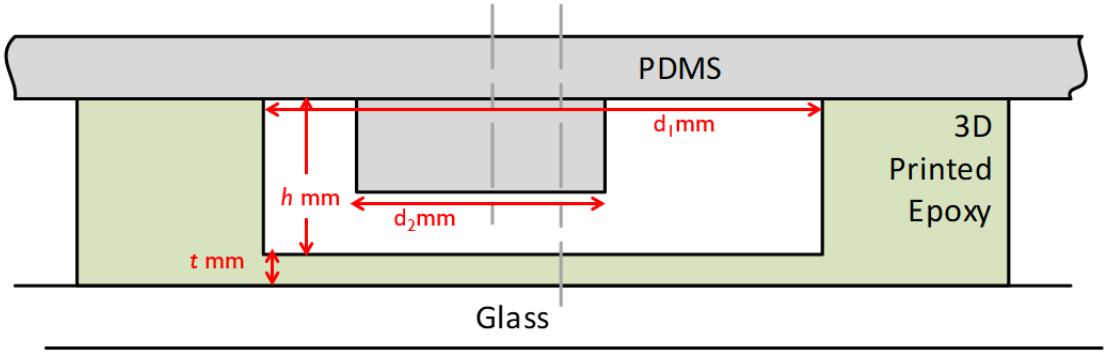

Figure 5.19 Schematic design of 3D printed circular device used in the attempt to reduce hydrogel swelling.

Table 5.2 Geometries of circular 3D printed device tested

d_1 [mm]	d_2 [mm]	h [mm]	t [mm]
8.00	3.00	2.50	0.05
6.00	2.00	2.00	0.10
-	-	1.75	0.20
-	-	1.50	-

The exact same experiment was conducted with this device as with the PDMS Layer 1 version. The Layer 1 well was filled to the brim with hydrogel prepolymer. Then Layer 2 was placed on top of Layer 1, taking care not to trap any air bubbles, and positioning the Layer 2 tab so that is was roughly centered with respect to the Layer 1 well. Once Layer 2 was properly positioned, the

hydrogel was UV-polymerised, cell solution dispensed into the reservoir, then the device immediately transferred to the microscope. Cell trajectory recorded using Time Lapse imaging at 30 second intervals for 15 minutes.

Unfortunately, the same results as with the PDMS layer 1 was observed (Figure 5.18 in Section 5.5.1.3). During the first 5-10 minutes of the Time Lapse recording, no significant cell motion was seen. Then at one sudden moment, flow would start. It is likely because the top surface of the hydrogel was still free to expand, even though the hydrogel was restricted from deforming at the sides and the bottom. Since the top surface of the hydrogel was still deforming, internal flow still existed.

5.5.2.2 Cell Trajectory on 3D Printed Linear Device with Thin Hydrogel Bottom

At this stage, the geometry of the device was changed back to the linear version, but with a 3D printed layer 1 instead of PDMS. The linear device has a reduced top surface area, such that the hydrogel top surface should deform less than the circular devices. Figure 5.20 and Table 5.3 shows the schematic design and geometries that were tested.

The experimental protocol for this device was the same as the circular devices. The Layer 1 channel was filled to the brim with hydrogel prepolymer. Then Layer 2 was placed on top of Layer 1, taking care not to trap any air bubbles, and positioning the Layer 2 tab so that is was roughly centered with respect to the Layer 1 channel. Once Layer 2 was properly positioned, the hydrogel was UV-polymerised, cell solution dispensed into the reservoir, then the device immediately

transferred to the microscope. Cell trajectory recorded with a 10x objective using Time Lapse imaging at 30 second intervals for 15 minutes.

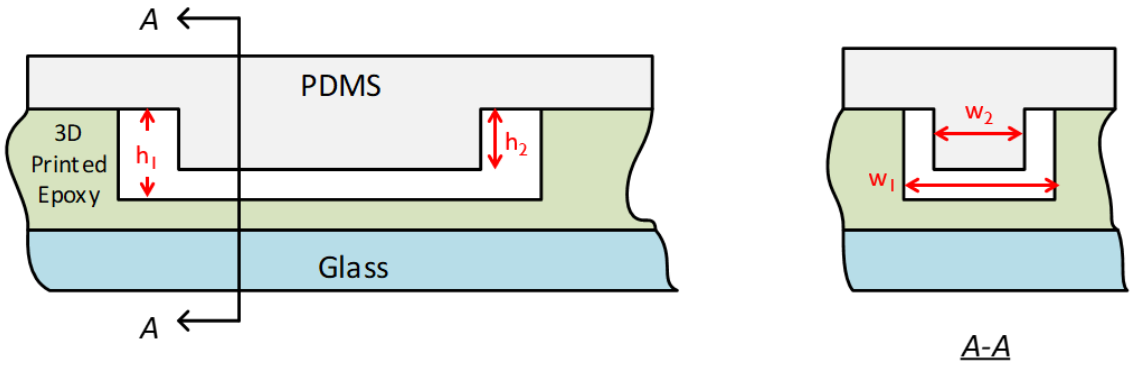

Figure 5.20 Schematic design of 3D printed linear device used in the attempt to reduce hydrogel swelling.

Table 5.3 Geometries of linear 3D printed device tested

h_1 [mm]	w_1 [mm]	h_2 [mm]	w_2 [mm]
1.25	1.25	1.00	1.00
1.50	1.50	1.25	1.25
1.75	1.75	1.50	1.50
2.00	2.00	-	1.75
-	2.25	-	2.00
-	2.50	-	2.25

Figure 5.21 shows the cell trajectory at the center of the channel with the configuration h_1 = 1.75 mm and h_2 = 1.50 mm, which gives a hydrogel bottom thickness of 250 μm. It can be seen that there is no significant cell trajectory.

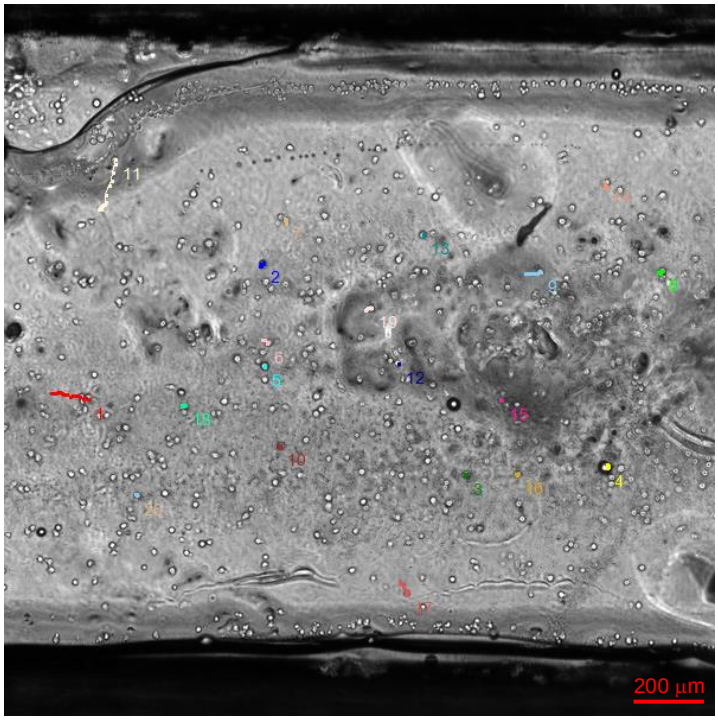

Figure 5.21 Time lapse over 15 minutes showing typical cell trajectory of PC3 cells dispensed in 3D printed linear device with hydrogel bottom thickness of 250 µm. The numbers indicate the last tracked position for each cell. There is no significant cell trajectory. Therefore, making the PEGDA bottom floor very thin and using 3D printed Layer 1 successfully eliminates internal flow in then microchannel.

In summary, a microchannel with a PEGDA surface and no internal flow has been achieved by restricting the PEGDA's tendency to deform. There are 2 factors restricting PEGDA swelling: (i) the bottom side of PEGDA is so thin that it has reduced capacity to absorb water, and so does not swell significantly, and (ii) fusion of polymerised PEGDA to the walls and bottom of the 3D printed microchannel constrains the PEGDA deformation.

5.6 Chemotaxis Experiment to Validate Functionality of 3D Printed Device

Having eliminated the internal flow failure mode, the functionality of the device needed to be tested once again by performing a chemotaxis experiment.

The experiment was conducted on Version 2 of the device, which was manufactured and prepared as described in Section 3.3 in Chapter 3. dHL60 cells were used with 100 nM fMLP chemoattractant, prepared as described in Section 3.1 in Chapter 3. Chemical gradients were generated in 8 of the 10 microchannels (referred as 100 nM gradients); the remaining 2 were filled with hydrogel prepolymer only (no chemoattractant, referred as 0 nM gradients).

After the cells were dispensed, the device was transferred to the stage-top adapter on top of the microscope stage, and left for 15 minutes for the cells to settle. The microscope was set up so that the center of each channel could be observed simultaneously. 10x objective was used for all experiments. Time Lapse of the microchannels was conducted at 30 second intervals for 15 minutes.

Figure 5.22 shows the typical cell trajectories of dHL60 cells at the center of the microchannel in an fMLP gradient. Figure 5.22a shows the cell trajectory in a 100 nM fMLP gradient. The fMLP concentration is higher on the left side, so it is expected that cells will move towards the left. Figure 5.22b shows the cell trajectory in 0nM gradient (no fMLP). It is expected that cells in 0 nM gradient will show no biased directional movement.

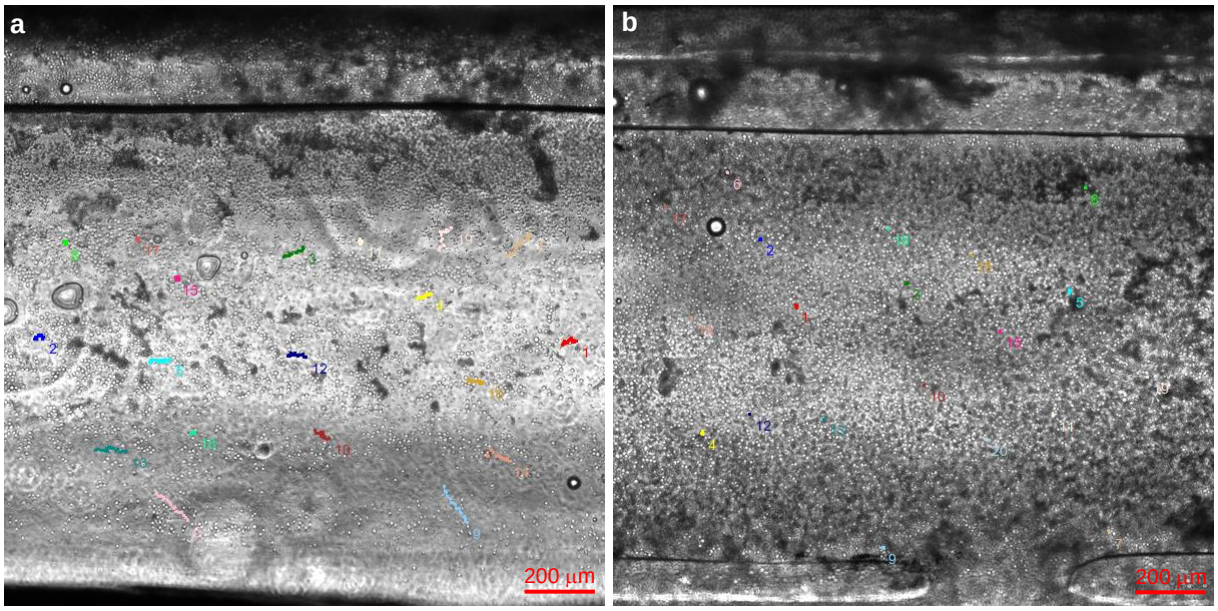

Figure 5.22 Time lapse image over 15 minutes showing results of a chemotaxis experiment in Version 2 device with dHL60 cells in gradient formed using (a) 100 nM and (b) 0 nM fMLP. The numbers indicate the position of the last tracked position for each cell. The fMLP concentration is higher on the left hand side. Cells in 0 nM gradient show limited motion, as expected. Cells in 100 nM gradient appear to show a low velocity trajectory bias towards the right; i.e. the end with lower concentration of chemoattractant.

Indeed, the cells in the 0 nM gradient show limited motion, as expected. However, cells in the 100 nM gradient exhibit low velocity motion towards the end with lower concentration of chemoattractant (the right).

To summarise, all failure modes that can be resolved through geometrical design, manufacturing methods, and device operation protocol have been resolved. The device has been validated to generate a reasonably consistent gradient at the channel center. Simulation of chemical effusion from polymerised hydrogel also verifies that a concentration profile exists in the cell vicinity. However, the cell response to the chemical gradient is still not as expected.

The remaining possible causes for the unexpected results are primarily biochemical. It is possible that 100 nM is not an appropriate concentration to induce dHL60 chemotaxis in this device; a lower or higher concentration may be more suitable. Also, it is possible that the cells have not adhered sufficiently to the hydrogel surface in order to respond to the chemical gradient. Now that the internal flow failure mode has been eliminated, modifying the PEGDA composition using techniques such as embedding 100 nm polystyrene beads or mixing dopamine may yield positive results. This is further discussed in Section 6.1.2 Future Work (Chapter 6).

Chapter 6: Conclusion

6.1.1 Summary of Results

In this thesis, I have developed a microfluidic chemotaxis assay that generates a stable chemical gradient by fixing the gradient inside a UV polymerized hydrogel. This phenomenon of gradient fixation occurs because the diffusion constant of the chemical in polymerised hydrogel is lower than that in hydrogel prepolymer. I designed 2 versions of this assay: Version 1 is manufactured using PDMS, and Version 2 is manufactured using 3D printing of epoxy resin.

Version 1 of the microfluidic device exhibited several failure modes, including (i) leakage between PDMS layers, (ii) air bubble formation in liquid, (iii) inconsistent gradient generation, and (iv) internal flow within the microchannel. I optimised the manufacturing method and operation protocol for Version 1 to eliminate failure modes (i)-(iii). To validate device functionality, I conducted chemotaxis experiments on Version 1 with: (i) dHL60 cells on fMLP gradient, and (ii) PC3 cells on FBS gradient. However, significant and similar cell motion was observed on both channels with gradient and control channel with no chemoattractant. Attempts to improve cell adhesion to the hydrogel by modifying the hydrogel composition also failed. Therefore an investigation was launched, and I discovered that internal flow within the microchannel was caused by polymerised hydrogel swelling by absorbing water from the cell solution. Hydrogel deformation was further aggravated because polymerised hydrogel does not adhere to PDMS. Since polymerised hydrogel irreversibly bonds to epoxy resin, I designed Version 2 of the device with a reduced hydrogel floor thickness of 250 μm, which successfully eliminated internal flow.

For Version 2, I experimentally validated the gradient formation. The gradient in the prepolymer forms due to internal flows induced by a combination of weight of fluid at the inlet well and evaporation at the inlet. I verified that, once polymerised, the gradient is indeed stable. 80% consistency has been demonstrated in generating a linear gradient in the middle of multiple channels. I set up a COMSOL simulation based on Version 2 geometry and experimental gradient data, and verified that the chemical gradient indeed applied to the cell sample.

Despite these results, chemotaxis experiments of dHL60 cells in an fMLP gradient did not yield positive results. However, I have resolved all failure modes that can be resolved through geometrical design, manufacturing methods, and device operation protocol. Thereby I have set the path for future work on this project to focus on the biochemical aspects of the device design.

6.1.2 Future Work

The current device has been verified to be able to produce consistent, stable gradients which are imposed on the cell sample using a simple operational protocol. The next step would be to improve the biochemical aspects of the device design. The following next steps are proposed:

- **Vary Chemoattractant Concentration.** Conduct multiple chemotaxis experiments with varying concentrations of chemoattractant. 100 nM may not be an appropriate concentration to induce dHL60 chemotaxis.
- **Explore Cell adhesion to PEGDA.** Now that internal flow has been resolved, chemotaxis experiments with 100 nm polystyrene bead and dopamine should be repeated. Other possible techniques to improve cell adhesion to PEGDA should also be explored.

- **Explore PEGDA Preparation Protocol.** The current PEGDA preparation protocol consists of a 50% PEGDA formulation and 10 second UV curing time. The effect of varying the concentration of PEGDA and UV curing time should be explored.

References

[1] B. Petri and M. Sanz, "Neutrophil Chemotaxis," *Cell Tissue Res.*, vol. 371, no. 3, pp. 425-436, Mar. 2018.

[2] Z. Liang, T. Wu, H. Lou, X. Yu, R. S. Taichman, S. K. Lau, S. Nie, J. Umbreit and H. Shim, "Inhibition of Breast Cancer Metastasis by Selective Synthetic Polypeptide against CXCR4," *Cancer Res.*, vol. 64, no. 12, pp. 4302-4308, Jun. 2014.

[3] J. Rossant and L. Howard, "Signalling Pathways in Vascular Development," *Annu. Rev. Cell Dev. Biol.*, vol. 18, no. 1, pp. 541-573, Nov. 2002.

[4] L. Cai, J. Lu, S. Volney and S. Wang, "Optimal Poly(L -lysine) Grafting Density in Hydrogels for Promoting Neural Progenitor Cell Functions," *Biomacromolecules*, vol. 13, no. 5, pp. 1663-1674, May 2012.

[5] N. Kramer, A. Walzl, C. Unger, M. Rosner, G. Krupitza, M. Hengstschläger and H. Dolznig, "In vitro cell migration and invasion assays," *Mutat. Res. Rev. Mutat. Res.*, vol. 752, no. 1, pp. 10-24, Jan. 2013.

[6] T. M. Keenan and A. Folch, "Biomolecular gradients in cell culture systems," *Lab Chip*, vol. 8, no. 1, pp. 34-57, Jan. 2008.

[7] S. Toetsch, P. Olwell, A. Prina-Mello and Y. Volkov, "The evolution of chemotaxis assays from static models to physiologically relevant platforms," *Integr. Biol.*, vol. 1, no. 2, pp. 170-181, Feb. 2009.

[8] E. Berthier, J. Surfus, J. Verbsky, D. Huttenlocher and D. Beebe, "An arrayed high-content chemotaxis assay for patient diagnosis," *Integr. Biol.*, vol. 2, no. 11-12, pp. 630-638, Nov. 2010.

[9] H. Somaweera, A. Ibraguimov and D. Pappas, "A review of chemical gradient systems for cell analysis," *Anal. Chim. Acta,* vol. 907, pp. 7-17, Feb. 2016.

[10] N. L. Jeon, H. Baskaran, S. K. W. Dertinger, G. M. Whitesides, L. Van De Water and M. Toner, "Neutrophil chemotaxis in linear and complex gradients of interleukin-8 formed in a microfabricated device," *Nat. Biotechnol.*, vol. 20, no. 8, pp. 826-830, Aug. 2002.

[11] World Health Organization, "The top 10 causes of death," World Health Organization, 24 May 2018. [Online]. Available: https://www.who.int/news-room/fact-sheets/detail/the-top-10-causes-of-death. [Accessed 10 Apr. 2019].

[12] International Agency for Research on Cancer, "Latest global cancer data: Cancer burden rises to 18.1 million new cases and 9.6 million cancer deaths in 2018," 12 Sep. 2018. [Online]. Available: https://www.iarc.fr/wp-content/uploads/2018/09/pr263_E.pdf. [Accessed 10 Apr. 2019].

[13] Ibidi, "μ-Slide Chemotaxis," Ibidi GmbH, 2019. [Online]. Available: https://ibidi.com/channel-slides/9--slide-chemotaxis-ibitreat.html. [Accessed 07 Apr. 2019].

[14] V. Biswenger, N. Baumann, J. Jürschick, M. Häckl and C. Battle, "Characterization of EGF-guided MDA-MB-231 cell chemotaxis in vitro using a physiological and highly sensitive assay system," *PLoS One,* vol. 13, no. 9, pp. 1-17, Sep. 2018.

[15] J. Wu, X. Wu and F. Lin, "Recent developments in microfluidics-based chemotaxis studies," *Lab chip,* vol. 13, pp. 2484-2499, May 2013.

[16] S. Boyden, "The Chemotactic Effect of Mixtures of Antibody and Antigen on Polymorphonuclear Leucocytes," *J. Exp. Med.,* vol. 115, no. 3, pp. 453-466, Mar. 1962.

[17] F. Lin and E. C. Butcher, "T cell chemotaxis in a simple microfluidic device," *Lab Chip,* vol. 6, no. 11, pp. 1462-1469, Sep. 2006.

[18] S. H. Zigmond, "Ability of polymorphonuclear leukocytes to orient in gradients of chemotactic factors," *J. Cell Biol.,* vol. 75, no. 2, pp. 606-616, Nov. 1977.

[19] D. Zicha, G. A. Dunn and A. F. Brown, "A new direct-viewing chemotaxis chamber," *J. Cell Sci.,* vol. 99, pp. 769-775, Aug. 1991.

[20] A. J. Muinonen-Martin, D. M. Veltman, G. Kalna and R. H. Insall, "An Improved Chamber for Direct Visualisation of Chemotaxis," *PLoS One,* vol. 5, no. 12, Dec. 2010.

[21] N. L. Jeon, S. K. W. Dertinger, D. T. Chiu, I. S. Choi, A. D. Stroock and G. M. Whitesides, "Generation of solution and surface gradients using microfluidic systems," *Langmuir,* vol. 16, no. 22, pp. 8311-8316, Oct. 2000.

[22] D. Irimia, D. A. Geba and M. Toner, "Universal Microfluidic Gradient Generator," *Anal. Chem.,* vol. 78, no. 10, pp. 3472-3477, Apr. 2006.

[23] W. Saadi, S. W. Rhee, F. Lin, B. Vahidi, B. G. Chung and N. L. Jeon, "Generation of stable concentration gradients in 2D and 3D environments using a microfluidic ladder chamber," *Biomed. Microdevices,* vol. 9, no. 5, pp. 627-635, Oct. 2007.

[24] L. Soon, G. Moumeimne, J. Segall, J. Wyckoff and J. Condeelis, "Description and characterization of a chamber for viewing and quantifying cancer cell chemotaxis," *Cell Motility and the Cytoskeleton,* vol. 62, no. 1, pp. 27-34, Sep. 2005.

[25] B. Heit and P. Kubes, "Measuring chemotaxis and chemokinesis: the under-agarose cell migration assay," *Science's STKE,* vol. 2003, no. 170, pp. 1-12, Feb. 2003.

[26] O. Moreno-Arotzena, G. Mendosa, M. Cóndor, T. Rüberg and J. M. García-Aznar, "Inducing chemotactic and haptotactic cues in microfluidic devices for three-dimensional in vitro assays," *Biomicrofluidics,* vol. 8, no. 6, p. 064122, Dec. 2014.

[27] W. J. Rosoff, R. McAllister, M. A. Esrick, G. J. Goodhill and J. S. Urbach, "Generating controlled molecular gradients in 3D gels," *Biotechnol. Bioeng.,* vol. 91, no. 6, pp. 754-759, Sep. 2005.

[28] Neuro Probe, "Chemotaxis Chambers," Neuro Probe Inc., 2019. [Online]. Available: http://www.neuroprobe.com/product-category/chemotaxis_chambers/. [Accessed 07 Apr. 2019].

[29] Ibidi, "μ-Slide III 3in1," Ibidi GmbH, 2019. [Online]. Available: https://ibidi.com/channel-slides/55--slide-iii-3in1.html. [Accessed 07 Apr. 2019].

[30] I. Meyvantsson, E. Vu, C. Lamers, D. Echeverria, T. Worzella, V. Echeverria, A. Skoien and S. Hayes, "Image-based analysis of primary human neutrophil chemotaxis in an automated direct-viewing assay," *J. Immunol. Methods,* vol. 374, no. 1-2, pp. 70-77, Nov. 2011.

[31] S. Kanegasaki, Y. Nomura, N. Nitta, S. Akiyama, T. Tamatani, Y. Goshoh, T. Yoshida, T. Sato and Y. Kikuchi, "A novel optical assay system for the quantitative measurement of chemotaxis," *J. Immunol. Methods,* vol. 282, no. 1-2, pp. 1-11, Nov. 2003.

[32] Essen BioScience, "Chemotactic Migration Assay for Live-Cell Analysis," Sartorius, 2019. [Online]. Available: https://www.essenbioscience.com/en/applications/measure-cell-migration-and-chemotaxis-in-real-time/incucyte-chemotaxis-system/. [Accessed 07 Apr. 2019].

[33] A. E. Lynch, J. Triajianto and E. Routledge, "Low-Cost Motility Tracking System (LOCOMOTIS) for Time-Lapse Microscopy Applications and Cell Visualisation," *PLoS One,* vol. 9, no. 8, pp. 1-13, Aug. 2014.

[34] J. Wu, L. Ouyang, N. Wadhawan, J. Li, M. Zhang, S. Liao, D. Levin and F. Lin, "A compact microfluidic system for cell migration studies," *Biomed. Microdevices,* vol. 16, no. 4, pp. 521-528, Aug. 2014.

[35] K. Yang, J. D. Wu, H. Peretz-Soroka, L. Zhu, Z. G. Li, Y. S. Sang, J. Hipolito, M. Zhang, S. Santos, C. Hilier, R. L. de Faria, Y. Liu and F. Lin, "M-kit : A cell migration assay based on microfluidic device and smartphone," *Biosens. Bioelectron. ,* vol. 99, pp. 259-267, Jan. 2018.

[36] N. A. Evensen, J. Li, J. Yang, X. Yu, N. S. Sampson, S. Zucker and J. Cao, "Development of a High-Throughput Three-Dimensional Invasion Assay for Anti-Cancer Drug Discovery," *PLoS One,* vol. 8, no. 12, pp. 1-11, Dec. 2013.

[37] W. Yang, H. Yu, G. Li, Y. Wang and L. Liu, "Facile modulation of cell adhesion to a poly(ethylene glycol) diacrylate film with incorporation of polystyrene nano-spheres," *Beiomed. Microdevices,* vol. 18, no. 6, p. 107, Dec. 2016.

[38] J. Z. Paxton, K. Donelly, R. P. Keatch and K. Baar, "Engineering the Bone-Ligament Interface Using Polyethylene Glycol Diacrylate Incorporated with Hydroxyapatite," *Tissue Eng. Part A,* vol. 15, no. 6, pp. 1201-1209, Jun. 2009.

[39] M. V. Turturro and G. Papavasiliou, "Generation of Mechanical and Biofunctional Gradients in PEG Diacrylate Hydrogels by Perfusion-Based Frontal Photopolymerization," *J. Biomater. Sci., Polym. Ed.,* vol. 23, no. 7, pp. 917-939, Apr. 2012.

[40] S. A. DeLong, A. S. Gobin and J. L. West, "Covalent immobilization of RGDS on hydrogel surfaces to direct cell alignment and migration," *J. Controlled Release,* vol. 109, no. 1, pp. 139-148, Mar. 2005.

[41] J. Crank, THE MATHEMATICS OF DIFFUSION, Oxford: Clarendon Press, 1975.

[42] COMSOL AB, "Diffusion Equation," COMSOL AB, 22 Mar. 2017. [Online]. Available: https://www.comsol.com/multiphysics/diffusion-equation. [Accessed 16 Apr. 2019].

[43] S. Seiffert and W. Oppermann, "Systemic evaluation of FRAP experiments performed in a confocal laser scanning microscope," *J. Microsc.,* vol. 220, no. 1, pp. 20-30, Oct. 2005.

[44] J. Schindelin, I. Arganda-Carreras and E. Frise, "Fiji: an open-source platform for biological-image analysis," *Nature Methods,* vol. 9, no. 7, pp. 676-682, Jun. 2012.

[45] P. -O. Gendron, F. Avaltroni and K. J. Wilkinson, "Diffusion Coefficients of Several Rhodamine Derivatives as Determined by Pulsed Field Gradient–Nuclear Magnetic

Resonance and Fluorescence Correlation Spectroscopy," *J. Fluoresc.*, vol. 18, pp. 1093-1101, Apr. 2008.

[46] Y. Du, J. Shim, M. Vidula, M. J. Hancock, E. Lo, B. G. Chung, J. T. Borenstein, M. Khabiry, D. M. Cropek and A. Khademhosseini, "Rapid generation of spatially and temporally controllable long-range concentration gradients in a microfluidic device," *Lab Chip,* vol. 9, no. 6, pp. 741-848, Dec. 2008.

[47] W. Yang, H. Yu, G. Li, Y. Wang and L. Liu, "Facile modulation of cell adhesion to a poly(ethylene glycol) diacrylate film with incorporation of polystyrene nano-spheres," *Biomed Microdevices,* vol. 18, no. 6, p. 107, Nov. 2016.

[48] M. V. Turturro, S. Sokic, J. C. Larson and G. Papavasiliou, "Effective tuning of ligand incorporation and mechanical properties in visible light photopolymerized poly(ethylene glycol) diacrylate hydrogels dictates cell adhesion and proliferation," *Biomed. Mater.*, vol. 8, no. 2, p. 025001, Apr. 2013.

[49] S. H. Ku, J. Ryu, S. K. Hong, H. Lee and C. B. Park, "General functionalization route for cell adhesion on non-wetting surfaces," *Biomaterials,* vol. 31, no. 9, pp. 2535-2541, Dec. 2009.

[50] Y. Tabei, H. Fukui, A. Nishioka, Y. Hagiwara, K. Sato, T. Yoneda, T. Koyama and M. Horie, "Effect of iron overload from multi walled carbon nanotubes on neutrophil-like differentiated HL-60 cells," *Sci. Rep.*, vol. 9, no. 2224, pp. 1-13, Feb. 2019.